1979

I The interaction of ammonia with single crystal rhodium catalysts II Hydrogen and nitrogen adsorption on a W(111) surface: A theoretical molecular orbital approach

Atis Vavere
Iowa State University

I. The interaction of ammonia with single crystal rhodium catalysts

II. Hydrogen and nitrogen adsorption on a W(111) surface: A theoretical molecular orbital approach

by

Atis Vāvere

A Dissertation Submitted to the
Graduate Faculty in Partial Fulfillment of
The Requirements for the Degree of
DOCTOR OF PHILOSOPHY

Department: Chemistry
Major: Physical Chemistry

Approved:

Signature was redacted for privacy.

In Charge of Major Work

Signature was redacted for privacy.

For the Major Department

Signature was redacted for privacy.

For the Graduate College

Iowa State University
Ames, Iowa

1979

TABLE OF CONTENTS

PART I. THE INTERACTION OF AMMONIA WITH SINGLE CRYSTAL RHODIUM CATALYSTS

INTRODUCTION

Chemical reactions which involve ammonia (NH_3) have fascinated scientists for many years. These reactions are probably the most studied of any catalytic processes since the turn of the century. The two most important ammonia reactions are (a) NH_3 synthesis from elemental N_2 and H_2, and (b) the decomposition of NH_3 to N_2 and H_2. These processes are depicted in the following reactions:

$$2NH_3 \rightleftharpoons N_2 + 3H_2 \qquad \text{(I-1)}$$

Both of these reactions require a catalyst as the homogeneous gas phase reactions are severely kinetically hindered. The catalyst used in this study is rhodium (Rh) and the reaction of interest is the decomposition of NH_3 to N_2 and H_2.

The importance of NH_3 in the chemical and manufacturing industries cannot be overemphasized. NH_3 is used extensively as a source of fixed nitrogen in the fertilizer industry. It is used throughout the world in cleaning solutions, solvents, and as a source of nitrogen in polymer and nitrate formation. Because of this extensive usage, the NH_3 synthesis represents one of the most important catalytic processes in the industrialized world.

The decomposition of NH_3 is also of extreme importance. Due to recent EPA standards, the auto industry must concern

itself with reducing the amounts of nitrogen effluents emitted into the atmosphere. In general, most catalysts tend to convert the NO_x produced in engines to NH_3 rather than N_2 as desired. As discussed by Schlatter and Taylor (1), Ru and Rh have a high selectivity toward N_2 formation but NH_3 is postulated as a reaction intermediate. Hence, NH_3 decomposition studies on these metals could be important to NO_x conversion. However, small amounts of O_2 tend to be detrimental to Ru catalysts, making the Rh catalysts most appealing for catalytic converters.

NH_3 is also important in the fuel cell industry, both as a fuel itself and as an efficient source of H_2. The latter requires the catalytic decomposition of NH_3, the subject of this dissertation. As NH_3 is supposedly an intermediate in the decomposition of hydrazine, N_2H_4, the study of its reaction may be relevant to the microrocket industry where N_2H_4 is used in the propellant mixture. Hence, it is clear that NH_3 is indeed a most important chemical.

The NH_3 synthesis/decomposition system is experimentally of great interest for several reasons. First, the NH_3 reactions comprise one of the few examples of a practical reversible chemical system. Under proper conditions of pressure and temperature, either the synthesis or decomposition reaction will dominate. The latter reaction is much

simpler to study experimentally due to the mild pressure conditions ($\leq$ 1 atm). Due to the microscopic reversibility principle, any information gained from a decomposition study should be useful in understanding the synthesis process.

Second, the system is chemically simple. The number of species is small, facilitating mathematical data interpretation, and the species are well-suited for instrumental quantitative analysis. Yet, the study of these reactions can provide generally useful information which can be applied to more complex catalytic systems.

Finally, even though the ammonia synthesis and decomposition reactions comprise basically a simple chemical system, a complete explanation of the reaction mechanism(s) has yet to be proposed. The NH_3 decomposition kinetics vary quite drastically from catalyst to catalyst and activation energies range from 20 to 140 kcal/mole as reported by Bond (2). With few exceptions, only a semiempirical explanation of the reaction kinetics has been developed. The most important questions to be asked are what are the surface intermediates, what do they "look" like, and how do they react to produce products? It is the purpose of this study to shed some new light on these and other questions concerning the NH_3 decomposition reaction.

This paper presents work done on the NH_3 decomposition reaction on clean, single crystal rhodium (Rh) catalysts. A

variety of surface chemical techniques was used to specifically characterize the catalytic reaction. The studies performed at pressures of less than 1 torr and in the temperature range of 273 to 723K aid in the development of a specific reaction mechanism for the NH_3 decomposition on Rh. Following a review of the pertinent literature, the experimental procedures and results and discussion will be presented. Then, the important conclusions of the study concerning both specific and general aspects of the NH_3 reaction on Rh will be given.

LITERATURE REVIEW

This review will consist mainly of three parts. First, the work done on the NH_3 synthesis reaction will be discussed followed by a presentation of a number of NH_3 decomposition studies on various metals. Finally, the often cited Temkin-Pyzhev theory for NH_3 reaction kinetics will be discussed. As the NH_3 reactions have been extensively reviewed in the literature, only the most important aspects of the studies will be mentioned here. This review will basically show that our understanding of the catalytic decomposition of NH_3 is still far from complete.

Ammonia Synthesis

The catalytic synthesis of ammonia was developed between 1908 and 1913 in Germany. The reaction has probably been studied more intensely in the last half century than any other. The subject of the NH_3 synthesis reaction has been thoroughly reviewed by a number of authors (2-9). Hence, only a summary concerning the important catalysts and processes involved will be presented.

The most effective (until recently) and best known NH_3 synthesis catalyst is a doubly promoted iron (Fe) catalyst:

$$Fe/Al_2O_3^*/K_2O^* \qquad (*\text{concentrations on the order of a few percent})$$

A process utilizing this type of catalyst was developed by Fritz Haber after the turn of the century for the Badische Anilin and Soda Fabrik (BASF) (3). Since that initial success, a variety of catalysts has been produced and studied.

The most active catalysts found in these early studies were Fe, Os, Re and the nitrides of Mo, W and U (6). The conditions leading to optimum rates and efficiencies were 200-300 atmospheres pressure, temperatures near 723K and an H_2/N_2 ratio of about 3:1. Conversions of nearly 30% are obtained under these conditions (6).

In the study of the NH_3 synthesis reaction, the important items investigated are: a) optimum reaction conditions, b) the effect of the various promoters used, and c) the kinetics and mechanisms of the synthesis reaction. The reaction conditions are controlled both by kinetics and thermodynamics. Thermodynamically, the reaction is more favored the lower the temperature, but it also proceeds more slowly. Hence, to obtain a reasonable conversion in a short period of time, a "compromise" temperature ($\sim$700K) is required. High pressures of N_2 and H_2 and low space velocities are also conducive to the NH_3 synthesis reaction.

The effect of promoters on the catalytic activity is also of interest. In general, most of the studies have been done with promoted Fe so that direct correlation to

industrial processes could be made. It appears, in theory (4), that the Al_2O_3 promoter has two important functions. First, it suppresses sintering of the Fe metal, leading to a reproducible and stable activity. Secondly, the slight "acidic" nature of the Al_2O_3 (H^+ from strongly adsorbed H_2O?) on singly promoted Fe appears to contribute to the formation of NH and/or NH_2 radicals. The addition of the alkali neutralizes this acidic character to produce a totally different reactive catalyst surface.

The effect of the K_2O is even more interesting than that of the Al_2O_3. In a number of papers co-authored by Ozaki (10-14), the effects of both Al_2O_3 and K_2O on the synthetic capabilities of an Fe catalyst were thoroughly studied. Their findings indicate that the alkali metal acts as an electron donor to the transition metal, increasing the electron density available to the impinging N_2 molecule. This type of electronic environment is conducive to dissociative N_2 adsorption (13). Consistent with this idea, a ruthenium catalyst promoted with Cs showed greater activity than one promoted with K (14); the ionization potential of cesium is much lower than that of potassium.

The most interesting feature of the NH_3 synthesis studies is the diversity of kinetic and mechanistic results and conclusions. Summaries of the kinetic results for Fe are adequately presented by several authors (2,6,9). In general,

the synthesis reaction is positive order in both N_2 and H_2 and inhibited by NH_3. Before 1940, no feasible theoretical explanation for the kinetics had been given. In 1940, Temkin and Pyzhev (15) developed a general theory, henceforth referred to as the T-P theory. The following assumptions are made in the theoretical development (2):

1) The adsorption of N as atoms is rate limiting and N atoms are the principal surface nitrogen species.
2) The activation energies for N adsorption and desorption vary linearly with increasing N coverage such that:

$$r_{ads} = k_a P_{N_2} \exp(-g\theta_N)$$

$$r_{des} = k_d \exp(h\theta_N)$$

where r_{ads} and r_{des} are the rates of adsorption and desorption of nitrogen, respectively, and θ_N is the surface coverage of $\dot{N}$ atoms.
3) θ_N is in equilibrium with P_{H_2} and P_{NH_3} (but not P_{N_2}).

The theoretical development continues and finally produces the famous equation as shown by Bond (2):

$$r_{synth} = k_1 P_{N_2} \left(\frac{P_{H_2}}{P_{NH_3}^2}\right)^{\alpha} - k_2 \left(\frac{P_{NH_3}^2}{P_{H_2}^3}\right)^{1-\alpha} \qquad (I\text{-}2)$$

where α equals g/g+h. This equation actually gives the rate of both the forward (decomposition) and reverse (synthesis) reactions depicted in equation I-1. It is seen that the first term (synthesis) of equation I-2 does indeed predict the proper trend in reaction orders. As will be discussed later, the second term of equation I-2 corresponds to the decomposition reaction.

Equation I-2 has been used extensively to explain kinetic results obtained in numerous laboratories. The parameter, α, is generally adjusted to fit the experimental data, which gives the theory considerable flexibility. Emmett and Kummer (16) showed that the T-P theory explained their synthesis results on doubly promoted Fe. Some years later, Temkin et al. (17) developed a more general equation which is to have more universal application than equation I-2. Other less used equations, which use most of the same assumptions as the T-P theory but different derivations, have been developed by Ozaki et al. (10), Brill (18) and Nielsen et al. (19).

The largest controversy in the NH_3 synthesis concerns the identification of the major surface species. Ozaki et al. (14) postulate that on pure and singly promoted Fe, N atoms are dominant while on doubly promoted Fe, an imino species (NH) was the most populous surface species (10). However, in discussing Ozaki's results, Emmett states that

their findings indicate the exact opposite conclusion (14). Logan and Philp (20) interpret the results of Ozaki et al. (10) as indicating that N is the predominant surface species on doubly promoted Fe. Clearly, there is much controversy concerning the adsorbed species in the synthesis reaction.

Even if nitrogen is assumed as the predominant surface species, one can find disagreement as to its adsorbed form. In general, atomic adsorption of N was assumed in all theoretical considerations. However, as discussed by Brill (18), there is increasing evidence that molecular nitrogen adsorption is important. Brill derived a kinetic expression assuming molecular N_2 adsorption, an analog to the expression derived by Ozaki et al. (10) assuming atomic adsorption. Surprisingly, both expressions fit the available data on Fe quite well! Carrá and Ugo (21) postulate a species called dehydrodiimide (N_2H) as the active intermediate as a means of explaining observed N_2 adsorption enhancement in the presence of H_2. The reaction scheme they postulate, however, predicts different pathways for NH_3 decomposition and synthesis. Concluding, the NH_3 synthesis reaction has many interesting aspects which could indirectly be studied via the decomposition reaction. It is quite evident that there is still much controversy in the interpretation of experimental NH_3 synthesis results over Fe.

Finally, there have been a few recent studies of interest concerning NH_3 synthesis on nonferrous metals. As mentioned earlier, Os, Re and several nitrides have been found to be active for the reaction. Though they have been somewhat ignored throughout the literature, several nonferrous group VIII metals are known to be excellent synthesis catalysts. Ozaki et al. (22) initially indicated that K promoted Rh on charcoal was very inactive for the synthesis reaction. However, upon reexamination (23), an activity equal to a doubly promoted Fe catalyst was observed for Rh. They also found that both promoted Ru and Os were nearly an order of magnitude higher in activity than the standard iron catalyst. Though cost prohibits wide spread use of promoted catalysts like Rh, Os or Ru, information gained from the study of the synthesis reaction over these catalysts could be useful for improving commerical processes now in use. The behavior of the promoted Rh catalyst will be correlated with the results and conclusions of the NH_3 decomposition studies presented in this dissertation.

Ammonia Decomposition

The decomposition reaction has been investigated over a number of different types of catalysts, from doubly promoted catalysts to metal single crystals. Though many authors have reviewed the subject, Bond (2) presents the most

comprehensive summary of the results up to 1962. Since that time, numerous studies have been reported; some will be discussed in this review. Supported catalysts, in general, were used in most of the earlier studies. However, with the advent of ultra-high vacuum technology, it was possible to study the decomposition reaction on "clean", well-defined surfaces. In the following discussion, the pertinent and sometimes controversial results obtained and concepts postulated are presented. It will be clear that a more thorough understanding of the specific surface reactions involved in the NH_3 decomposition is needed.

As Fe is the most important NH_3 synthesis catalyst, it has been extensively used in studies of the "sister" reaction: NH_3 decomposition. Love and Emmett (24) reported results on doubly promoted Fe which correlated with the T-P theory. The rate law determined was of the form:

$$-\frac{dNH_3}{dt} \propto \frac{(NH_3)^{.6}}{(H_2)^{.9}} \qquad \text{(I-3)}$$

where the value of α for the second part of equation I-2 (decomposition) was chosen as .7. However, on Al_2O_3 promoted Fe, the kinetics were inverted under certain conditions:

$$-\frac{dNH_3}{dt} \propto \frac{(H_2)^{1.2}}{(NH_3)^{.8}} \qquad \text{(I-4)}$$

The authors cautiously postulated that in this case, the rate limiting step may not be N_2 desorption.

Logan et al. (25) produced an explanation for the above phenomena. They obtained similar results on Fe films. It appears that under certain conditions, an Fe nitride (Fe_4N) is formed and this layer inhibits N_2 desorption until the layer itself decomposes at high temperatures. They claim that this layer may produce the anomalous kinetics observed. By making certain assumptions, Logan et al. predict reaction orders very close to the inversion kinetics observed. This theoretical development was all within the bounds of the T-P theory such that there should be no rate limiting step change. Löffler and Schmidt (26) also observed a positive order in H_2. Their belief is that H_2 reduces the surface nitride to reactive clean Fe metal at high pressures. They fit their pure NH_3 data to a Langmuir-Hinshelwood expression thus avoiding the T-P theory. They were unable to develop a mechanism consistent with their results.

There has been some controversy concerning the rate limiting step of the NH_3 decomposition reaction on Fe. Takezawa and Toyoshima (27) indicated that at low temperatures, N_2 desorption was rate limiting while at high temperatures, the dehydrogenation of an NH_x ($1 \leq x \leq 3$) species limited the reaction rate.

A determination of the stoichiometry number for the reaction (as discussed by Emmett (9)) can help determine which step is rate limiting. As discussed by Kazusaka (28),

the stoichiometry number for the NH_3 decomposition reaction on Fe was determined as 2 by Enomoto *et al.* (29), indicating a dehydrogenation step as rate limiting. Kazusaka states that he and numerous other workers determined the stoichiometry number as 1; *i.e.*, N_2 desorption is rate limiting. Hence, a definite controversy exists in the Fe-NH_3 decomposition system. Sources of this controversy may be varying extents of surface nitridation and different forms of the catalysts.

In general, the only transition metals which readily form stable nitrides (with a few exceptions) are the body centered cubic elements (30). It appears that those metals forming "quasi-stable" nitrides are relatively active for the NH_3 reactions (4). So, Fe, W and Mo are considered reasonably good decomposition catalysts. Some reported studies on the latter two metals will now be discussed.

In recent years, tungsten (W) has been extremely popular as an NH_3 decomposition catalyst. Examples of work performed since 1965 include papers co-authored by Hansen (31-35) and investigations from Dawson's laboratories (36-40). The consensus is that the decomposition takes place on a surface nitride layer. Surface intermediates of the form $W_2N_2H_2$ (32), W_2N_3H (37) and $W_2N_3H_2$ (35) have been postulated, the latter two seemingly the most reasonable.

McAllister and Hansen (35) postulated one of the few specific mechanisms for NH_3 decomposition. They propose a "rate limiting step" which consists of the concurrent decomposition of $W_2N_3H_2$ and WNH, producing the two-thirds order in NH_3 as observed experimentally. The decomposition of the surface nitride (WN) also contributes to the overall rate of N_2 production. Even though the stoichiometry of the surface intermediates are given, no specific surface structures are postulated. An isotope effect of about 1.5 was observed on the W(111) face (35) and was interpreted as indicating the rate limiting step includes the breaking of an N-H bond (35,38).

However, Sheets and Blyholder (41) attribute the above isotope effect to what is called a β-secondary isotope effect. This would be compatible with N_2 desorption being rate limiting in the NH_3 decomposition reaction. Dawson and Peng (38) argue strongly against the interpretation of Sheets and Blyholder, and conclude emphatically from their results that N_2 desorption is not rate limiting. The studies discussed above on W were generally done in ambient pressures less than 10 torr; quite near the experimental conditions of this study on Rh. Generally, most kinetic studies reported have been at pressures much greater than 1 torr.

Molybdenum, also a nitriding metal, has also been studied quite extensively for the ammonia reactions. As discussed by Matsushita and Hansen (42), Mo behaves very similarly to W in both kinetics and surface structure. Abon et al. (43) reported that their field emission studies on Mo predict that the Mo(100) plane should be the most active for the NH_3 decomposition reaction. This is in marked contrast to the findings on W single crystal catalysts (35). They further claim that NH_3 will preferentially adsorb on the Mo(110); the opposite conclusion obtained on W(110) where NH_3 and N_2 do not adsorb very well at all (44). There is obviously some controversy remaining in the study of Mo.

From the discussion given above, it seems that the processes involved in the decomposition of NH_3 on nitriding metals are relatively complex. The involvement of the surface nitride in the intermediate formation can present problems if under the conditions studied, the nitride is not fully developed. In some cases, for example NH_3 decomposition on vanadium nitride (VN) (45), the kinetics are quite similar to those observed in this and other studies on nonnitriding metals. By studying the decomposition reaction on transition metals not forming stable bulk nitrides, a simpler basis for mechanistic interpretation should be established.

Though most hcp and fcc metals do not form any type of bulk nitrides (30), several of them are quite active for the NH_3 decomposition reaction (2) and the synthesis reaction (22). Only in the past few decades has interest sufficed to spawn studies of the NH_3 decomposition reaction on these metals, including comprehensive studies by Logan and Kemball (46) and Sokol'skii et al. (47). The former group found the following reactivity series for the decomposition reaction on films at 673K:

Ru>Fe, Co>Ni, Rh>Re>Pt

On supported metals, Sokol'skii et al. observed a different reactivity trend at 673K:

Ru>Os>Rh>Ir>Ni>Co>Pt>Pd>Fe

The reaction conditions on the films (46) included a large excess of H_2 while only pure NH_3 was used with the supported catalysts (47). The discrepancies are quite dramatic and will be discussed in conjunction with the results of this study. Of the metals mentioned above, Ni, Pt and Ru will be discussed as examples due to either their high reactivity or large number of studies reported. Then the work done with Rh as an ammonia decomposition catalyst will be examined.

Although Ni can form a stable metal-rich nitride under certain conditions (30), the metal itself appears to be the

catalytic species for the ammonia decomposition reaction (2,4). The reaction obeys T-P kinetics with NH_3 and H_2 orders of .96 and -1.53, respectively, on Ni films between 573 and 773K (46). Tamaru et al. (48) support these findings on a supported Ni catalyst at lower temperatures. The major surface species was postulated as NH_2 in the latter study.

Mardaleishvili, Sin-Chou and Smorodinskaya (49,50) observed different kinetics on supported Ni at $T \geq 723K$ and pressures less than 130 torr. Their results indicate an H_2 order of -1.0 rather than -1.5. Also, the NH_3 order decreases from 1.0 to .50 at low H_2 pressures, a trend observed in this study on Rh. A very simple mechanism with NH_2 surface species is postulated. Friedlander et al. (51) also observed a -1.0 H_2 order on supported Ni in the presence of H_2O vapor. Via mathematical manipulation, they show that the revised T-P equation (17) predicts this H_2 order at low pressures. There is an obvious controversy concerning the H_2 order on Ni; this is also the case on other nonnitriding metals.

The NH_3 decomposition reaction on Pt has been studied quite extensively as summarized by Mardaleishvili et al. (up through 1965) (49). Robertson and Willhoft (52) determined an H_2 order of -.25 on a Pt filament at very low pressure. They postulate the formation of a surface nitride

which has no precedence in the literature at the pressures of interest. Sokol'skii et al. (47) found Pt to be over 150 times less active than Ru with an NH_3 order of +1.0

The most comprehensive kinetic studies to date on Pt were done by Löffler and Schmidt (53,54). These experiments were done over Pt wires (53) and Pt single crystals (54) over a wide temperature ($600 \leq T \leq 1400K$) and pressure ($10^{-2} \leq P \leq 1$ torr) range. These conditions are very close to those in the experiments reported here.

Löffler and Schmidt found that their steady state flow reaction kinetics could be fit to a Langmuir-Hinshelwood unimolecular rate expression (53):

$$r_R = \frac{k_R K_{NH_3} P_{NH_3}}{1 + K_{NH_3} P_{NH_3} + K_H P_{H_2}^{3/2} + K_N P_{N_2}} \qquad (I\text{-}5)$$

This expression fit all of their data under all conditions generally within 20%. At low temperatures, the NH_3 order approached zero at high P_{NH_3} ($P_{H_2} = 0$) as is predicted. The inhibiting effect of N_2 is very slight and the H_2 order is -1.5 at high P_{H_2}. The kinetics observed "fit" the T-P theory but the authors tend to avoid correlation to the semiempirical T-P expression.

A large face specificity for the decomposition reaction was observed (54) with the least densely packed faces being most reactive (i.e., 210, 110). This agrees with the

results of McAllister and Hansen on W single crystals discussed earlier (35).

The studies on Pt provide an opportunity to compare absolute reaction rates determined in different laboratories under reasonably similar conditions. As shown by Bond (2), the activity of the Pt film prepared by Logan and Kemball (46) was about 10^8 molecules cm^{-2} sec^{-1} at 673K in a highly H_2 inhibited gas mixture (6:1 H_2/NH_3). Applying these conditions to Löffler and Schmidt's expression (equation I-5), a rate of about 4×10^{12} molecules cm^{-2} sec^{-1} is calculated, over four orders of magnitude higher than the film results! The results of this dissertation indicate that the same type of discrepancy exists for Rh. The apparently anomalous rates observed by Logan and Kemball will be analyzed in detail in the Results and Discussion section.

Ruthenium, as mentioned previously, is the most active NH_3 decomposition catalyst studied to date (46,47). In an early study, Amano and Taylor (55) found that Ru was more active than Rh or Pd; Friedlander et al. (56) observed that it was more active than Ni or Pd. Reaction orders determined vary from .6 and -.9 for NH_3 and H_2, respectively (55), to +1.2 and -2.0 (46). Therefore, it is evident that the kinetics on Ru need to be fully resolved and analyzed.

Finally, there have been very few studies in the literature using Rh as an NH_3 decomposition catalyst. The study of

Amano and Taylor (55) appears to be the earliest investigation. The temperature range of their study (633-723K) was nearly identical to that reported in this dissertation. Over a supported Rh catalyst, an activation energy of 25 kcal/mole in pure NH_3 was obtained and the energy increased with increasing H_2 pressure. An approximate H_2 order of -1.0 can be extracted from figure 1 of their publication. However, the lack of quantitative data and the small quantity of experimental results allow only qualitative comparisons to be made.

The study of Logan and Kemball (46) provides an interesting controversy concerning the NH_3 decomposition reaction on Rh. First, they state that Rh films have about the same activity as Co and Ni and are much less active than Fe. This trend has not been observed before and is questionable. For a 6:1 N_2-to-NH_3 mixture, Logan and Kemball report an activation energy of 57 kcal/mole in the temperature region of 593 to 773K, quite high relative to other results (47,55). The most startling results are NH_3 and H_2 orders of +1.35 and -2.45, respectively! These results are almost unprecedented in studies of NH_3 decomposition on metal catalysts. No mechanistic arguments concerning these kinetics are given. Later in this dissertation, these results will be further compared with results on Rh single crystal catalysts.

Experiments done by Pignet and Schmidt (57) provide a direct means of comparing their findings with results reported here. Part of their work concerned NH_3 decomposition on Pd, Rh and Pt wires and the results are displayed in figure 1 of their paper. An approximation of the decomposition rate on Rh at conditions used in this single crystal study can be made for comparison. The results will be of interest in light of the Logan-Kemball controversy mentioned earlier.

Finally, Sokol'skii's group (47) used supported Rh as a decomposition catalyst in its survey study. Only Ru and Os (both hcp packing) were determined to be more active than Rh. The Russian group reported only NH_3 orders which were stated as being "virtually first order" for all metals studied. As to the true meaning of "virtually", one can only speculate. An activation energy of 20.8 kcal/mole was reported with pure NH_3 only. As before, no mechanistic arguments were presented though some correlations with physical properties were attempted. The above mentioned investigations are the only direct investigations of the NH_3 decomposition reaction on pure Rh catalysts.

Numerous other reactions have been studied on Rh catalysts. A few examples are the decomposition of hydrazine (58,59), NO reduction reactions (60,61,62,1) and CO-CO_2 interactions with O_2 and H_2 (63,64). There have been

a number of studies done on Rh single crystals which are relevant to this thesis. These will be discussed when appropriate.

Limitations of Temkin-Pyzhev Theory

The literature review shows that the T-P theory has provided the interpretive basis for a large part of published work on ammonia synthesis and decomposition, and has also pointed out that this stems in large part from its empirical flexibility. Yet, several of the assumptions underlying this theory are open to serious questions and objections.

First, it is indeed not clear that the adsorption (or desorption) of N_2 is the rate limiting reaction. The isotope effects observed generally do not correlate with this assumption. Also, as presented above, the possibility exists that NH species (10) are the major surface constituent in some cases. It appears that different surface species may be present under different reaction conditions; the T-P theory does not include this possibility.

The coverage of nitrogen, θ_N, on the catalyst surface is assumed to be in equilibrium with both H_2 and NH_3 according to the T-P theory. This implies that at high P_{H_2} the coverage of N should be small. However, as discussed by Bond (2), there are several instances where H_2 enhances N_2 exchange and adsorption. This phenomenon is not implied in the T-P theory

and yet it may well be very important to the overall kinetics of the processes involved.

The linear variation of the heat of adsorption of N_2 with coverage is not universal for all metals. As discussed by Hansen and Mimeault (65), ΔH_{ads} for N on W is nearly independent of coverage. In general, one would expect a linear dependence in ΔH_{ads} if the adsorbed phase was immobile and the adatom-adatom interactions were minimal (66). This may indeed be the case at very low temperatures where the activation energy for surface diffusion is much greater than kT. However, at NH_3 reaction temperatures (500-800K), nitrogen should be quite mobile on most metal surfaces. Miller (66) has shown that the heat of adsorption for a mobile layer changes very nonlinearly with coverage. If strong adatom-adatom interactions are also included (as is probably the case for N), even larger deviations result. Hence, the T-P theory assumption of a linear variation of ΔH_{ads} with N coverage should be valid only over a very narrow range in θ_N. As the amounts of N_2 adsorbed on transition metals vary drastically from metal to metal, the universal validity of the assumption is not substantiated. This assumption, however, is very important to the Temkin-Pyzhev theoretical development and hence raises doubts as to the theory's applicability to all NH_3 reaction systems.

Furthermore, the rate constant, k_1, in equation I-2 should be independent of space velocity, H_2/N_2 ratio and the total pressure. According to Bond (2), the constant does tend to vary with the H_2/N_2 ratio on Fe catalysts. Also, the Temkin isotherm, which is used in the Temkin-Pyzhev derivation, is valid only in the intermediate coverage range as it does not predict $\theta=0$ for $P=0$ and $\theta=1$ for large values of P. Both of these facts tend further to show the limited applicability of the Temkin-Pyzhev theory to the NH_3 reactions.

It is clear from the literature that the T-P equation fits kinetics in the NH_3 synthesis/decomposition system over doubly promoted Fe catalysts. As discussed by Emmett (9), the value of α in the T-P equation has been independently determined from N_2 adsorption studies and correlates very well with the NH_3 decomposition value of $\sim.3$ (24). However, this type of independent determination is clearly necessary for other metals also if the choice of α is to be more than empirical. It may be possible to adjust enough parameters and make enough assumptions to cause the T-P theory to fit observed data but the physical validity of the fit must definitely be questioned without corroborating evidence.

From the above comments, it is clear that each catalytic system should be treated separately to incorporate the

varying conditions such as surface structure and stoichiometry, reactive intermediates, adsorption-desorption properties, etc. This is clearly the case for NH_3 decomposition on W (35), where the kinetics are drastically different from those predicted by the T-P theory. In this study of NH_3 decomposition on Rh, a specific mechanism and rate law with few assumptions are developed with all intermediates specified. There is no proof of applicability to other metal catalysts but the generalities (and hence inherent arbitrariness) of the T-P theory are avoided.

One of the reasons for choosing the rhodium system for study was the obvious disparity of the NH_3 decomposition results reported in the literature. The wide variation in reaction orders and activation energy reported indicates a need for more definitive experimental work. None of the four Rh-NH_3 studies cited (46,47,55,57) presents any mechanistic arguments whatsoever. No isotope studies (useful in predicting the rate limiting step of the reaction) have been reported for Rh. The complete characterization of the reactive surface and intermediates has received no emphasis in the literature. The work reported here will at least partially fill the void which obviously exists in the study of the decomposition of NH_3 on Rh and other catalysts. By using well-defined single crystal Rh catalysts in conjunction with a variety of catalytic techniques, a

complete characterization of the NH_3/Rh system can be attempted.

EXPERIMENTAL

Several different experiments were performed to characterize the NH_3 decomposition reaction on single crystal Rh. Most of the work was devoted to establishing steady state kinetics of the reaction over Rh(110), (100) and (111) single crystals. Other experiments included flash desorption spectroscopy, structure symmetry determinations by LEED, and surface composition analysis by Auger spectroscopy. The various procedures used in these experiments will be presented in detail.

Vacuum System Design

The schematic of the ultra-high vacuum system used in the kinetic and flash desorption experiments is shown in Figure I-1. The system was fabricated almost entirely of Pyrex glass, sections being interconnected by ultra-high vacuum valves. Pressure measuring devices included Bayard-Alpert ionization gauges, a differential capacitance manometer and a quadrupole mass spectrometer. The apparatus consisted basically of a high pressure (to 1 torr) section (shaded area, Figure I-1) and an ultra-high vacuum mass spectrometer chamber. The entire system was bakeable to 673K and pumped to a minimum pressure of 2×10^{-10} torr.

The ultra-high vacuum pumps consisted of a three-stage mercury diffusion pump in series with a two-stage pump; two

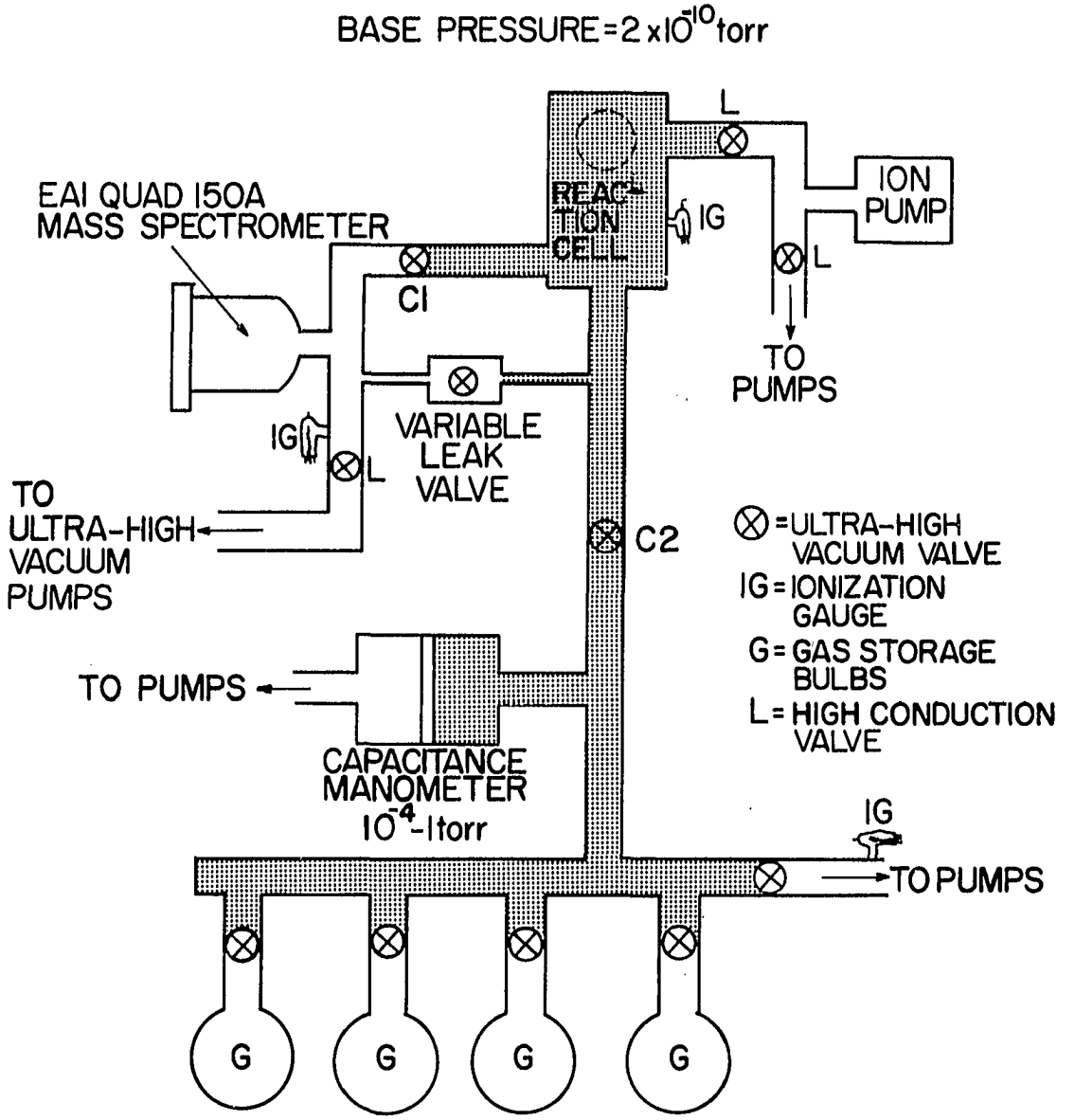

Figure I-1. Schematic of ultra-high vacuum system used in kinetics and flash desorption experiments. (Shaded area = reaction volume ≅ 1.1 ℓ)

liquid nitrogen (ℓ-N_2) traps were between the mass spectrometer chamber and the Hg pumps. The gas handling manifold and ion pump (during bakeout) were pumped by two, two-stage Hg pumps in series with a ℓ-N_2 trap. The reference side of the capacitance manometer was maintained at $\sim 10^{-7}$ torr with a single two-stage Hg pump and a ℓ-N_2 trap. A 20 ℓ/sec differential ion pump (Ultek, Model #202-2000) was used to pump the reaction cell during sample outgassing. In general, valve C1 remained closed to keep the background pressure in the mass spectrometer chamber as low as possible. The reaction cell pressure was reduced to 10^{-7} torr within 1 hour, after a series of kinetic runs, using the ion pump.

The variable leak valve (Granville Phillips, Series 203) shown in Figure I-1 was used to control the flow of reactants and products into the mass spectrometer chamber. By properly adjusting this valve, the pressure could be reduced by a factor of 10^6 between the reaction cell and mass spectrometer. The size of the leak was such that a negligible fraction of the reactants was "lost" during a typical experiment.

The capacitance manometer (Granville Phillips, Series 212) was used to measure the reactant and product pressures in the reaction volume. The pressure range of the instrument was approximately 0.1 to 1000 microns (μ), i.e., 10^{-4} to 1 torr. The capacitance manometer head was thermostatted via a constant temperature water jacket to alleviate large zero drifts due to room temperature variations.

The manometer was calibrated against a McLeod gauge (Consolidated Vacuum Corp., Rochester, N.Y.) using argon (Ar). The pressure changes were indicated by a meter deflection on the manometer control unit. There were five separate pressure ranges with full scale values of approximately 10, 30, 100, 300 and 1000 μ. Although the calibration data were approximately linear, they fit very well to a power formula of the form:

$$\text{Pressure } (\mu) = A\ (\text{Scale Deflection})^{b} \quad (.96 \leq b \leq 1.10) \qquad (I\text{-}6)$$

the parameters for which were determined for each scale and used in the kinetic data analysis. The calibration was checked several times over a period of months with a variation of 10% or less observed.

The mass spectrometer was an EAI model QUAD 150A which was rebuilt and modified by the R. M. Jordan Co., Mountain View, CA. The operating range of the instrument was 10^{-11} to 10^{-5} torr with the usual experimental pressure region being 10^{-7} torr or less. All of the reactants and products encountered were in the range of 1-30 a.m.u , a region which was displayed every 2.5 seconds on a two-channel, time-drive strip chart recorder (Brush Instruments, model MARK 780). Rapid scans for leak testing, etc., were displayed on an oscilloscope (Tektronix, Inc., type R.M. 503).

Sample Preparation

The Rh single crystal samples were cut from a single crystal quarter-inch rod from Materials Research Corporation. Back reflectance Laue x-ray diffraction was used to determine the crystal orientations after which several (110), (100) and (111) discs were spark cut. The discs were mechanically polished, the final polish using .03 μ particle size Linde B alumina. The disc orientations were within ∿1.0° of those desired following this preparation procedure. Figure I-2 shows the ideal surface atom arrangements for the three crystal faces used in this study. The sample crystals, in general, were disc-like with a diameter of ∿7 mm and ∿.6 mm thick. The edge areas were ∿10% of the total surface areas. The approximate surface areas of the (110), (100) and (111) crystal faces are .70, .63 and .78 cm^2, respectively.

Following the kinetic experiments, several Rh samples were analyzed *via* ESCA, atomic emission spectroscopy and Auger electron spectroscopy. The results showed a Pt impurity in the samples in a concentration of a few atom %. The effect of this impurity was considered negligible as according to Sokol'skii *et al.* (47), Pt is approximately 1/20th as active for the NH_3 decomposition reaction as Rh. Therefore, the rates determined should not vary from those of pure Rh by more than the experimental error in these studies.

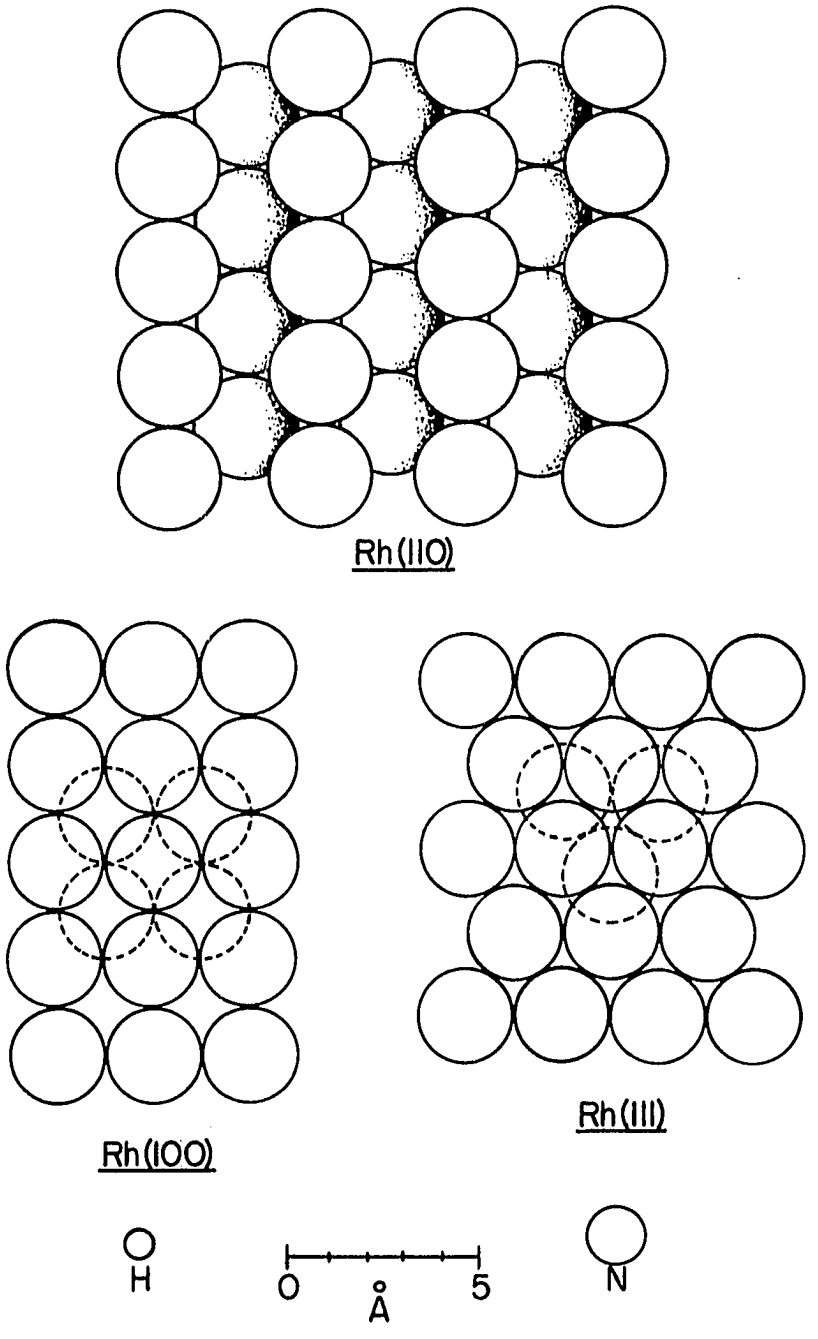

Figure I-2. Surface atom arrangement for the Rh single crystal catalysts used in the kinetic experiments. N, H diameters are included for comparison. (Dotted circles = atoms in next layer down; Rh(110) row atoms have a nearest neighbor directly "below" them)

The Rh single crystal samples were mounted in the reaction vessel as shown in Figure I-3. The crystals were spotwelded to a 10 mil (.254 mm) support wire which in turn was welded to a 45 mil (1.14 mm) rod for stability. This arrangement was then attached to a 4-lead dewar and glass blown to the cell. The thermocouple wires spotwelded to the crystals were 3 mil (.08 mm) W/5% Re, W/26% Re (Hoskins Manf. Co., Detroit).

The Rh crystal faces were heated *in vacuo via* electron bombardment using a thoria-coated iridium filament as an electron source. By applying a +400 volt d.c. potential to the sample and heating the filament to obtain a suitable emission, the samples could be heated to 1500K.

Producing what appeared to be a clean Rh surface was very difficult. The common procedure for cleaning Rh surfaces involves the sequence of heating *in vacuo* to 1500K, heating in 10^{-7} torr O_2, argon bombardment, and annealing (63,67,68). When the Rh(110) sample was initially cycled through a sequence of heating to 1400K for extended periods, O_2 cleaning (10^{-7} torr, 970K, 5 min) and argon bombardment (300 eV, 10 μamps, 5 min) with annealing, its activity toward NH_3 decomposition was at first very low and erratic. Between experiments, the crystal was flashed to 1400K and maintained at 900K until the next "cleaning" cycle. Over a long period of time, the activity of the (110) sample increased steadily,

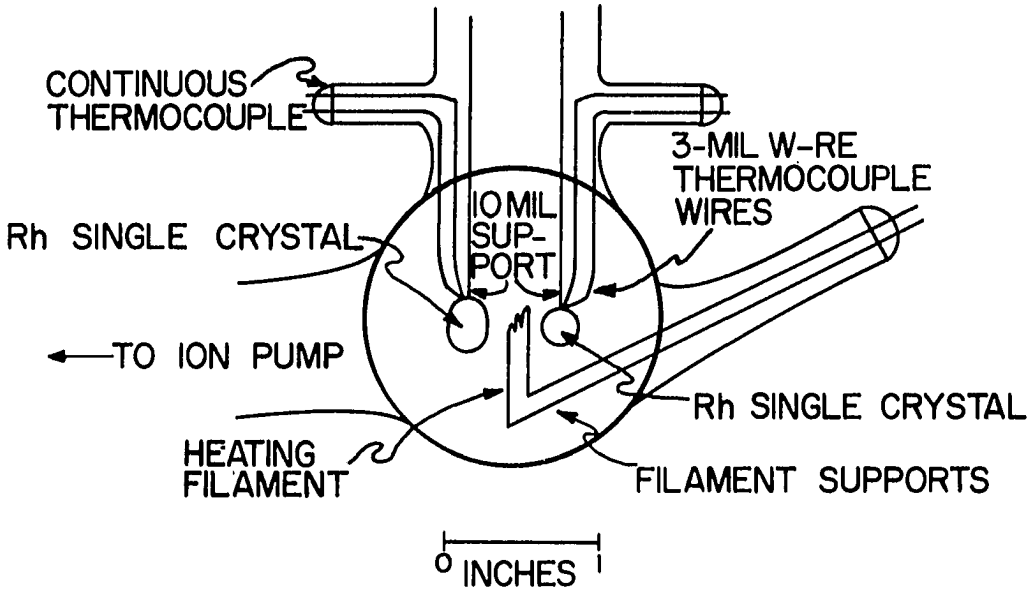

Figure I-3. Reaction cell design

with the absolute rates of N_2 production being very irreproducible; the reaction orders remained constant, however. After numerous cleaning cycles over an extended period of time, the Rh surface finally exhibited high, constant activity for the duration of the kinetic experiments. Catalytic activity was maintained (within 15%) merely by flashing the crystal to 1400K and maintaining at ∿900K between series of experiments. Occasional O_2 cleaning had no effect on the NH_3 decomposition activity.

Grant and Haas (69) could clean their Rh sample by heating to ∿1600K for a few minutes. Tucker (70,71), using the same procedure, obtained "clean" LEED patterns of Rh single crystals. Marbrow and Lambert (72) seem to indicate that heating to 1300K in vacuo for long periods of time plus an O_2 treatment is sufficient to remove C, O, S and B from Rh surfaces. This procedure is clearly not sufficient to produce clean surfaces using the samples in this study.

As will be discussed in the LEED/Auger section, the major surface contaminant of the Rh samples was boron (B). Only by numerous Ar^+ bombardments and O_2 cleaning cycles could the B be substantially removed. This observation explains the initial low activity of the Rh(110) surface; B was poisoning the surface to NH_3 adsorption. Over the extended cleaning period, the B was depleted from the bulk, leaving a clean surface which could be regenerated by mild heating alone. Both the Rh(111) and (100) faces used in

these studies were bombarded and O_2 cleaned extensively before they were mounted in the vacuum system for this study. Auger and XPS analysis of the Rh(110) and (100) faces indicated that no detectable B was present. Furthermore, a Rh(100) sample which had only been heated to 1400K *in vacuo* showed almost no activity for the NH_3 decomposition. Therefore, the treatment of the Rh crystals discussed above was sufficient to produce clean surfaces whose catalytic activity was reproducible.

Kinetics Procedure

During a kinetic and/or flash desorption experiment, the catalyst was heated by focusing light from a 1200 watt projector bulb onto the single crystal of interest. The heating arrangement is shown in Figure I-4. A maximum crystal temperature of ∿1070K was obtained *in vacuo* using this procedure. The heating capabilities were substantially reduced upon admission of the reactant gases, especially H_2.

A solid state constant temperature controller (Ames Lab electronics service group) was used to maintain the catalyst temperature at a preset value. The controller monitored the thermocouple e.m.f. and adjusted the bulb voltage to keep the thermocouple reading constant. The temperature varied by ±3K during an experiment.

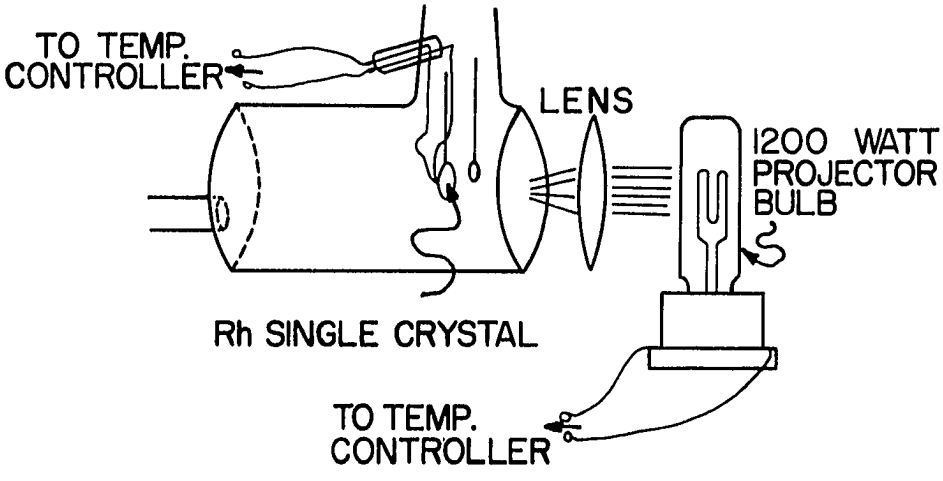

Figure I-4. Crystal heating arrangement. (Catalysts could be cooled to 250K with a Dry Ice, acetone slurry in the cell dewar).

To prepare for a kinetic experiment, the catalyst was cooled in vacuo to ~550K. The reaction cell walls were saturated with an initial dose of NH_3; the catalyst was maintained between 600-750K. During this period, the leak valve (Figure I-1) was adjusted to produce readily detectable N_2 and H_2 signals on the mass spectrometer output; the valve was then not adjusted again.

There were three types of reaction mixtures which were dosed into the reaction cell. These were pure NH_3 (or ND_3 for isotope studies), NH_3/H_2 mixtures and NH_3/N_2 mixtures. Whenever possible, N_2 production was monitored as its mass spectrometer signal was most stable and reproducible. In the pure NH_3 case, the ratio of H_2 production rate to N_2 rate was within 15% of the stoichiometric 3:1 value in all cases.

A typical kinetic experiment using only pure NH_3 involved dosing a known pressure of NH_3 into the entire reaction cell with the catalyst at reaction temperature, monitoring product production for $\leq$ 100 seconds, and then pumping the cell to less than 10^{-4} torr for the next experiment. Identical rates (within 10%) were observed if the NH_3 was "predosed" in the manifold and then into the reaction cell or NH_3 was dosed into the cell with the catalyst at less than 573K and the temperature then raised after several minutes. Hence, the NH_3 doses equilibrated with the walls and the manometer within 5 seconds in most cases.

The NH_3/H_2 and NH_3/N_2 mixtures were always prepared in the manifold and then dosed through valve C2 into the reaction cell. During these experiments, several runs were made at different pressures of pure NH_3 to correlate absolute rates from day to day. The importance of this will be made clear in the Results and Discussion section.

There were several limitations placed on the reaction conditions for the kinetic studies. First, the temperature region was limited at the low end by low reactivity and at the high end by high percent NH_3 conversion (>10%) over the reaction time period as the reaction system is basically a static reactor. The temperature limits for the Rh(110) crystal (the one used in most of the experiments) were 573 to 698K.

The pressure limitations were set by two factors. Due to the thermal conductivity of the gas, a temperature between 633 and 673K could be maintained only if the NH_3 pressure was < 500 μ. The maximum H_2 pressure usable was about 150 μ for this reason also. Secondly, the pressure of NH_3 had to be limited to avoid decomposition in the mass spectrometer chamber. Normally, with P_{NH_3} < 150 μ, the NH_3 took several minutes to diffuse appreciably through the leak valve. At very high NH_3 pressures, the "mass spectrometer" decomposition interfered with the detection of the Rh-NH_3 decomposition products.

The absolute rates of product formation (μ/min) were obtained by calibrating the mass spectrometer output against the capacitance manometer; the N_2 or H_2 mass spectrometer peak heights varied linearly with pressure up to 20 μ. The presence of varying amounts of background gases decreased the detected product sensitivity (example: sensitivity = μ N_2 in cell/mv(m/e = 28) on recorder). This phenomenon is due to pressure dependent flow through the leak valve into the mass spectrometer chamber. This sensitivity change has been seen previously and is discussed by Masterson (73). The N_2 sensitivity was reduced by 10% at about 50-60 μ total pressure and decreased to a maximum correction of ∿25% at very high pressures.

The system volume was required for conversion of the "experimental" rates (i.e., μ N_2 min^{-1}) to structurally sensitive rates (molec N_2 cm^{-2} sec^{-1}). The volumes were determined via Ar expansion, using the capacitance manometer. The manifold volume (Figure I-1, shaded area "below" valve C2) was 0.28 ℓ; the reaction cell volume was 0.82 ℓ, giving a total reaction volume of 1.1 ℓ.

The NH_3 decomposition reaction did not occur in the gas phase as moving the focused light beam slightly from the crystal "stopped" all catalytic activity. The heating filament was active only when the direct light struck it, which never occurred during the kinetic experiments.

The following outline is given as a summary of the types of kinetic experiments to be reported and analyzed in subsequent sections:

1) Pure NH_3 decomposition ($1 \leq P_{NH_3} \leq 500$ μ).
   a) Gives NH_3 order with initial $P_{H_2} = P_{N_2} = 0$.
2) NH_3/H_2 mixture studies ($P_{TOT} \leq 150$ μ in general).
   a) H_2 order determination at constant P_{NH_3}.
   b) NH_3 order determination at constant P_{H_2}.
3) NH_3/N_2 mixture studies ($P_{TOT} \leq 250$ μ).
   a) N_2 order at constant P_{NH_3}.
4) Comparison of pure NH_3 and ND_3 decomposition rates.
   a) Determination of isotope effect.

Flash Desorption Procedure

Three types of flash desorption experiments were performed using the Rh(110) crystal face. These were H_2 desorption (H_2 dose), N_2 desorption (N_2 dose) and H_2/N_2 desorption (NH_3 dose). The basic flash desorption experiment proceeds as follows:

1) Clean Rh(110) sample and cool to 253K <u>via</u> a Dry Ice-acetone slurry in cell dewar.
2) Dose a known amount of gas; doses usually expressed in terms of langmuir (L), $1L = 10^{-6}$ torr sec.
3) Increase the crystal temperature at ∿8K/sec with the focused light beam while continually pumping.

Temperature region flashed is 253K to 1000K at most.

4) Observe desorption peaks on both ionization gauge and mass spectrometer outputs.

By observing the shifts and temperatures of the peak maxima, qualitative information concerning order of desorption and strength of binding can be obtained.

The NH_3 flash desorption experiments required some modifications of the above procedure. During dosing, the cell ion gauge was off to prevent large scale decomposition of the NH_3. Only the ion pump current was used as a qualitative indication of the dose. Therefore, the only means of detecting the desorption peaks was the mass spectrometer. The peaks indicated by the mass spectrometer were generally slightly broader than those obtained from the cell ion gauge due to the low conductance C-valve (C1, Figure I-1). The temperatures of the maxima were the same, however. Furthermore, once NH_3 had been dosed, the NH_3 ambient never decreased much below 10^{-8} torr so that the sample was "redosed" by simply cooling to 253K after a flash experiment. Hence, one initial dose provided sufficient background pressure for several flash desorption experiments in succession. It is clear that the absolute dose of NH_3 could not be determined in this system.

It is known that N_2 generally does not adsorb on the fcc Group VIII metals (2). Therefore, a means of activating

N absorption on Rh is required. The procedure of Matsushita and Hansen (74) was used in an attempt to activate nitrogen adsorption using electron impact. The thoria-coated iridium filament was used as the electron source and the Rh(100) crystal as the "grid" (+200 v d.c.) and $P_{N_2} \sim 10^{-6}$ torr to adsorb N on the Rh(110) crystal face.

LEED/Auger Procedure

LEED (Low Energy Electron Diffraction) is useful for surface analysis because it provides information concerning the order and symmetry of a surface structure. Auger election spectroscopy (AES) establishes what species are present on the surface in a given experiment. Hence, information obtained by these techniques can be used to infer the condition of the surface under reaction conditions.

The LEED/AES experiments were performed in a Varian 981-2000 vacuum system with 4-grid LEED optics and Auger arrangement with a cylindrical mirror analyzer (base pressure = 2×10^{-10} torr). The Auger experiments were generally run at 10 μ amps beam current, 2.0 KeV beam energy, 100-1100 eV scan width (3.3 eV/sec), 10 volts peak to peak modulation. Ordered LEED patterns were observed at 78 eV and 144 eV. A polished Rh(110) crystal (with 1.5° of proper orientation) was mounted on the offset manipulator and a W/5% Re,W/26% Re thermocouple spotwelded to the exposed face.

The sample was heated by an indirect heater block; the maximum temperature was 1600K.

The crystal was initially outgassed to 1400K and Auger analysis showed P, S and B as major contaminants. Repeated Ar^+ bombardment (1000 eV, 1 μ amp) and O_2 cleaning (1×10^{-6} torr, 700-1300K) completely removed the P and S but the B kept segregating to the surface upon cooling from 1300K. Over a period of days, the B concentration was reduced substantially but not totally. Any C or O present could be removed by heating to > 1100K.

The basic objective of the LEED/AES experiments was to determine if the NH_3 decomposition reaction occurred on a nitrogen covered Rh surface. NH_3 was dosed into the system through a capillary leak to $\sim 10^{-7}$ torr with the crystal at ~320K. The N Auger peak (380 eV) was then monitored as a function of temperature. The electron beam was on only when obtaining spectra as it has been shown that the Auger beam can induce NH_3 adsorption on metals (75,76). Presumably, there was a dynamic equilibrium established in these experiments as the ambient NH_3 pressure remained at $\geq 1 \times 10^{-7}$ torr throughout. Finally, a high NH_3 pressure study was done. The vacuum chamber was isolated from the ion pumps and ~70 μ of NH_3 were introduced with the crystal at ~650K to simulate kinetic reaction conditions. After 5 minutes, the system was pumped down to $< 5 \times 10^{-7}$ torr

and Auger spectra were taken to determine the amount of N present.

Materials

Most of the gases used in this study were of ultra-high purity. The NH_3 (99.999%) was obtained from Scientific Gas Products in 1 liter Pyrex bulbs with breakable seals and used without further purification. Bulbs of N_2 (>99.999%) and H_2 (>99.999%) were purchased from Matheson Gas Products. The Linde Division of Union Carbide was the source for the argon (99.999%) used for expansions and calibrations. The H_2 used in the LEED/Auger experiments and the O_2 for sample cleaning were purified through Pd/25% Ag and Ag diffusers, respectively.

The ND_3 was loaded from a Stohler Isotope Chemicals lecture bottle (~98%) into a 1 ℓ bulb and vacuum distilled several times using liquid-N_2 and Dry Ice-acetone baths. A mass spectrometric check indicated no significant impurities.

RESULTS AND DISCUSSION

Surface Characterization

LEED, Auger spectroscopy and flash desorption spectroscopy were used to characterize the catalytic Rh surface. The nature of the Rh(110) surface under catalytic conditions can be inferred from the LEED/AES results. Flash desorption spectroscopy provided information concerning the major surface species. The mechanistic arguments developed later will be based on these conclusions.

An "untreated" Rh(110) crystal was chosen for the LEED/AES experiments to ascertain the reason for the initial inactivity of the Rh(110) crystal used in the kinetic studies discussed previously. The "untreated" crystal was subjected to a number of standard cleaning techniques. Figure I-5 shows the Auger spectra taken following these various treatments. Spectrum (a) was taken after only heating the crystal to 1400K for several hours. Besides the Rh peaks (200, 222, 256 and 302 eV), peaks at 118, 154 and 180 eV are attributed to P, S and B, respectively. Very little C (273 eV) or O (510 eV) was detected. In general, both C and O could be removed from the surface by heating to 1400K, presumably by desorption (O) or diffusion into the bulk (C,O). Several Ar^+ bombardments and flashes produced spectrum (b), showing that the S is easily removed. Lengthy

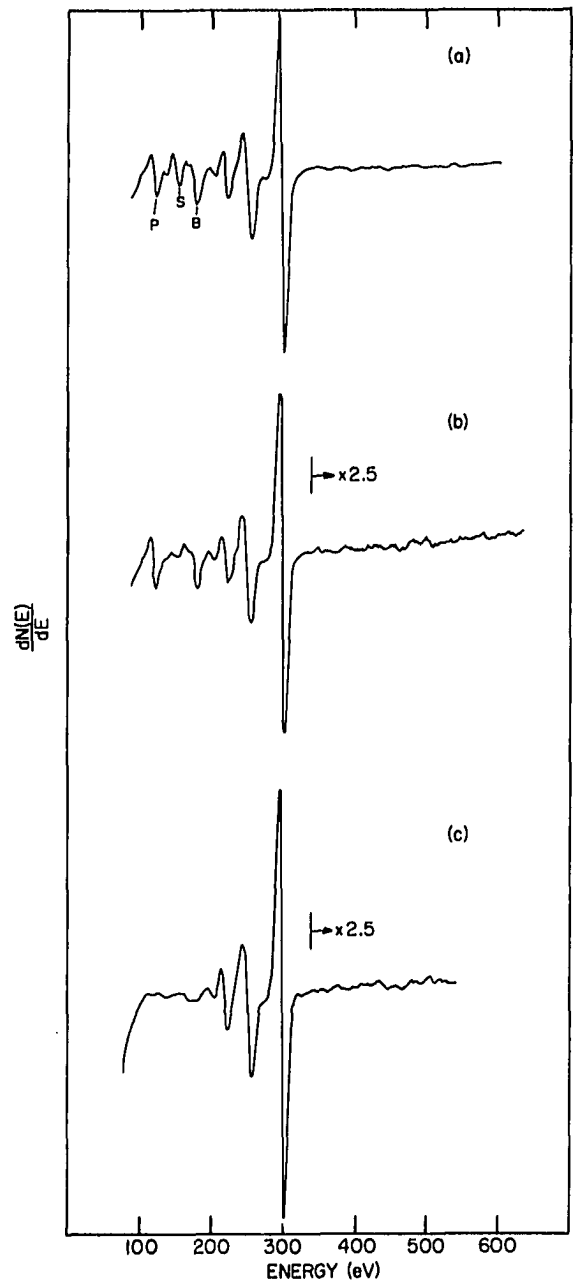

Figure I-5. Auger spectra of Rh(110) surface:
(a) Initial spectrum after heating
(b) Spectrum after initial Ar^+ and O_2 treatment
(c) "Clean" Rh(110) spectrum

oxygen treatments with high temperature flashes were required to remove the phosphorous and reduce the B. Figure I-5(c) is the "cleanest" spectrum obtained, with a small amount of B still present. This clean spectrum compares quite favorably with other Rh spectra reported in the literature (68,69,72). Figure I-6 shows the (1x1) LEED pattern of the clean Rh(110) crystal observed at 144 eV; the distortion presumably was due to nonsymmetrical magnetic fields. Most of the LEED work was done at 78 eV.

Initially, NH_3 was adsorbed at about 330K on a B contaminated surface. As the temperature was increased, the N (380 eV) peak decreased slightly but then began to increase when T > 770K. After heating to 1000K in a 10^{-7} torr NH_3 ambient, the Rh(110) crystal was cooled to 330K. This heating and cooling procedure caused B to diffuse to the surface. Figure I-7(a) shows the resulting Auger spectrum, indicating a relatively large amount of N (380 eV) and B (170-180 eV). The N peak would disappear only on heating to > 1200K. It appears that this nitrogen existed in the form of a boron nitride, which has been observed on Rh before (77). The presence of this nitride interfered with the detection of any N adsorbed on the Rh surface. According to B. A. Sexton at General Motors (77), this nitride layer is inert to further gas adsorption. Hence, by vigorous cleaning cycles, the B surface concentration was reduced to

Figure I-6. LEED pattern of the clean Rh(110) surface, 144 eV. (Most LEED work was done at 78 eV.)

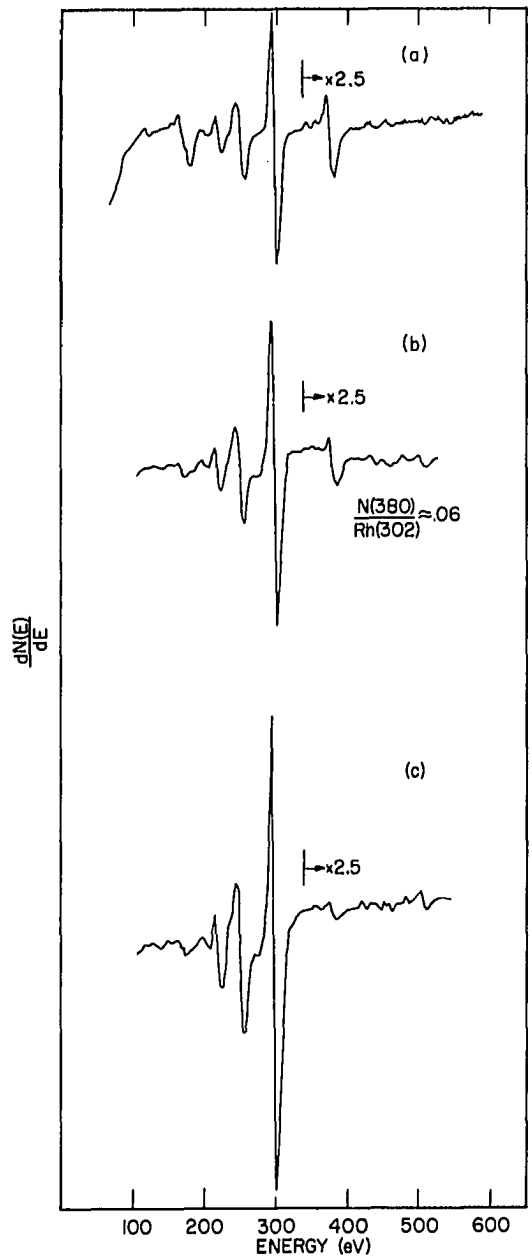

Figure I-7. Auger spectra obtained after NH_3 adsorption. (a) B covered surface, indicating formation of surface boron nitride. (b) Saturated, "clean" surface with N peaks at 380 eV (T = 360K). (c) Spectrum taken following 70 μ NH_3 dose at 650K

the extent that its interference was nearly negligible. It is now clear that the inactivity of the Rh(110) sample used in the kinetic studies was due to a large B contamination. Cleaning the sample over a long period of time finally completely removed the B, producing the active, stable surface used in the kinetic studies.

Once the Rh surface was clean (Figure I-5(c)), NH_3 was again adsorbed at 330K. After 2000 seconds at 10^{-6} torr NH_3 (Auger beam off), the spectrum shown in Figure I-7(b) was taken indicating that some NH_3 had adsorbed. The ratio N(380) peak height/Rh(302) peak height is approximately .06 which can be compared to .093 for the N(380)/Ru(273) produced by electron beam induced NH_3 adsorption on Ru(0001) (78). Danielson et al. determined, from an apparent (2x2) LEED pattern observed, that this ratio corresponds to .50 monolayer. Hence, it can be crudely estimated that the N concentration on the Rh(110) surface was about 1/3 of a monolayer following a 2000L dose at 330K. The temperature of the Rh(110) was progressively raised with Auger spectra taken at various intervals. Figure I-8 depicts the N(380) peak-to-peak height as a function of temperature. The surface concentration of B for the "solid line" data was somewhat higher than for the "dashed line" data. It is clear that under low pressure conditions ($<10^{-6}$ torr NH_3), the concentration of surface nitrogen was quite small (<0.1 monolayer)

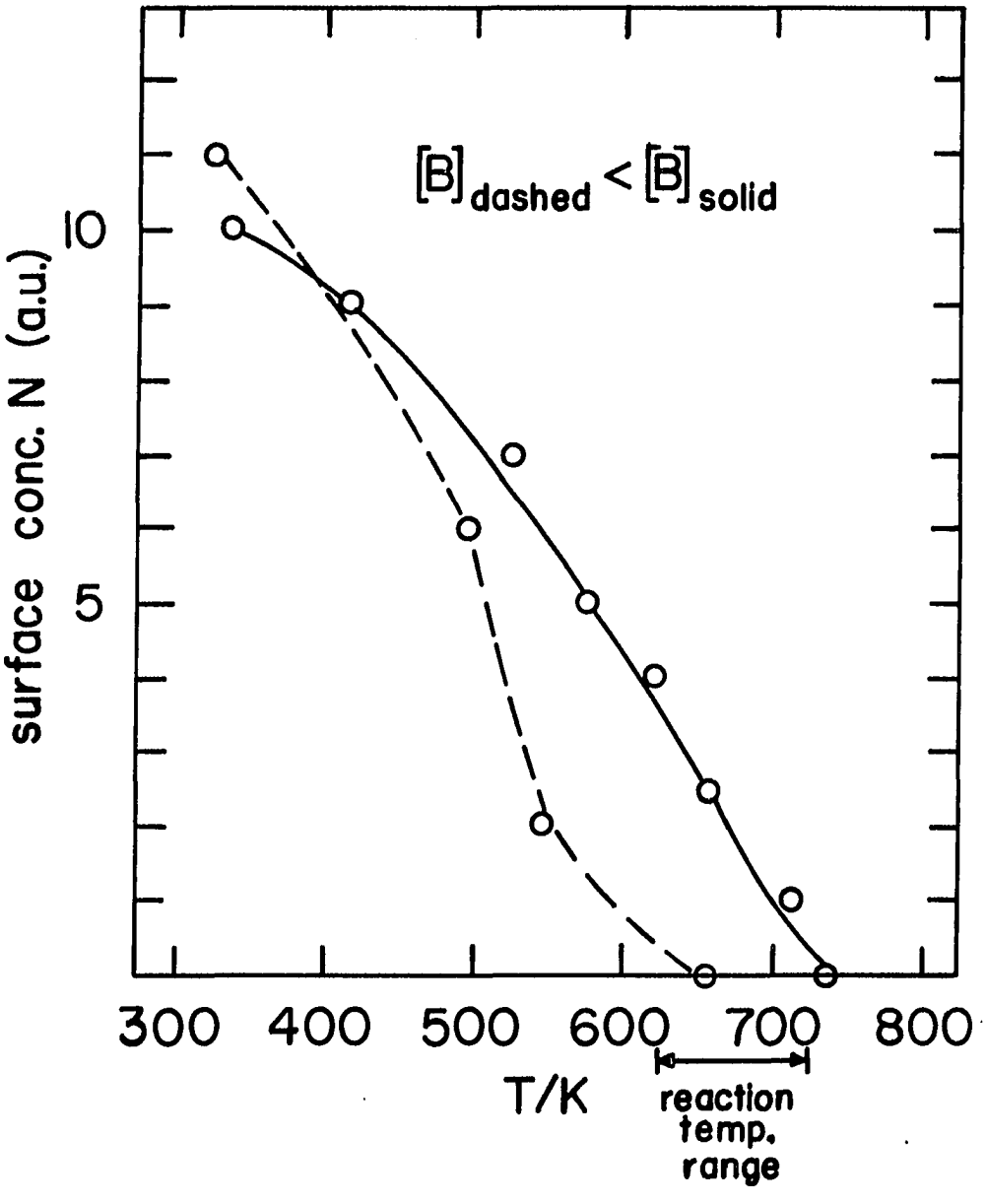

Figure I-8. Amount of adsorbed N as a function of catalyst temperature with $P_{NH_3} \approx 10^{-7}$-10^{-6} torr throughout the experiment. [3](Dashed curve represents a more B free surface than the solid curve.)

within the reaction temperature range. Following the high pressure reaction experiment (70 μ NH_3, 660K, 10 min), the spectrum shown in Figure I-7(c) was obtained, indicating that very little surface nitrogen was present. Hence, it is concluded from the Auger experiments that the Rh(110) surface was nearly devoid of N under reaction conditions.

The adsorption of NH_3 on the Rh(110) surface produced no new diffraction spots on the (1x1) LEED pattern at any reasonable temperature. Only the background intensified causing the pattern to become quite diffuse. This phenomenon has also been observed for NH_3 adsorption on Pt (75) and on a nonelectron bombarded Ru surface (76). It must be that the concentration of nitrogen-containing species on the surface was too low to give an ordered LEED pattern or that the adsorbate was totally disordered. Finally, dosing 10^{-5} torr N_2 onto the catalyst resulted in no N adsorption as indicated by Auger or LEED as was expected.

Some interesting phenomena were observed during the cleaning cycles and NH_3 interactions with a B contaminated surface. The boron clearly interacted with both the O_2 and NH_3 to form boron oxide and boron nitride. Chemical shifts due to the formation of these compounds were clearly observed, as shown in Figure I-9. Spectrum (a) shows the "pure" B peak at 180 eV for the contaminated surface. Heating in O_2 produced spectrum (b), showing a definite new

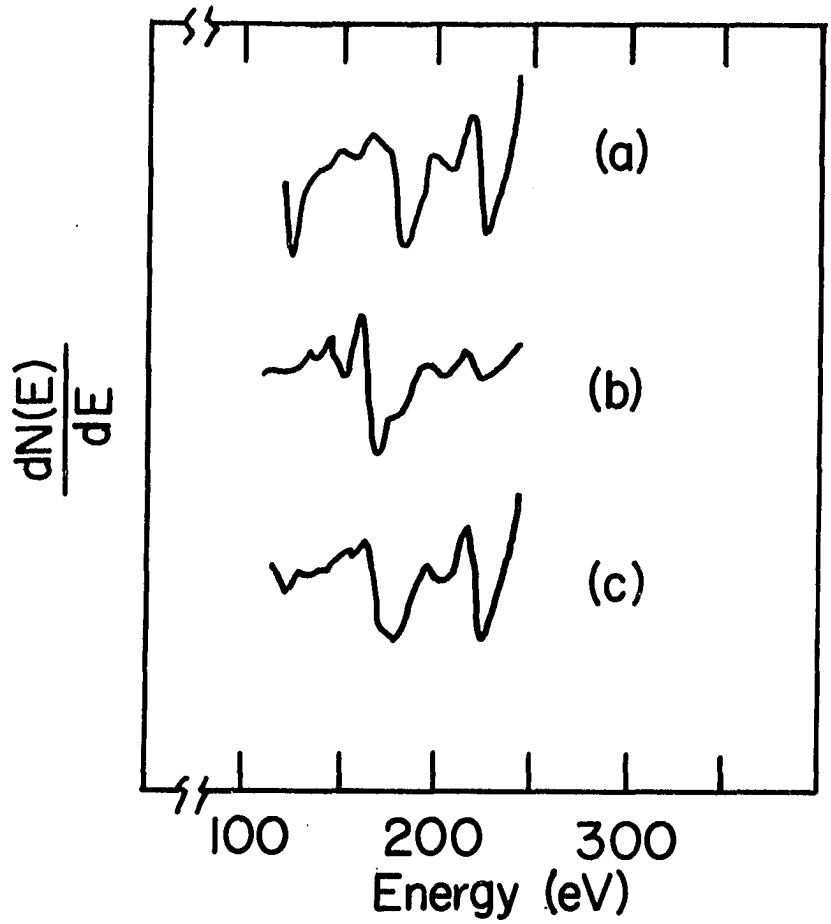

Figure I-9. Auger spectra of different B surface states. (a) "Pure" B (180 eV). (b) Surface boron oxide (170 eV). (c) Some boron nitride (~175 eV)

feature at 170 eV. This new peak appears to be due to a surface boron oxide. A shift of this magnitude has been seen for Si and SiO_2 where the major Si peak shifts from 92 eV to 76 eV, respectively (79). Spectrum (c) was obtained after a high temperature (>700K) interaction of 10^{-7} torr NH_3 and a B contaminated surface. Again, a peak begins to appear at a lower energy than for "pure" B, though the shift is not as large as for oxygen. The formation of these surface compounds is interesting in that actual changes in the electronic states of B due to modified chemical environments can be observed.

Flash desorption experiments involving adsorbed H_2, NH_3 and N_2 on the Rh(110) kinetic crystal were done. Figure I-10(a) shows the H_2 desorption curves obtained. The desorption temperature range of 320-360K compares very favorably with the H_2 desorption temperatures from a Rh(111) surface; Yates (80) observed H_2 desorbing between 300 and 370K from the surface. These desorption temperatures are significantly lower than those reported by Castner et al. (68); the cause of the discrepancy is not clear at this time. However, it is clear that there would be very little adsorbed H on a Rh surface under vacuum conditions at the reaction temperatures of interest.

Figure I-10(b) shows the flash desorption results from NH_3 adsorption at 250K. The H_2 and N_2 peaks at ∿350K may

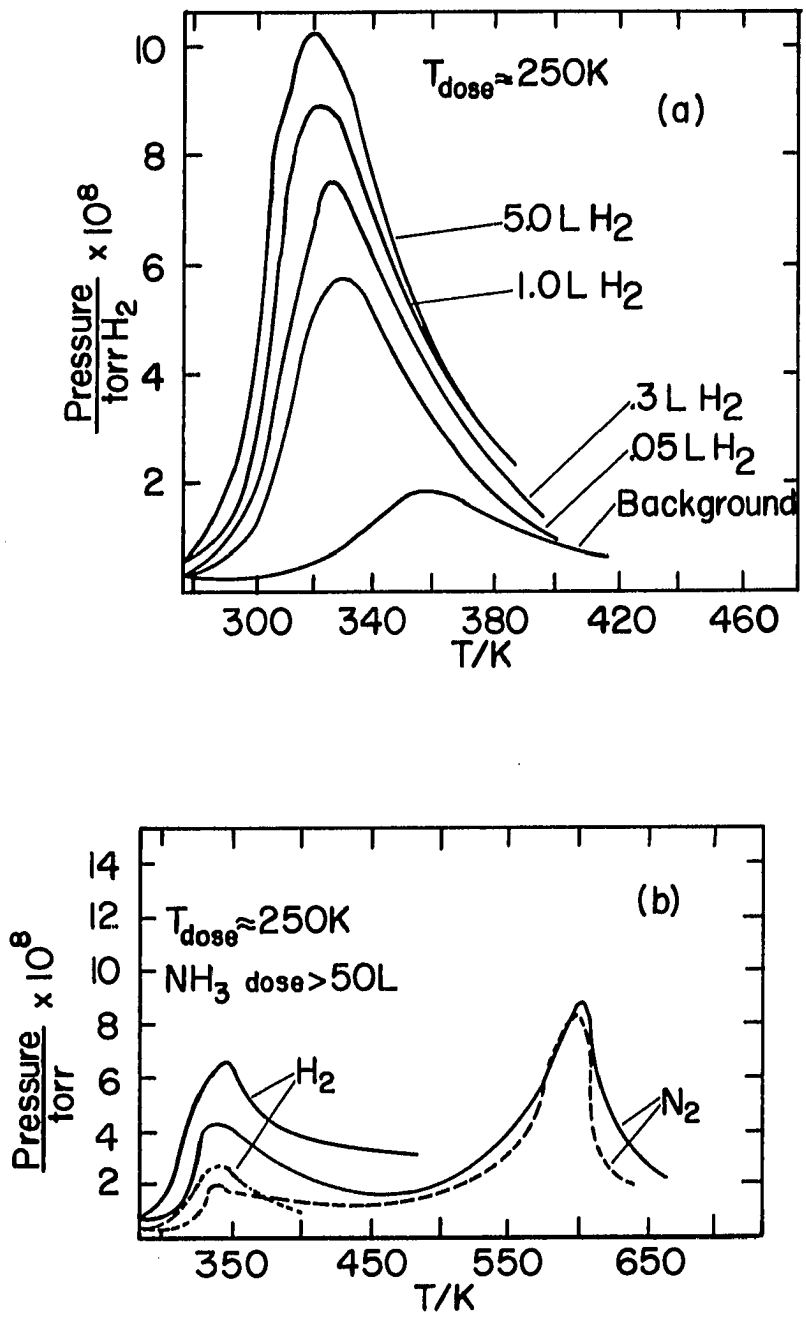

Figure I-10. Flash desorption spectra. (a) H_2 adsorption at 250K. (b) NH_3 adsorption at 250K, dashed curves obtained following initial (solid) flash (1L = 10^{-6} torr-sec)

have been due to a surface intermediate of some kind, probably not NH_3 as it would not diffuse to the mass spectrometer. The dominating feature of the spectrum is the N_2 peak at 600K. This correlates quite well with the 650K N_2 peak obtained by flash desorption of NO on a Rh wire (62). This N_2 peak appeared to be due to the atomic N on the surface as N adsorbed via activation also desorbed at ∿670K (62). In this study, very little activated N was adsorbed but the small peak observed at 600K did have a shoulder at ∿615K which correlates with the observations of Campbell and White (62). A CO peak at 540K was observed after "activated" N_2 adsorption, in agreement with the 530K peak of Campbell and White (64), probably due to "background" CO adsorption.

The decrease in the low temperature N_2, H_2 peaks for subsequent doses can be rationalized by the fact that the Rh(110) crystal was cooling in an ammonia ambient following a flash to 900K, so that atomic N was deposited at $T \leq 600K$. At 250K, where the flash was started, no more NH_3 could adsorb as all the sites were blocked by the atomic nitrogen.

The flash desorption results correlate very well with the Auger findings, supporting the contention that the Rh surface was nearly devoid of nitrogen species at typical reaction temperatures for the NH_3 decomposition. Therefore, in most cases, the surface of the Rh catalysts will be considered bare for mechanistic purposes.

Kinetics Introduction

As discussed previously, the kinetic experiments involved the study of the NH_3 decomposition under a variety of conditions. The results of interest are the NH_3 orders, H_2 orders and N_2 orders for all reaction conditions. Table I-1 summarizes the results obtained from the active Rh(110) single crystal. The results obtained on the Rh(100) and Rh(111) surfaces were generally the same as for the (110) and will also be reported.

Figure I-11 shows the "pure" NH_3 kinetic order plots for the three crystal faces studied. Approximately 1/2 order in NH_3 is indicated for all three faces. Clearly, the NH_3 decomposition reaction on Rh is markedly face specific with the rates being in the ratio 20:2:1 for the Rh(110), (100) and (111), respectively. This trend will be interpreted in subsequent discussion. The 700K data (Rh(110)) clearly show the 1/2 order dependence on NH_3.

Other kinetic results are shown in Figures I-12 and I-13. The H_2 order trend is depicted in Figure I-12(a) for the Rh(110) and (111) samples. As the temperature increased, a higher P_{H_2} was required for clear inverse first order inhibition of the reaction. Figure I-12(b) implies that the ammonia order exceeds +1/2 upon addition of H_2 on the Rh(111) surface. The trend will be more striking when the Rh(110) results will be considered. As seen in Figure I-13, N_2 had

Table I-1. Summary of the kinetic results on the Rh(110) single crystal

Conditions	NH_3 Order
NH_3 Orders[a]	
1) Low P_{NH_3} (P_{NH_3} < 30 μ), P_{H_2} = 0	∿+1/2
2) Moderate to high P_{NH_3} (P_{NH_3} > 30 μ), P_{H_2} = 0	∿+1/3
3) Low P_{NH_3} (P_{NH_3} < P_{H_2}), P_{H_2} = constant ≠ 0	∿+1
4) Moderate P_{NH_3} (P_{NH_3} > P_{H_2}), P_{H_2} = constant ≠ 0	∿+1/2
H_2 Orders[b]	
Conditions	H_2 Order
1) Low P_{H_2} (P_{H_2} < P_{NH_3}), P_{NH_3} = constant	0→fractional(-)
2) High P_{H_2} (P_{H_2} > P_{NH_3}), P_{NH_3} = constant	∿-1
N_2 Orders	
Conditions	N_2 Order
1) All temperatures and pressures	0

[a]Dependence on P_{H_2} and temperature is discussed in the text.

[b]Dependence on P_{NH_3} and temperature is discussed in the text.

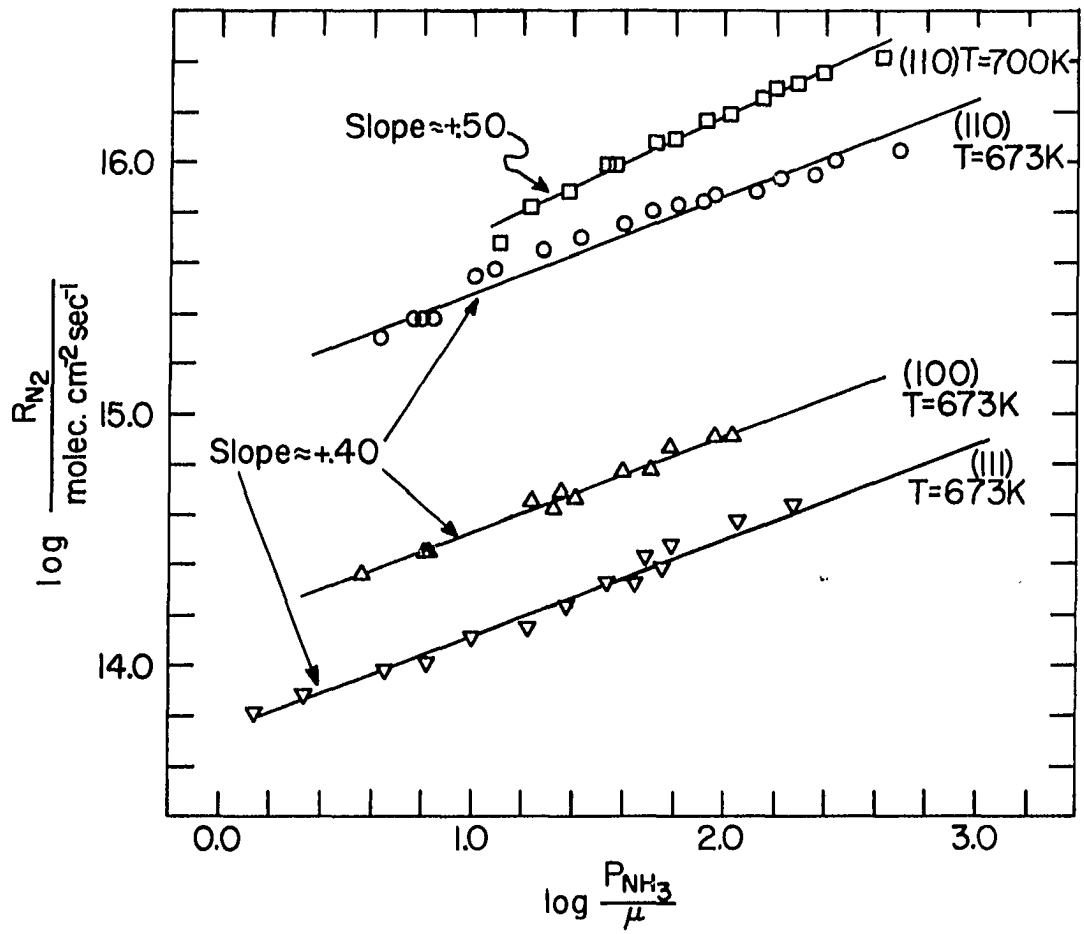

Figure I-11. The dependence of the reaction rate on ammonia pressure in pure NH_3 for the three crystal faces at 673K. The face specificity is quite evident. (Top curve shows data at 700K on the Rh(110))

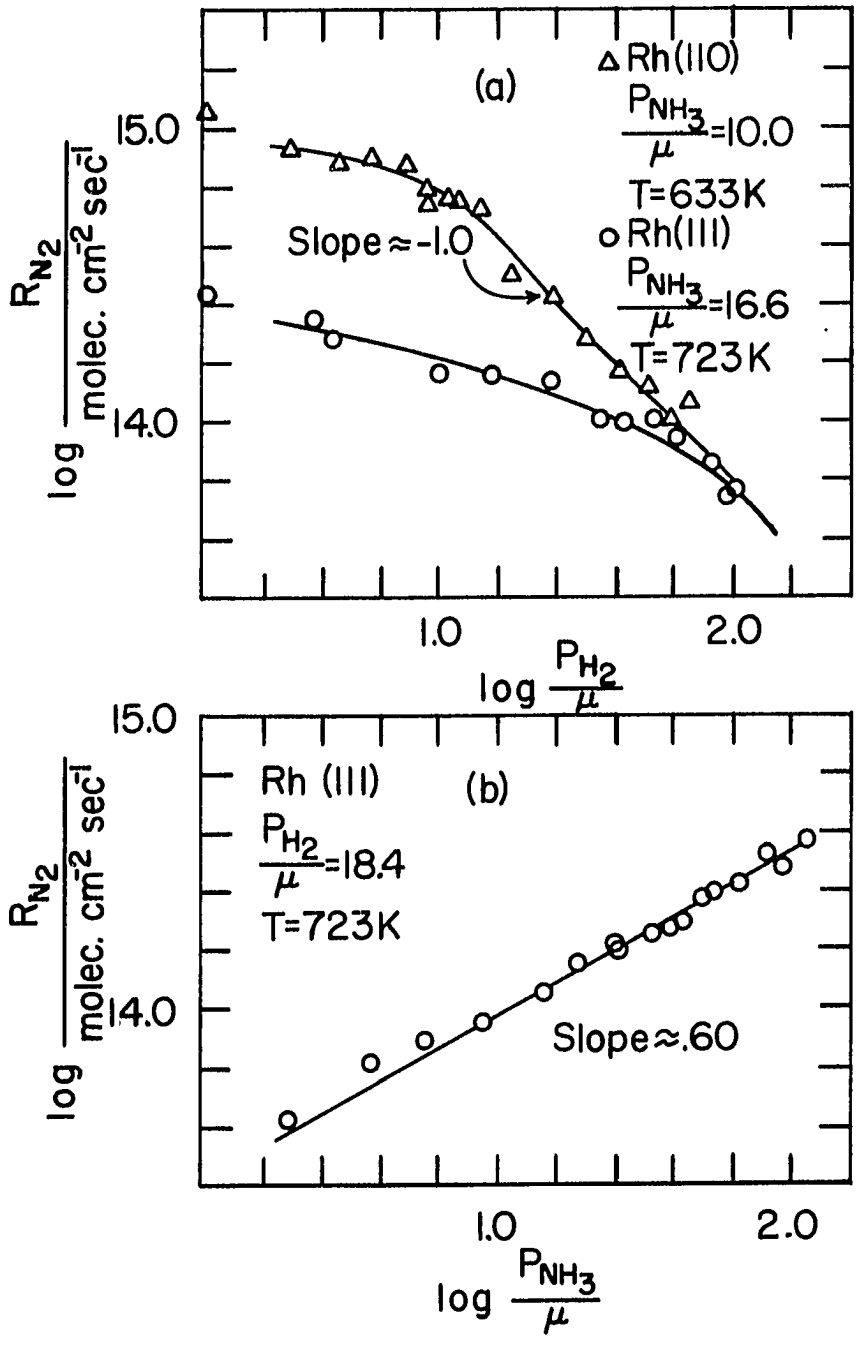

Figure I-12. Other examples of kinetic results: (a) H_2 order data on Rh(110) and Rh(111) indicating -1.0 order at high P_{H_2}. (b) NH_3 order for NH_3/N_2 mixture on Rh(111), indicating deviation towards first order

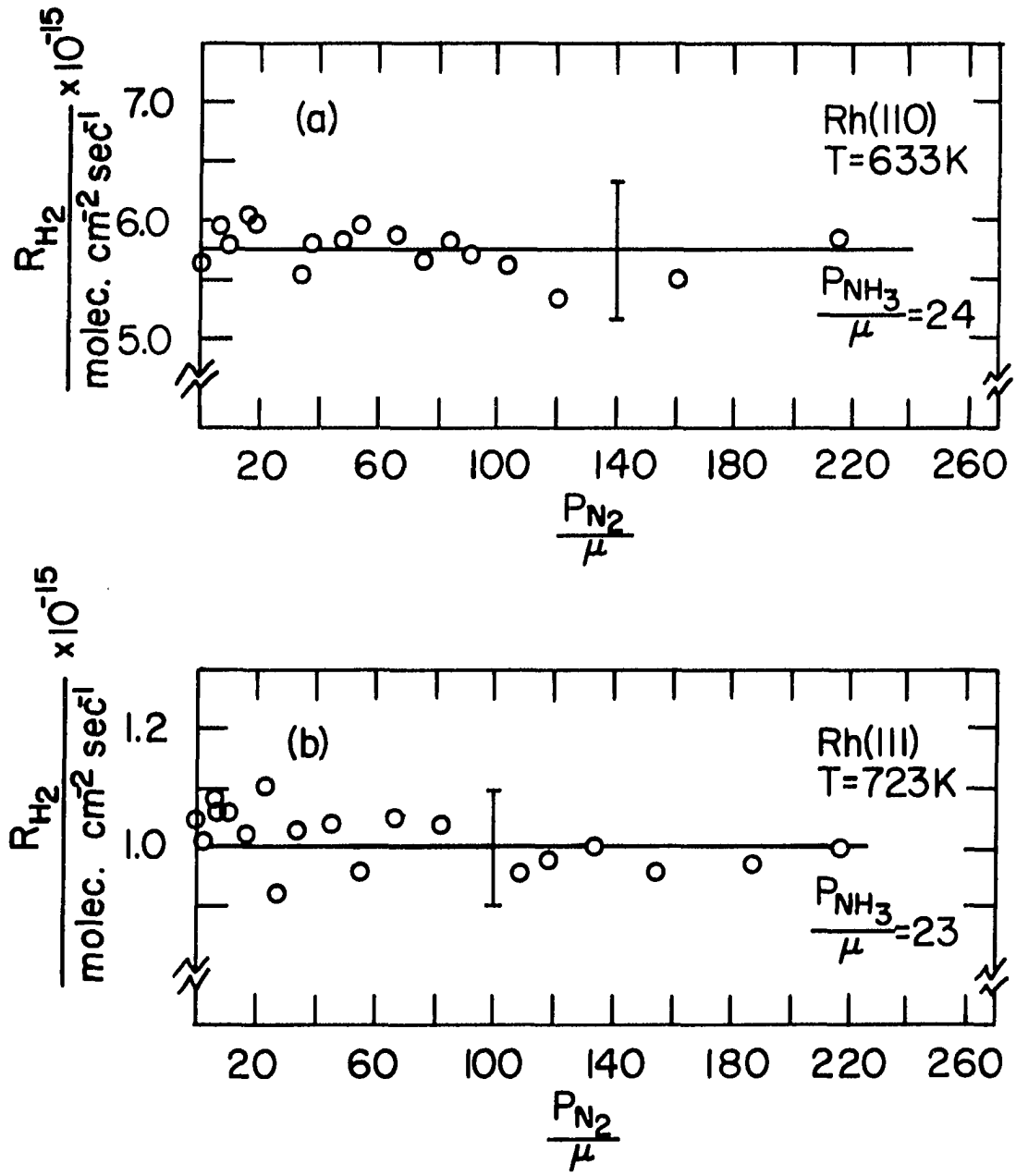

Figure I-13. Rate of H_2 production as a function of N_2 pressure: (a) Rh(110). (b) Rh(111) (Error bars are ~±10% of "average rate".)

no effect on the NH_3 decomposition rate. This result is reasonable in that adsorption experiments in this study indicated that N_2 will not adsorb on Rh and hence will probably not affect the surface reactions. The effect of N_2 has been found usually to be negligible in NH_3 decomposition studies on transition metals (2).

There is clearly an isotope effect in the NH_3 decomposition reaction on Rh as shown in Figure I-14. In general, the NH_3 rates were $\sim$1.4-1.6 times greater than the ND_3 rates; this effect was similar to the value of 1.47 observed on W (35). The existence of the isotope effect implies that the rate limiting process includes the breaking of an N-H bond. As discussed by Van Hook (81), the high temperature limit ($kT>>h\nu_{ovib}$) of an isotope effect (in this case RH/RD) is simply the ratio of the vibrational frequencies of the bond "designated" as the reaction coordinate. If we assume that stretching the N-H bond is the reaction coordinate in this study, the ratio of the vibrational frequencies (as calculated from the reduced masses of N-H and N-D) is $\sim$1.36 which will be the theoretical minimum. This correlates very well with the effects noted in Figure I-14. The Rh(110) isotope effect decreased with temperature as required by theory (81).

The apparent activation energies of the NH_3 decomposition reaction can be extracted from Figure I-15. The apparent

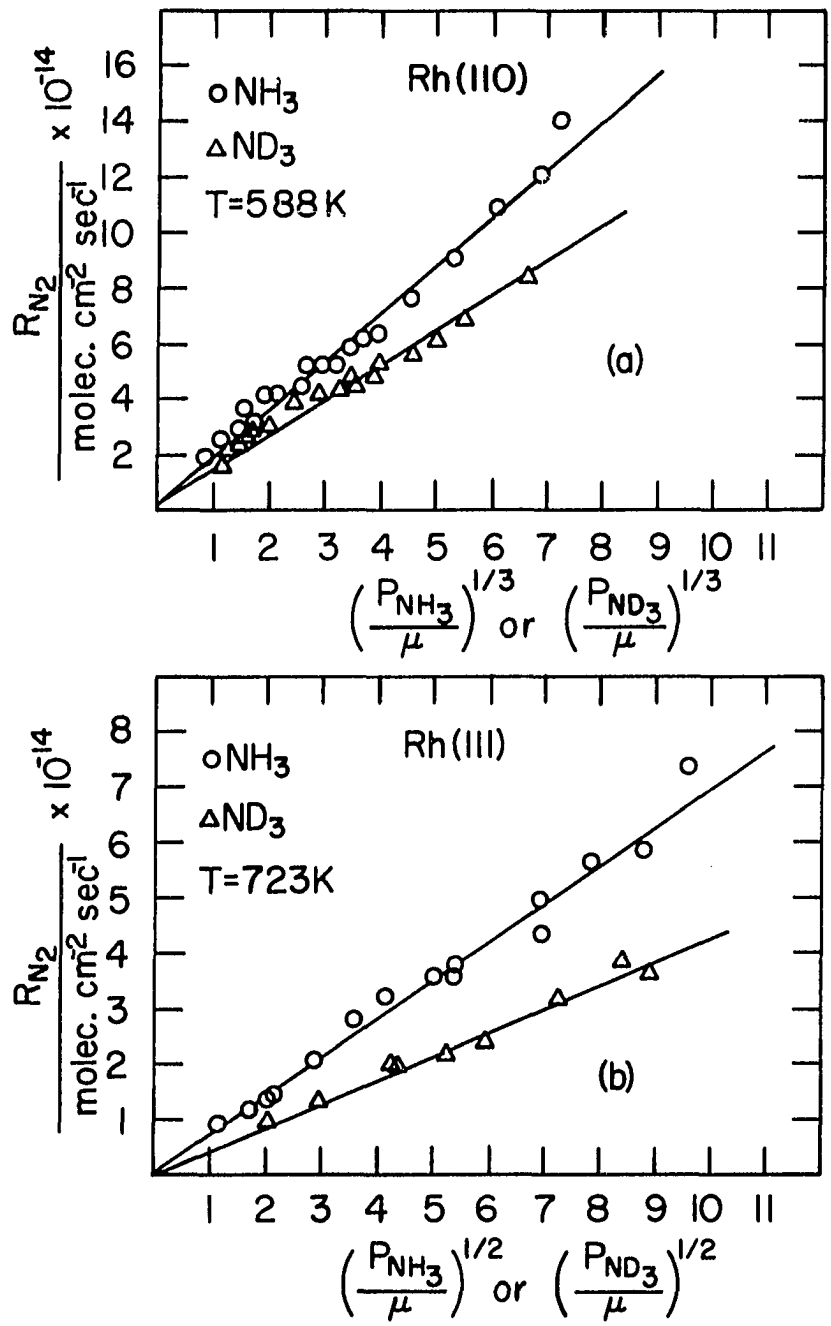

Figure I-14. Decomposition of NH_3 and ND_3 on: (a) Rh(110); $r \approx 1.4$. (b) Rh(111); $r \approx 1.6$. r = Rate (NH_3)/Rate (ND_3)

activation energies (NH_3 only) for the three crystal faces studies were approximately the same (∿19 kcal/mole) and were found not to vary appreciably with NH_3 pressure. The equality of the energies is not without precedence as Löffler and Schmidt (54) observed equal reaction activation energies for different Pt single crystal faces (though the (110) was an anomaly). In this study, the (110) face appears to have "behaved" the same as the other faces. Below ∿670K, the activation energy on the Rh(110) increased to ∿23 kcal/mole. The possible significance of this will be discussed subsequently. It is clear that the apparent activation energy increased with added H_2 (Figure I-15(b)). This phenomenon may partially "explain" the large activation energy (∿57 kcal/mole) found for a 6 to 1 H_2 to NH_3 reaction mixture on a Rh film by Logan and Kemball (46). The value of 19 kcal/mole for pure NH_3 from this study correlates reasonably well with those of Amano and Taylor - 26 kcal (55) and Sokol'skii et al. - 20.8 kcal/mole (47).

During the complete analysis of the kinetic data, it was noted that the rates varied by as much as 15% from day to day. This may have been due to inaccuracies in temperature and/or pressure determinations, differing amounts of surface contaminants on different days or mass spectrometer calibration variations. To facilitate analysis, the following normalization procedure was used. Most of the data reported here were taken at 633 and 673K with a set of standard

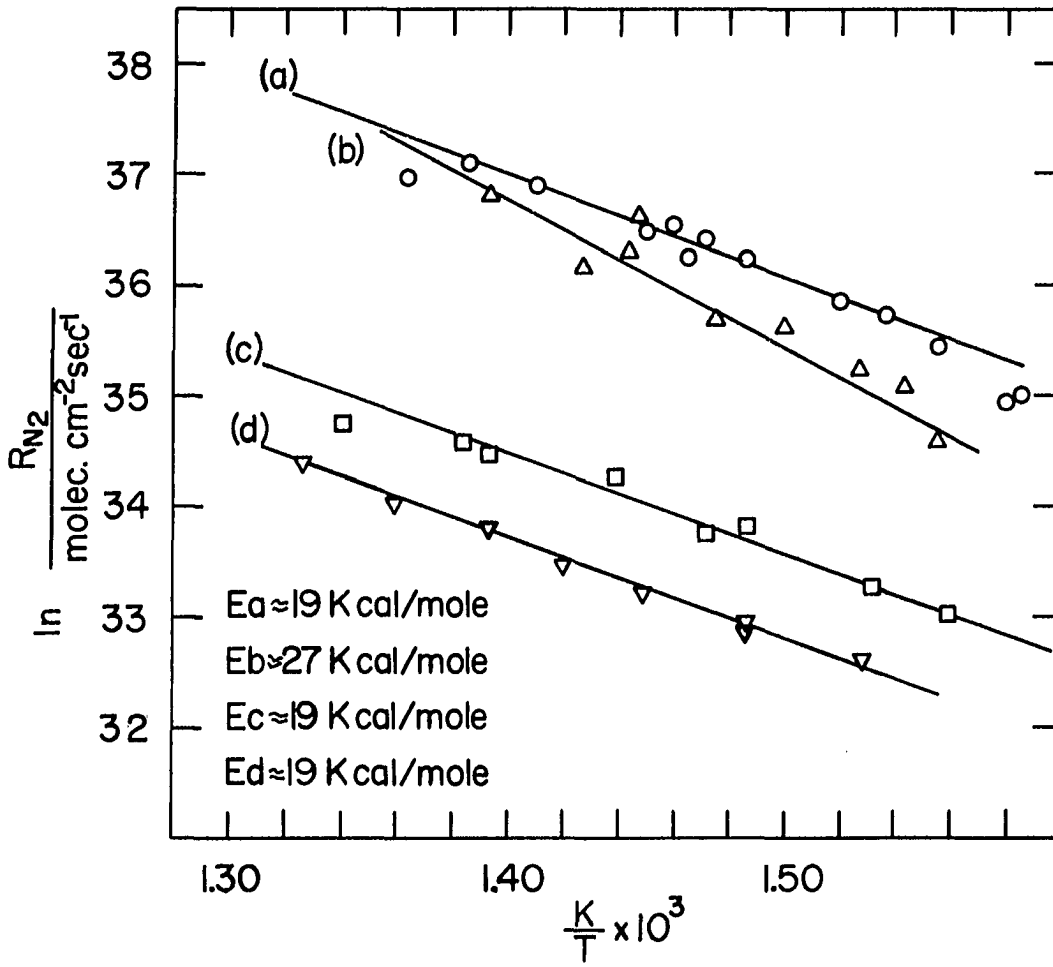

Figure I-15. Temperature dependence of decomposition rates: (a) Rh(110), P_{NH_3} = 29 μ. (b) Rh(110), P_{NH_3} = 29 μ, P_{H_2} = 31 μ. (c) Rh(100), P_{NH_3} = 24 μ. (d) Rh(111), P_{NH_3} = 29μ

"NH_3 only" runs performed after each experimental series. The rates determined from these runs were compared to a "standard" pure NH_3 order data set at the appropriate temperature. All of the data were then adjusted such that the set of "pure NH_3" runs correlated with the standard pure NH_3 order curve. As an example, if the "standard" rates from an H_2 order run series were 10% low on a particular day, then all the H_2 order rates were increased by 10% to compensate.

Mechanistic Considerations

In the following discussion, a specific mechanism for the NH_3 decomposition reaction on Rh will be presented. Semi-quantitative correlations of the kinetic data (from the Rh(110)) to the derived rate law will be made followed by a discussion of the surface intermediates.

As discussed previously, the active Rh surface under reaction conditions consisted largely of "bare" Rh atoms. The following reaction mechanism for the NH_3 decomposition on Rh is consistent with this fact and leads to the observed reaction kinetic orders:

$$\begin{aligned}
&\text{a)} \quad 4Rh + NH_3(g) \underset{k_{-1}}{\overset{k_1}{\rightleftharpoons}} Rh_2NH + 2RhH \\
&\text{b)} \quad Rh_2NH \xrightarrow{k_2} RhN + RhH \\
&\text{c)} \quad 2RhH \underset{k_{-3}}{\overset{k_3}{\rightleftharpoons}} 2Rh + H_2(g) \\
&\text{d)} \quad 2RhN \xrightarrow{k_4} 2Rh + N_2(g)
\end{aligned} \qquad \text{(I-7)}$$

In the subsequent analysis, the Rh surface atoms are assumed to be the major surface species whose concentration does not appreciably change during the reaction; i.e., [Rh] ≈ a constant, Q. This assumption will be analyzed in more detail later. Under steady state conditions, the following is assumed:

$$\frac{d[Rh_2NH]}{dt} = \frac{d[RhH]}{dt} = \frac{d[RhN]}{dt} = 0 \qquad \text{(I-8)}$$

From the mechanism, the following expressions are developed:

$$\text{a)}\quad \frac{d[Rh_2NH]}{dt} = 0 = k_1 P_{NH_3} Q^4 - k_{-1}[Rh_2NH][RhH]^2 - k_2[Rh_2NH] \qquad \text{(I-9)}$$

$$\text{b)}\quad \frac{d[RhH]}{dt} = 0 = 2k_1 P_{NH_3} Q^4 - 2k_{-1}[Rh_2NH][RhH]^2 + k_2[Rh_2NH] - 2k_3[RhH]^2 + 2k_{-3} P_{H_2} Q^2$$

$$\text{c)}\quad \frac{d[RhN]}{dt} = 0 = k_2[Rh_2NH] - 2k_4[RhN]^2$$

From equation I-9(c), we see that

$$k_2[Rh_2NH] = 2k_4[RhN]^2 \qquad \text{(I-10)}$$

i.e., reactions I-7(b) and I-7(d) are coupled. If the fourth step in the mechanism (N_2desorption) is rate limiting, the following is true:

$$\text{Rate}(N_2) = k_4[RhN]^2 = \tfrac{1}{2} k_2[Rh_2NH] \qquad \text{(I-11)}$$

Hence, by obtaining an expression for $[Rh_2NH]$, a rate equation can be derived.

From I-9(a) we obtain immediately:

$$a) \quad [Rh_2NH] = \frac{k_1 P_{NH_3} Q^4}{k_2 + k_{-1}[RhH]^2} \qquad (I\text{-}12(a))$$

Subtracting twice I-9(a) from I-9(b) and rearranging, we obtain

$$b) \quad [RhH]^2 = \frac{3}{2}\frac{k_2}{k_3}[Rh_2NH] + \frac{k_{-3}}{k_3} P_{H_2} Q^2 \qquad (I\text{-}12(b))$$

Substituting (b) into (a), a quadratic equation in $[Rh_2NH]$ is obtained. The physically sensible solution is given by:

$$[Rh_2NH] = \frac{(k_2k_3 + k_{-1}k_{-3}P_{H_2}Q^2)}{3k_2k_{-1}} \left[\left[1 + \frac{6k_2k_{-1}k_3k_1P_{NH_3}Q^4}{(k_2k_3 + k_{-1}k_{-3}P_{H_2}Q^2)^2}\right]^{1/2} - 1\right] \qquad (I\text{-}13)$$

Recalling that $Rate(N_2) = \frac{1}{2} k_2[Rh_2NH]$, the following is derived:

$$Rate(N_2) = \frac{(k_2k_3 + k_{-1}k_{-3}P_{H_2}Q^2)}{6k_{-1}} \left[\left[1 + \frac{6k_2k_{-1}k_3k_1P_{NH_3}Q^4}{(k_2k_3 + k_{-1}k_{-3}P_{H_2}Q^2)^2}\right]^{1/2} - 1\right] \qquad (I\text{-}14)$$

Equation I-14 is indeed relatively complex. It would be possible to fit this equation to the data using a "trial and

error" constant determination but the physical significance of this method is questionable.

Qualitatively, all the kinetic features observed are present in equation I-14 (and hence in the mechanism). At $P_{H_2} = 0$, the rate goes as $P_{NH_3}^{1/2}$ if $6k_{-1}k_1P_{NH_3}Q^4/k_2k_3 >> 1$. For $P_{H_2} \neq 0$, the NH_3 order is predicted to go from +1 to +1/2 depending on the NH_3/H_2 ratio. The expression correctly predicts the -1 order in H_2 at high P_{H_2}. The following development will show that the rate expression and hence the mechanism fit all of the kinetic data reasonably well.

A "superposition" procedure can be used to obtain some quantitative information about the kinetics. Considering expression I-14, define P_o by:

$$P_o \equiv \frac{(k_2k_3 + k_{-1}k_{-3}P_{H_2}Q^2)^2}{6k_2k_{-1}k_3k_1Q^4} \qquad \text{(I-15)}$$

Rearranging, the following is obtained:

$$\left(\frac{k_2k_3k_1Q^4P_0}{6k_{-1}}\right)^{1/2} = \frac{k_2k_3 + k_{-1}k_{-3}P_{H_2}Q^2}{6k_{-1}} \equiv R_o \qquad \text{(I-16)}$$

defining R_o. Hence, equation I-14 may be rewritten as:

$$\frac{R}{R_o} = \left[\left(1 + \frac{P_{NH_3}}{P_o}\right)^{1/2} - 1\right] \qquad \text{(I-17)}$$

$R = \text{Rate}(N_2)$

This expression contains dimensionless quantities which can be related to the NH_3 order data for constant P_{H_2} (see Table I-1). On a master curve plotting $\log(R/R_o)$ against $\log(P_{NH_3}/P_o)$, the NH_3 order data at constant P_{H_2} can be superimposed. Values of R_o and P_o can then be extracted for each set of data. The superposition was done by manually determining the "best" fit. A mathematical fit was not done as the superposition method only produces two rate constants. The data are scattered enough that a manual superposition seemed justified. As will be seen, the method produced internally consistent results.

Figure I-16 shows the best superposition of four data sets obtained at 673K. The fit to the theoretical curve is generally good except at the extremes. Figure I-17 shows the superposition of three data sets at 633K; the scatter is much more evident here. The data at P_{H_2} = 26.5 μ had to be adjusted quite drastically and will not be considered in further developments. It is clear that an excellent qualitative fit to the mechanism function is obtained, indicating that the mechanism predicts the proper trends in the kinetics. The information listed in Table I-2 was extracted from the superpositions discussed. Theoretically, the values of $R_o/P_o^{1/2}$ should be constant at a fixed T. This requirement is approximately met for the 673 and 633K data, providing some justification for the superposition method used. The

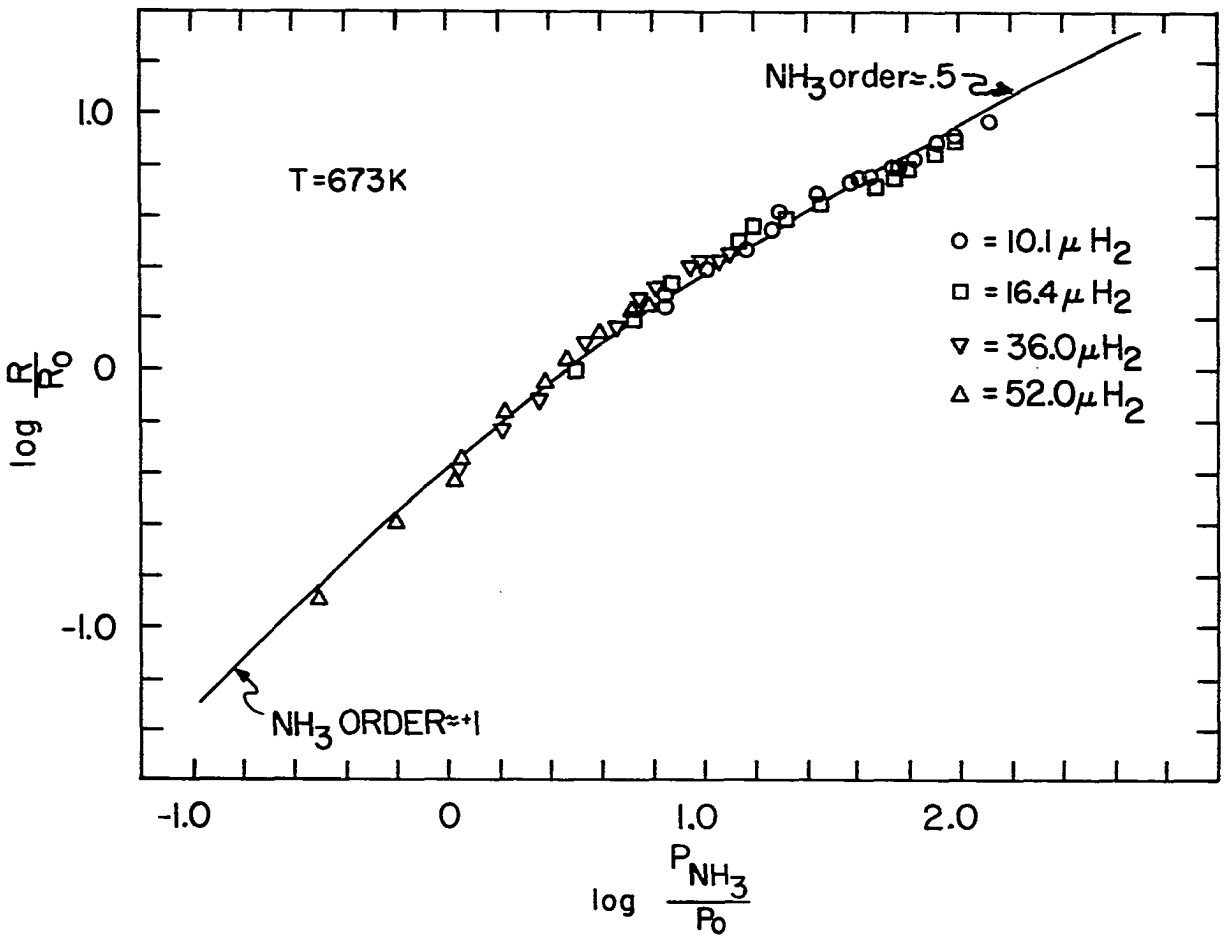

Figure I-16. Superposition of NH_3 order data at fixed P_{H_2} on log-log curve representing the function defined by equation I-17 at 673K (See Table I-2 for appropriate parameters.)

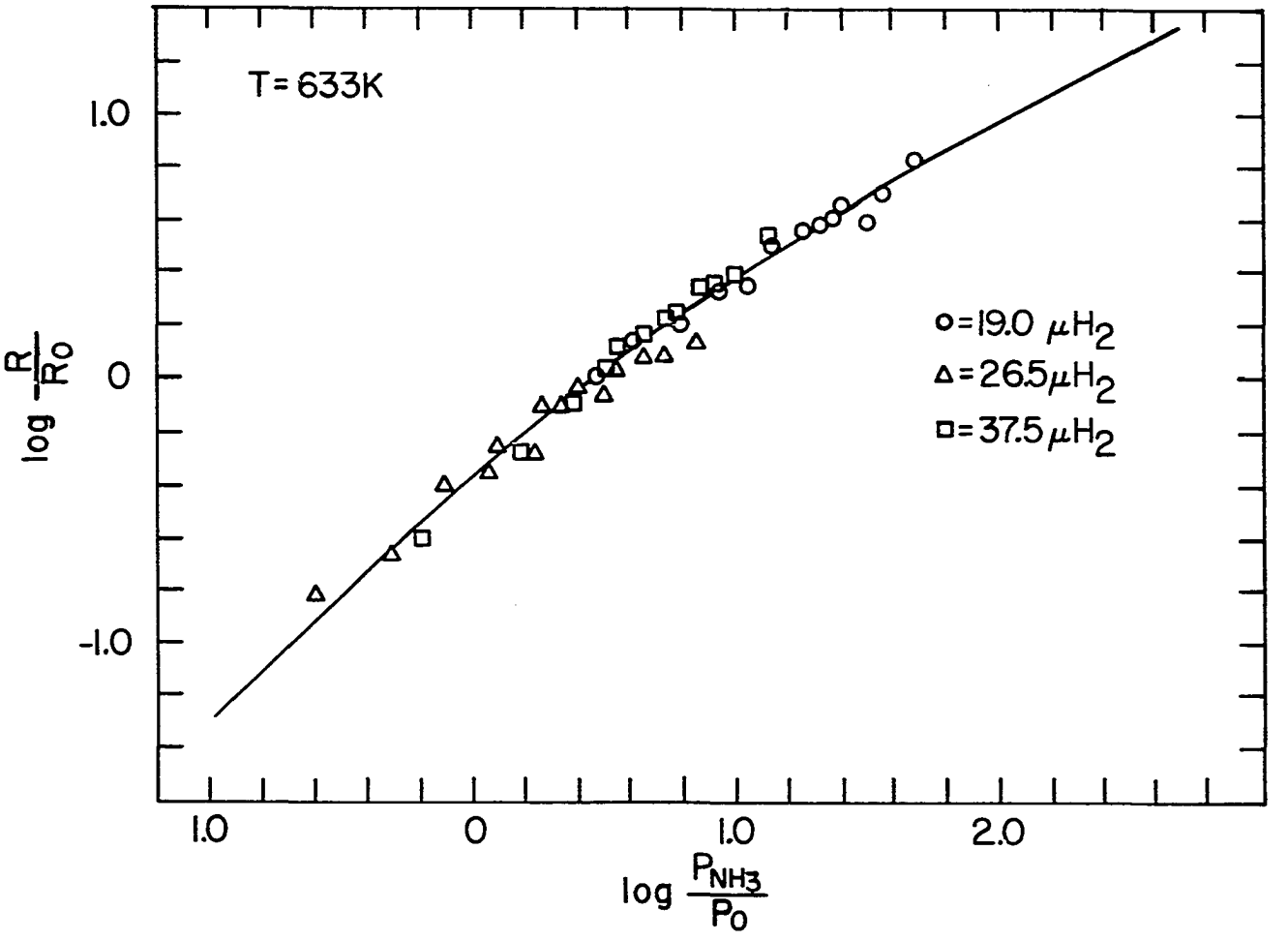

Figure I-17. Superposition of NH_3 order data at fixed P_{H_2} on log-log curve representing the function defined by equation I-17 at 633K (See Table I-2 for parameters)

Table I-2. Parameters obtained from superposition of data on log R/R_o, log P/P_o curve defined by equation I-17

T(K)	$P_{H_2}(\mu)$	R_o(molec $cm^{-2}sec^{-1}$)	$P_o(\mu)$	$P_o^{1/2}(\mu^{1/2})$	$R_o/P_o^{1/2}$(molec $cm^{-2}sec^{-1}\mu^{-1/2}$)
673	10.1	8.1×10^{14}	1.00	1.00	8.10×10^{14}
	16.4	1.05×10^{15}	1.86	1.37	7.67×10^{14}
	36.0	2.04×10^{15}	7.94	2.82	7.24×10^{14}
	52.0	2.82×10^{15}	15.85	3.98	7.08×10^{14}
633	19.0	4.0×10^{14}	3.16	1.78	2.24×10^{14}
	26.5[a]	5.6×10^{14}	3.98	2.00	2.81×10^{14}
	37.5	6.9×10^{14}	10.00	3.16	2.19×10^{14}

[a]This data set was not included in subsequent slope and intercept determination due to large rate correction.

average values of $M \equiv R_o/P_o^{1/2}$ are 7.53×10^{14} (673K) and 2.22×10^{14} (633K) molec cm^{-2} sec^{-1} $\mu^{-1/2}$.

From equation I-15, it is seen that $P_o^{1/2}$ is directly proportional to P_{H_2}. Hence, plotting $P_o^{1/2}$ *versus* P_{H_2} should give a straight line with slope and intercept given by:

$$S_P = \left[\frac{k_{-1}k_{-3}^2}{6k_2k_3k_1}\right]^{1/2} \qquad I_P = \left[\frac{k_2k_3}{6k_{-1}k_1Q^4}\right]^{1/2} \qquad \text{(I-18)}$$

A similar plot of R_o *versus* P_{H_2} should give a straight line with the following slope and intercept:

$$S_R = \frac{k_{-3}Q^2}{6} \qquad I_R = \frac{k_2k_3}{6k_{-1}} \qquad \text{(I-19)}$$

By noting that:

$$M = \left[\frac{k_1k_2k_3Q^4}{6k_{-1}}\right]^{1/2} = R_o/P_o^{1/2} \qquad \text{(I-20)}$$

the following can be seen:

$$M \times S_P = \frac{k_{-3}Q^2}{6} \qquad \frac{M}{I_P} = k_1Q^4 \qquad \frac{M^2}{I_R} = k_1 \qquad \text{(I-21)}$$

Figure I-18 shows the $P_o^{1/2}$, R_o *vs* P_{H_2} plots for both temperatures studied. Straight lines may be drawn through the points indicating a nonzero intercept in all cases. Now, if the surface Rh concentration (Q) is considered in terms of surface coverage, then $Q = \theta \simeq 1$ by the assumption made previously. Hence, by inserting the appropriate

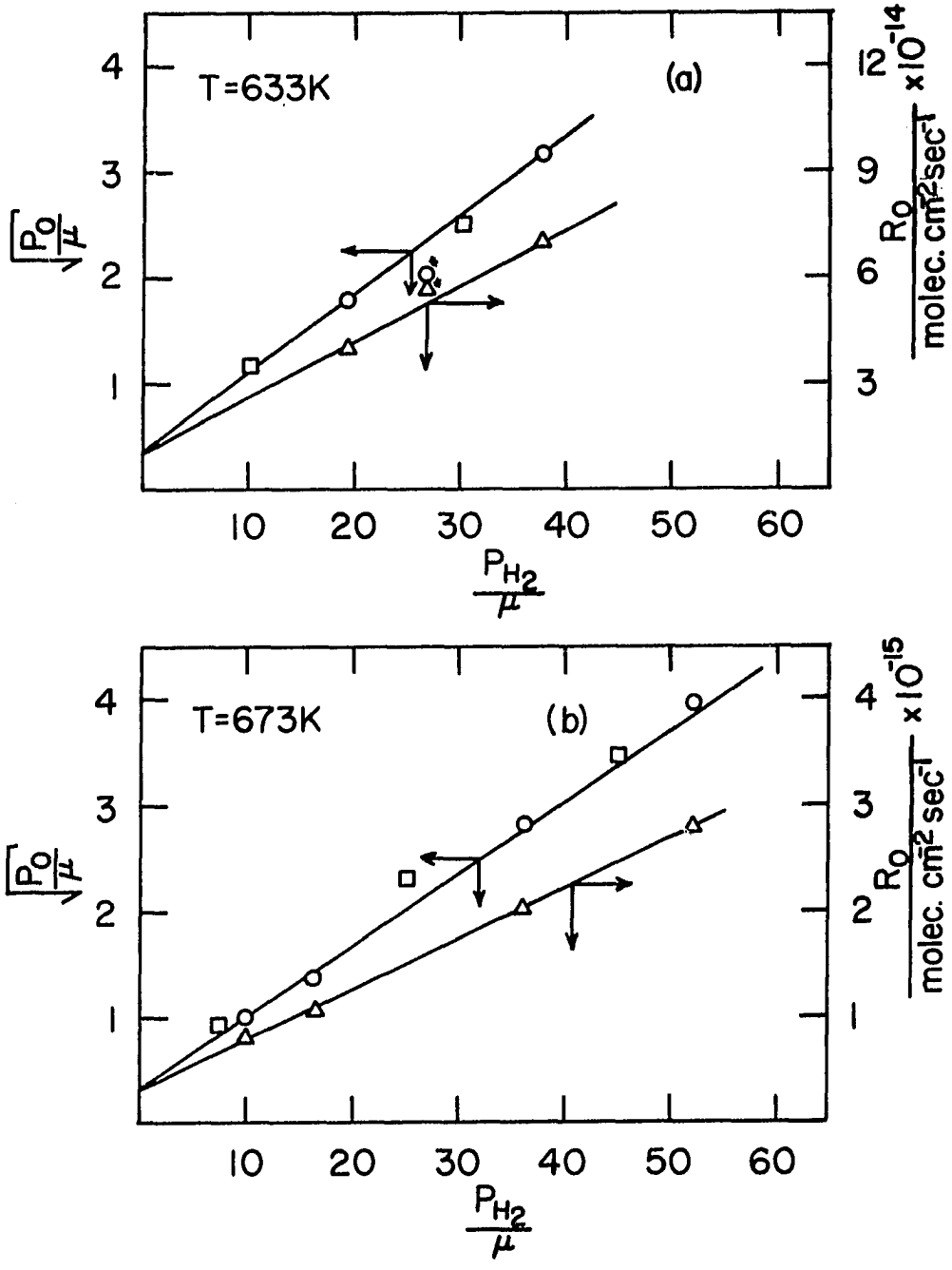

Figure I-18. Relation of $P_o^{1/2}$ (circles) and R_o (triangles) to hydrogen pressure at (a) 633K (see comments in text concerning starred points.) (b) 673K (The squares are empirically determined as discussed later in the text.)

quantities obtained from Figure I-18 into the above expression, values of k_1 and k_{-3} can be obtained. These results are shown in Table I-3. The overall fit of this development to the 633K data is not expected to be too accurate as the pure NH_3 order is nearer 1/3 than 1/2 (reasons are discussed later). The 673K data, as is clear, fit relatively nicely to the "mechanism" function.

An alternate means of checking the above results requires return to equation I-14. By assuming that $P_{H_2} = 0$, that the group of constants and P_{NH_3} within the square root is large compared to one and that $Q \approx 1$, the equation reduces to:

$$\text{Rate}(N_2) \approx \underbrace{\left(\frac{k_1 k_2 k_3}{6k_{-1}}\right)^{1/2}}_{a} P_{NH_3}{}^{1/2} \qquad \text{(I-22)}$$

The group of constants labeled (a) is the slope of a Rate *versus* $P_{NH_3}{}^{1/2}$ plot. The experimental value for this slope (a) at 673K (see Figure I-22(b), page 89) is 9.7×10^{14} molec cm^{-2} sec^{-1} $\mu^{-1/2}$. It is seen that slope (a) = $(k_1 \times I_R)^{1/2} = k_1 \times I_P$. Inserting the determined values gives a theoretical slope (a) of 7.6×10^{14} molec cm^{-2} sec^{-1} $\mu^{-1/2}$, reasonably close to the experimental value. As k_1 and k_{-3} correspondingly represent NH_3 and H_2 adsorption on the surface, it is clear that both processes are activated

Table I-3. Parameters obtained from Figure I-18 and rate constants calculated using the expressions from the text

T(K)	Ordinate[a]	S[b]	I	k_1 (molec $cm^{-2}sec^{-1}\mu^{-1}$)	k_{-3} (molec $cm^{-2}sec^{-1}\mu^{-1}$)
633	$P_o^{1/2}$	.075	.36	6.2×10^{14}	1.0×10^{14}
	R_o	1.60×10^{13}	1.0×10^{14}	5.0×10^{14}	9.6×10^{13}
673	$P_o^{1/2}$	.068	.33	2.3×10^{15}	3.1×10^{14}
	R_o	4.8×10^{13}	3.0×10^{14}	1.9×10^{15}	2.9×10^{14}

[a]Units of $P_o^{1/2}$ and R_o are $\mu^{1/2}$ and molec cm^{-2} sec^{-1}, respectively.

[b]Units of S_{P_o} are $\mu^{-1/2}$, units of S_{R_o} are molec cm^{-2} sec^{-1} μ^{-1}.

as the constants increase with temperature. Crude activation energies calculated from the data available are $E_1 \approx 27$ kcal/mole and $E_{-3} \approx 24$ kcal/mole.

In conclusion, the theoretical mechanism and equation I-14 appear to fit the NH_3 order data quite well. Two rate constants are estimated and will be used in later considerations. The H_2 order data cannot be fit as easily to equation I-14 over the entire H_2 pressure range. An empirical treatment of the H_2 order data will be presented and is correlated quantitatively to the mechanism rate expression.

As stated previously, the H_2 order varied from 0 to -1.0 on the Rh catalysts studied. As seen in the Literature Review, a number of catalysts exhibit -1.5 H_2 order at high P_{H_2} which is comparable to -1.0. About 80% of the H_2 order determinations fit better to a -1.0 order over the pressure region studied such that this order is assumed to be valid for this Rh study.

Empirically, the H_2 order data are fit to the following expression (a modified version is used in reference (50)):

$$\frac{R_{oH}}{R_H} = kR_{oH}P_{H_2} + 1 \qquad (P_{NH_3} = \text{constant}) \qquad \text{(I-23)}$$

which is not obviously suggested by equation I-14. Here, R_H is the decomposition rate for the H_2/NH_3 mixture, R_{oH}

is the rate for the particular NH_3 pressure ($P_{H_2} = 0$) and k is functionally an inverse rate constant. A plot of R_{oH}/R_H *vs* P_{H_2} will give a straight line of slope kR_{oH}. Figure I-19 shows these plots for the available data at 633 (a) and 673K (b). As mentioned previously, the data have been adjusted to a standard to compensate for day-to-day errors. In general, the linearity is quite good and using the experimentally obtained R_{oH}s, the appropriate ks are calculated. A plot of log k *vs* log P_{NH_3} will give the NH_3 dependence of k. Figure I-20 shows that at both temperatures there is an inverse dependence on P_{NH_3}:

$$k = \frac{1}{k'P_{NH_3}} \qquad (P_{NH_3} \neq 0) \tag{I-24}$$

Therefore, equation I-23 becomes:

$$\frac{R_{oH}}{R_H} = \frac{P_{H_2}}{k'P_{NH_3}} + 1 \tag{I-25}$$

Hence, the slopes from Figure I-19 will give values for k' which should be independent of pressure. The results to this point are listed in Table I-4.

At 633K, over the NH_3 pressure range of interest (see Figure I-22(a), page 89) the following is true: $R_{oH} \cong k'P_{NH_3}^{1/3}$. Substituting this into equation I-25 gives:

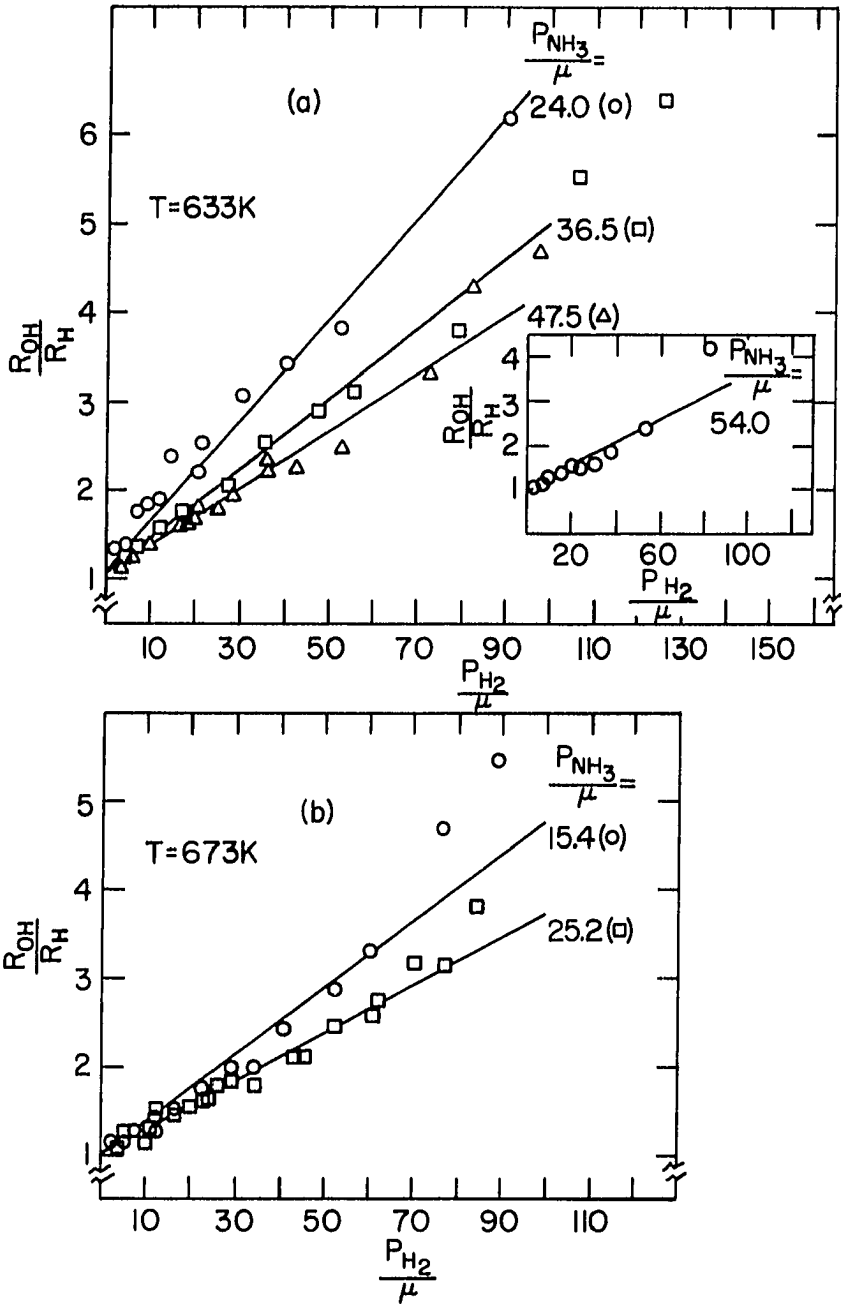

Figure I-19. Graphs of R_{oH}/R_H versus P_{H_2} at various ammonia pressures where:

$$\frac{R_{oH}}{R_H} = k\, R_{oH} P_{H_2} + 1$$

(a) 633K (b) 673K

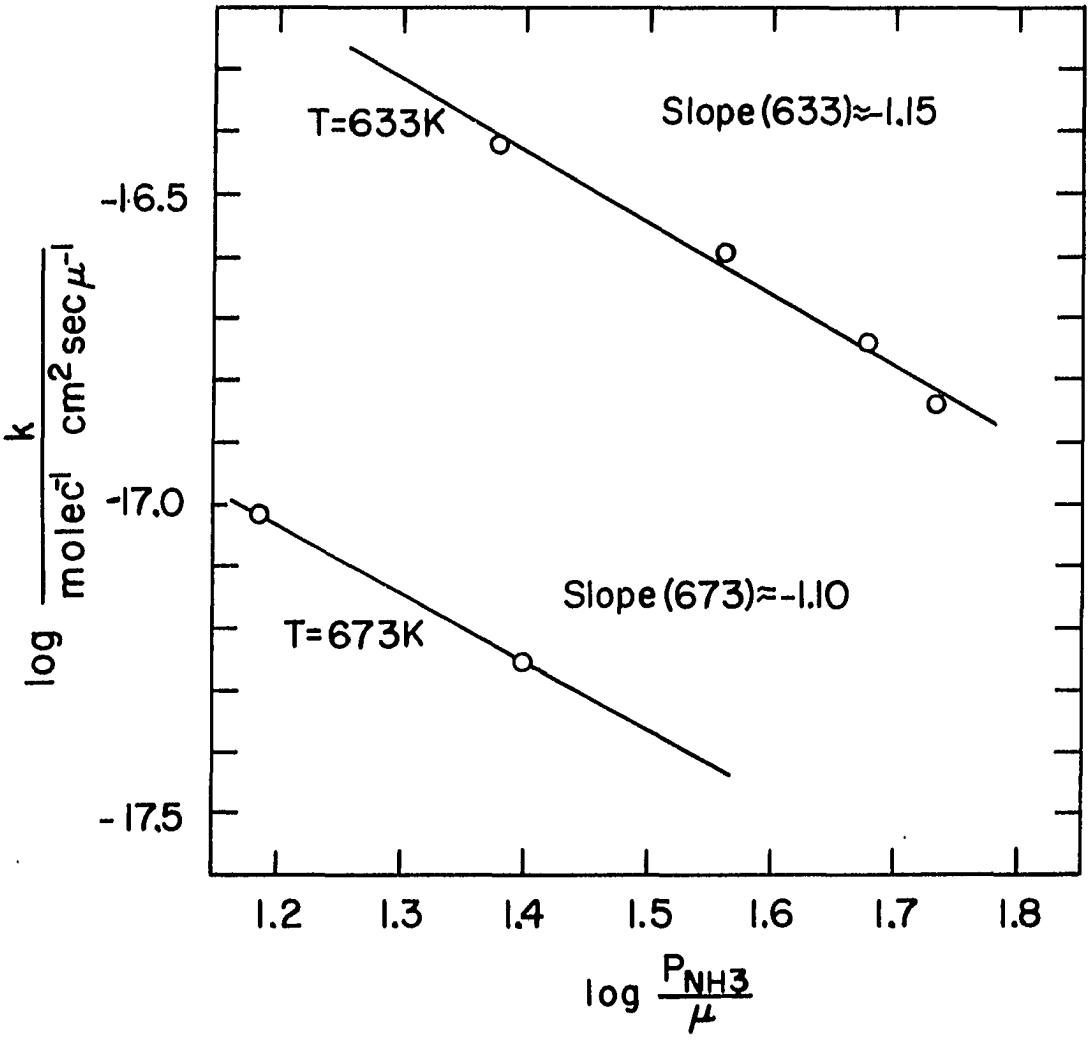

Figure I-20. Dependence of k on P_{NH_3} at 633 and 673K (Slopes of ∿-1.0 imply equation I-24.)

Table I-4. Calculated parameters relevant to equations I-23 and I-25. (Experimental values of R_{OH} are implied by the slope and k and hence are not listed)

T(K)	P_{NH_3} (μ)	Slope (μ^{-1})[Fig. I-19]	k (molec^{-1} cm^{2}sec μ^{-1})	k' (molec cm^{-2}sec^{-1})
633	24.0	.057	3.74×10^{-17}	1.12×10^{15}
	36.5	.040	2.53×10^{-17}	1.08×10^{15}
	47.5	.032	1.81×10^{-17}	1.16×10^{15}
	54.0	.077	1.48×10^{-17}	1.25×10^{15}
			Average	$\cong 1.14 \times 10^{15}$
673	15.4	.038	9.41×10^{-18}	6.90×10^{15}
	25.2	.027	5.47×10^{-18}	7.25×10^{15}
			Average	$\cong 7.07 \times 10^{15}$

$$R_H^{633} = \frac{k'' P_{NH_3}^{1/3}}{1 + k''' \frac{P_{H_2}}{P_{NH_3}^{2/3}}} \qquad k''' \equiv \frac{k''}{k'} \tag{I-26}$$

Similarly, at 673K (Figure I-22(b), page 89), R_{oH} can best be represented by: $R_{oH} \cong k'' P_{NH_3}^{1/2}$, which leads to:

$$R_H^{673} = \frac{k'' P_{NH_3}^{1/2}}{1 + k''' \frac{P_{H_2}}{P_{NH_3}^{1/2}}} \tag{I-27}$$

Now, by plotting R_{oH}/R_H vs $P_{H_2}/P_{NH_3}^{2/3}$ (for 633K) and R_{oH}/R_H vs $P_{H_2}/P_{NH_3}^{1/2}$ (for 673K), all the H_2 order data will be superimposed on a straight line of slope k'''. Figure I-21 shows that this is indeed the case at both temperatures. Then since both k' and k''' are known, k'' can be calculated. The final rate equations are then given by:

$$R_H(633) = \frac{5.13 \times 10^{14} P_{NH_3}^{1/3}}{1 + .45 \frac{P_{H_2}}{P_{NH_3}^{2/3}}} \tag{I-28}$$

$$R_H(673) = \frac{1.04 \times 10^{15} P_{NH_3}^{1/2}}{1 + .147 \frac{P_{H_2}}{P_{NH_3}^{1/2}}} \tag{I-29}$$

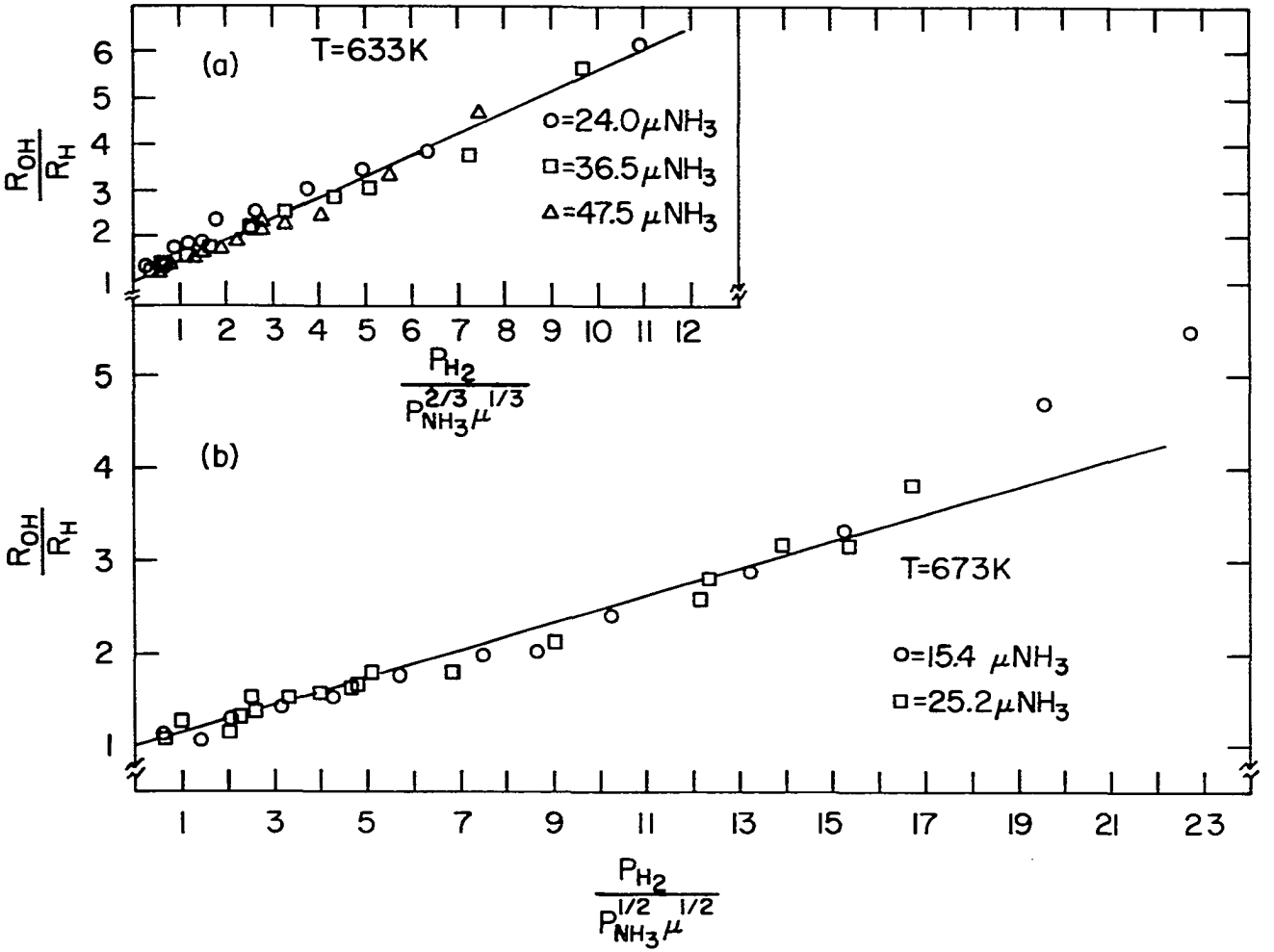

Figure I-21. Superposition of all H_2 order data on linear plots with slopes equalling k''' as defined in equation I-26: (a) 633K, $k''' = .45\ \mu^{-1/3}$ (P_{H_2} = 54 μ data omitted for clarity); (b) 673K, $k''' = .147\ \mu^{-1/2}$

These rate expressions should theoretically fit the kinetic data for any of the reaction mixtures.

Figure I-22 shows the NH_3 data ($P_{H_2} = 0$) at 633 and 673K with the straight lines being calculated from the above expressions. The fit in both cases is quite good. Two examples of calculated H_2 orders relative to the experimental data are shown in Figure I-23, the correlation being very good considering the scatter in the R_{oH}/R_H plots presented previously (Figure I-19).

Figure I-24 depicts two examples of experimental NH_3 order data ($P_{H_2} \neq 0$) with the solid curves calculated for the particular conditions using equations I-28 and I-29. The fit is poorer in these cases but still acceptable in that the reaction order trends are definitely maintained. It appears that all of the data presented are internally consistent to within about 20% which, considering the methods of analysis, is acceptable.

The data presented have been fit by two separate expressions. The first is equation (I-14) developed from the proposed mechanism. The second is the "empirical" expression discussed above. The two equations predict the same reaction orders but functionally are somewhat different. In general, at the two extremes of NH_3 pressure, the correlation between the two functions is not exceptional. However, in the pressure region of interest here (1→400 μ),

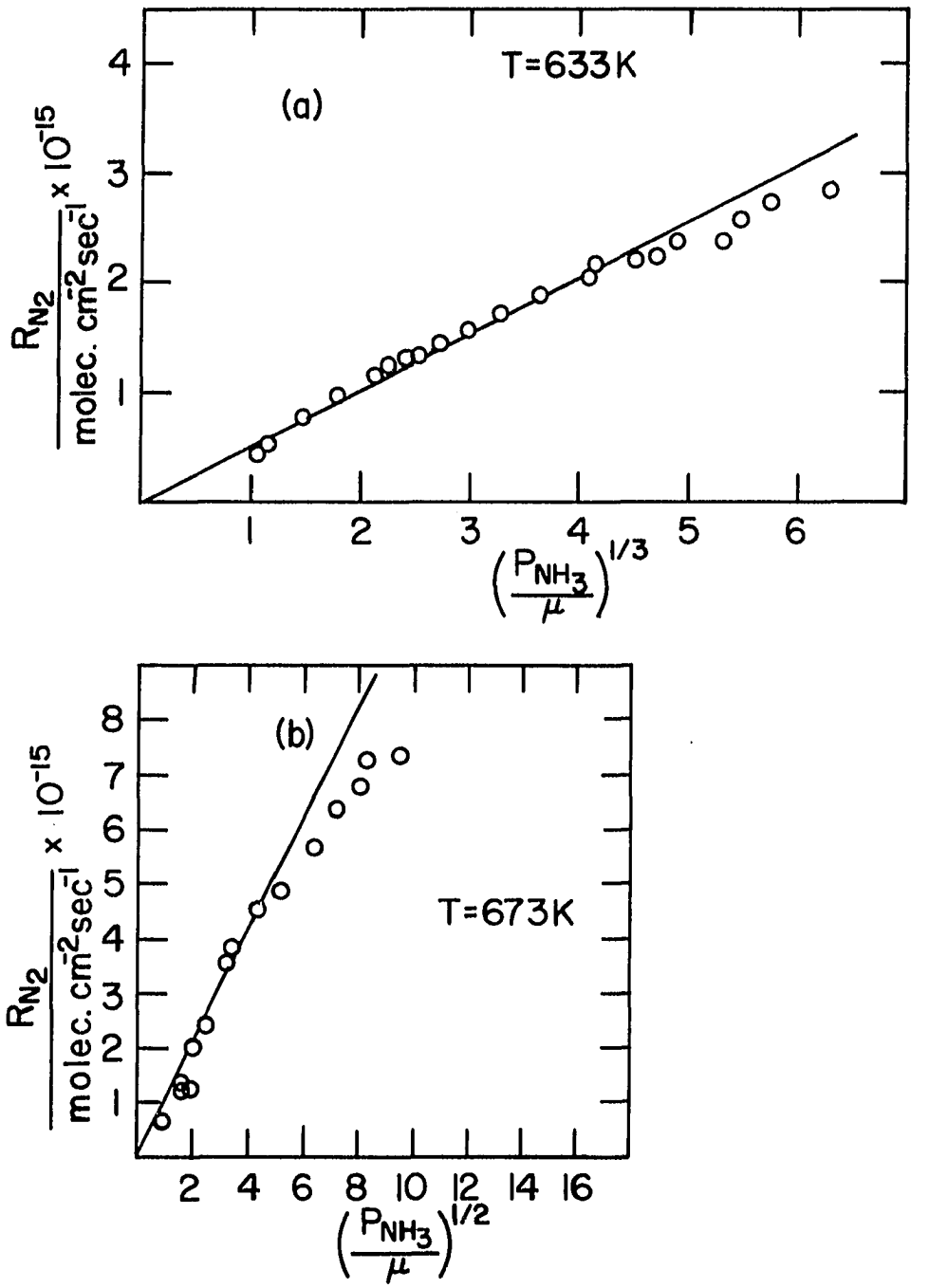

Figure I-22. Representation of NH_3 data (P_{H_2} = 0) with theoretical fits calculated from:
(a) Equation I-28, 633K
(b) Equation I-29, 673K

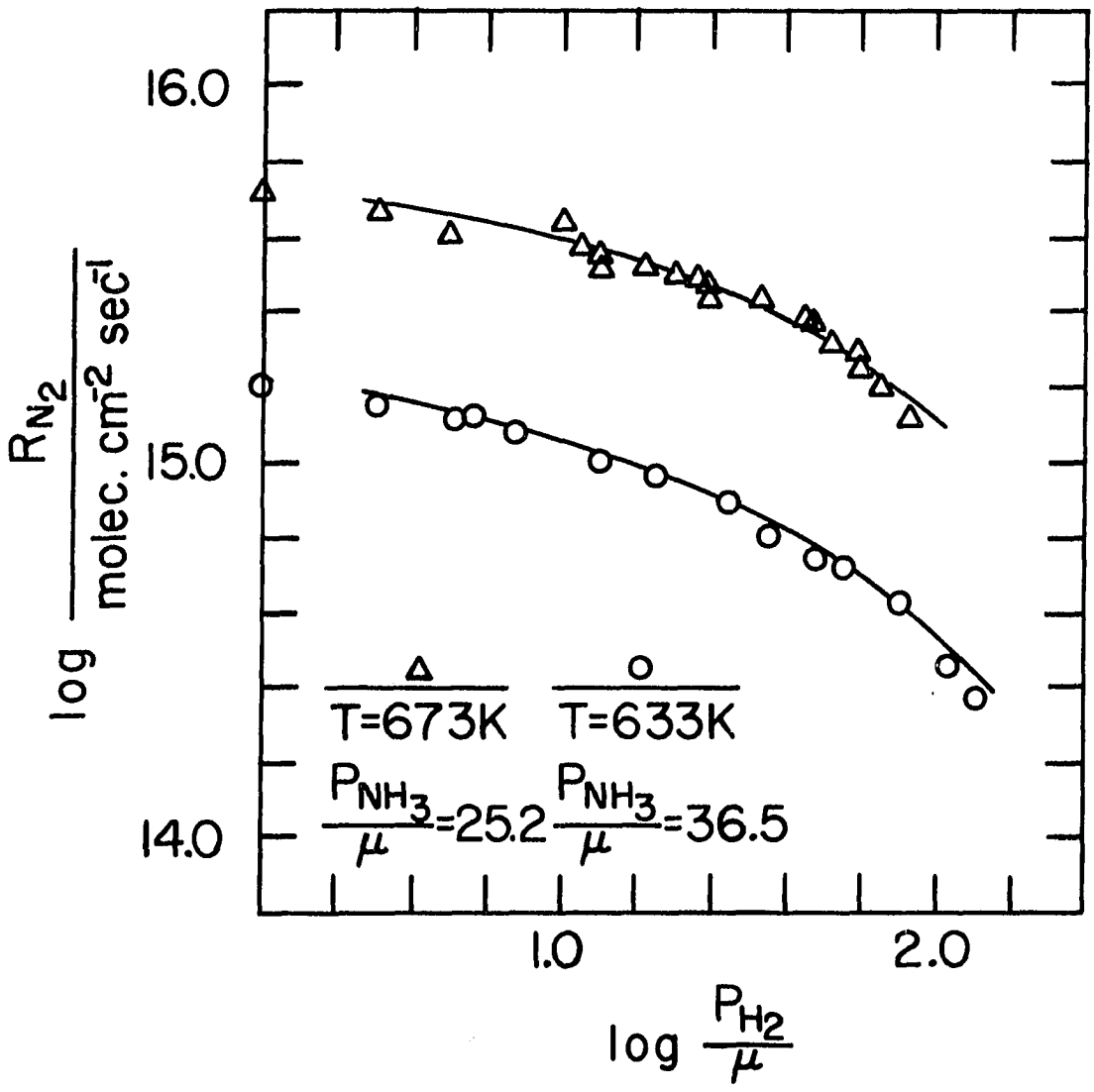

Figure I-23. Dependence of rate of N_2 production on hydrogen pressure with theoretical curves calculated from equation I-28 (633K) and equation I-29 (673K) (Points on ordinate correspond to R_{OH}.)

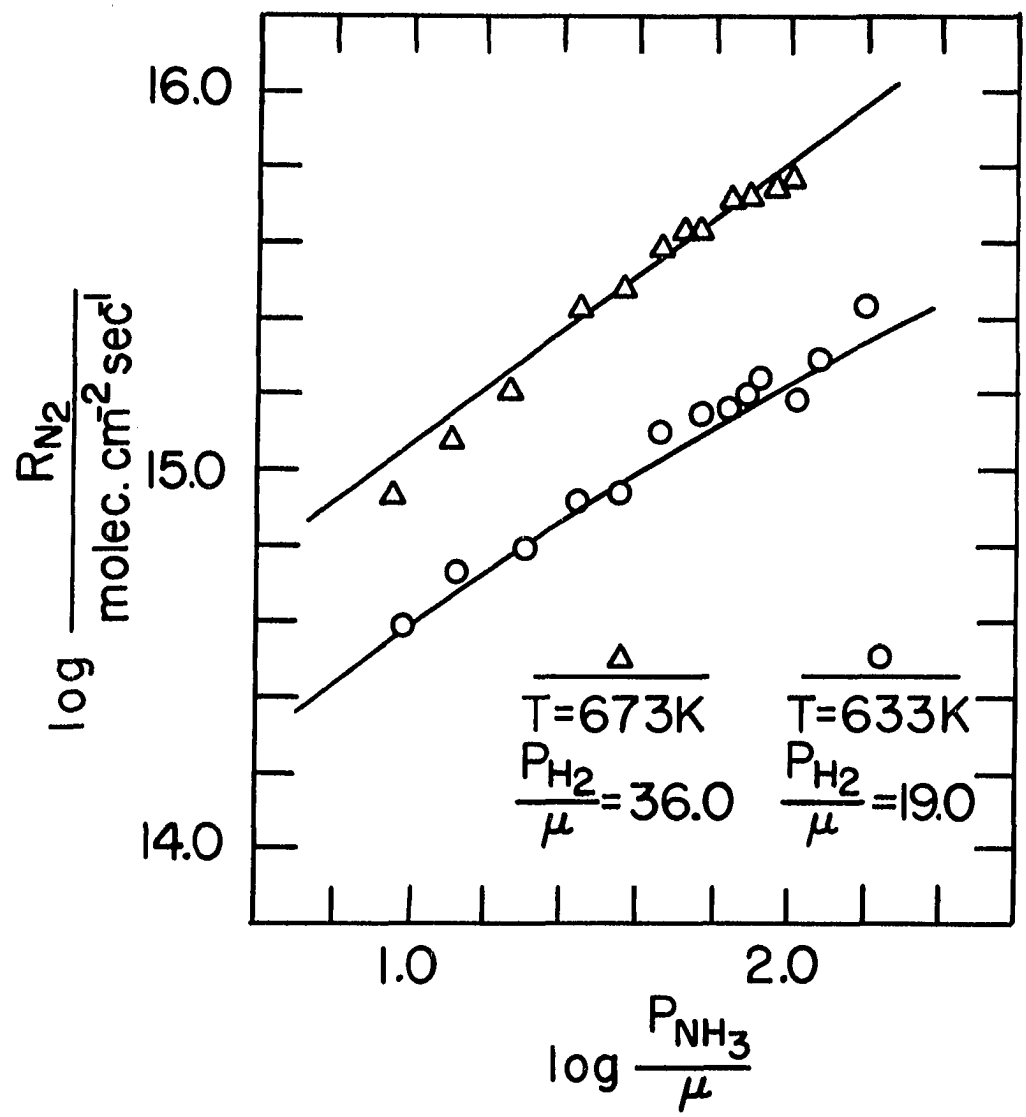

Figure I-24. Examples of NH_3 order data ($P_{H_2} \neq 0$) correlated with curves calculated from equations I-28 and I-29 for the specified conditions

the two functions are very similar. Figure I-25 shows this remarkable similarity. The circled points are calculated from either expression I-28 or I-29 at the given conditions. The solid curve is the best superposition of the "mechanism" function. It is obvious that the two functions correspond very nicely in both cases, at least as well as the experimental data correlate with the mechanism function. Values of P_o and R_o can be obtained from these superpositions; several examples of the $P_o^{1/2}$s are plotted as squared points on the graphs in Figure I-18. The excellent correspondence of these points to the experimental data indicates that the superposition method can at least be deemed semiquantitative.

The pure NH_3 data need further analysis as there are obvious deviations from the predicted 1/2 order in NH_3. At low temperatures ($\sim$590K), the NH_3 order is $\sim$1/3 throughout the pressure region. As the temperature is increased, the 1/2 order begins to develop at low pressures and becomes 1/2 order throughout at high temperatures ($\sim$700K). Most of the Rh(100) and (111) studies were done at T>700K and exhibited $\sim$1/2 order over the entire pressure region. The theory developed thus far does not predict this type of behavior but reasonable modifications do provide a qualitative explanation for the above phenomenon.

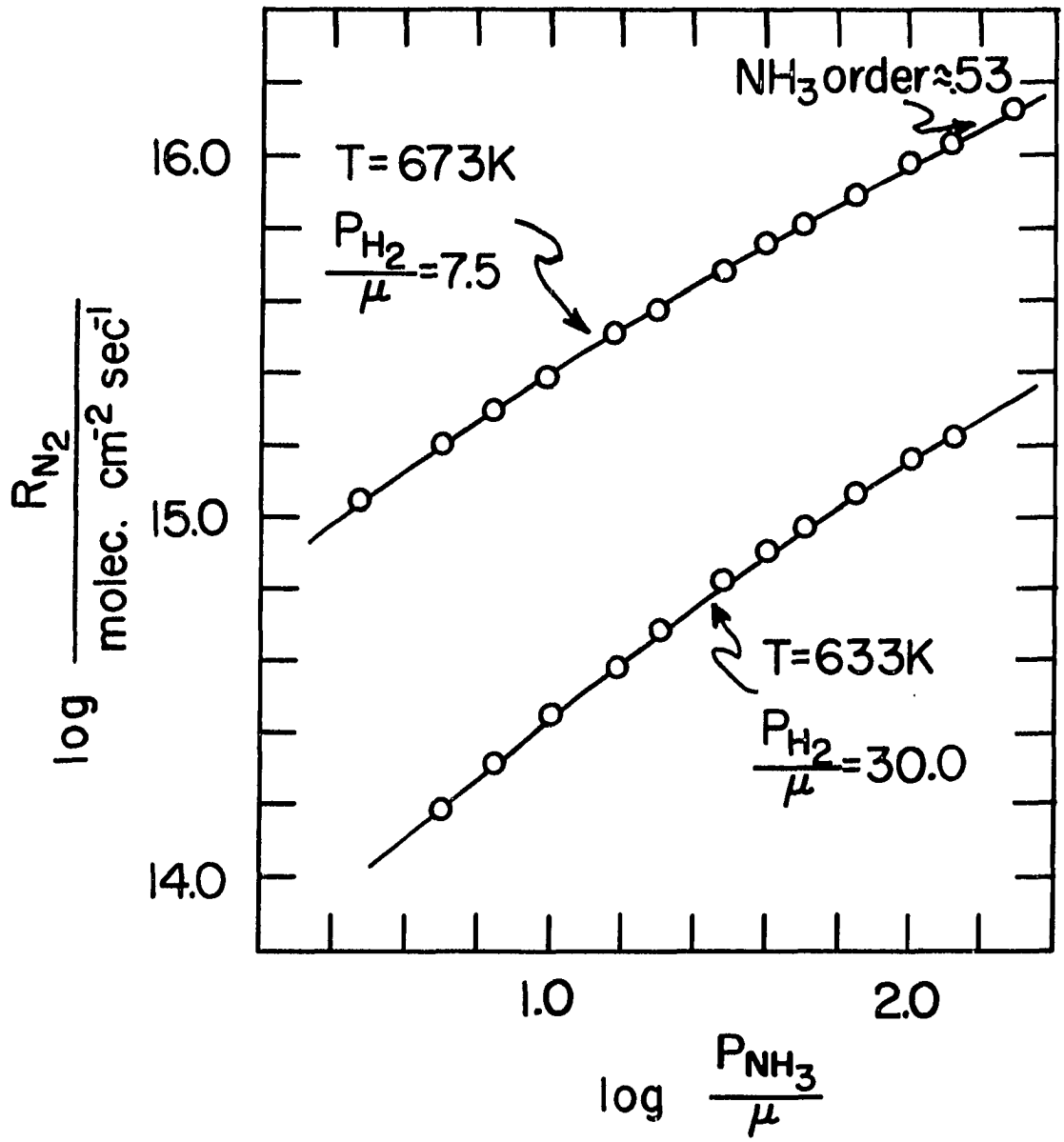

Figure I-25. Examples of the superposition of calculated data from equations I-28 and I-29 onto the mechanism "function". The values of $P_o^{1/2}$ obtained from these "empirical" superpositions are shown as squares in Figure I-18

In the derivation of the mechanism rate law (Equation I-14), it is assumed that [Rh] ≅ constant (Q) ≅ 1, i.e., that the fractional surface coverages of all adsorbed species are small compared to 1. Suppose this is not true for one species, e.g., RhN. Considering equation I-13 with the same assumptions used in the derivation of equation I-22, and recalling equation I-10, the following expression is derived:

$$\frac{[RhN]^2}{[Rh]^2} = \left(\frac{k_1 k_2 k_3 P_{NH_3}}{6 k_{-1} k_4^2}\right)^{1/2} \equiv \beta \qquad (I-30)$$

In this derivation, it will be assumed that the amount of RhN on the surface is nonnegligible at low temperatures, a valid assumption in light of the Auger and flash desorption results. Hence, if [RhN]≡θ, then [Rh] = 1-θ. Then equation I-30 becomes: $\theta^2/(1-\theta)^2 = \beta$. The rate of the decomposition reaction is $\propto \theta^2$ and $P_{NH_3} \propto \beta^2$. Therefore, a plot of log θ^2 versus log β^2 will provide another superposition curve which should correlate with the NH_3 order data under consideration. Figure I-26 shows this plot with the 633K data set superimposed as an example. The fits at the other temperatures studied are generally not as good. The 673K data show a greater curvature than the theoretical curve while the 588K data show less curvature. The theory is hence not quantitatively correct, quite possibly due to the presence of other species; for example, the surface

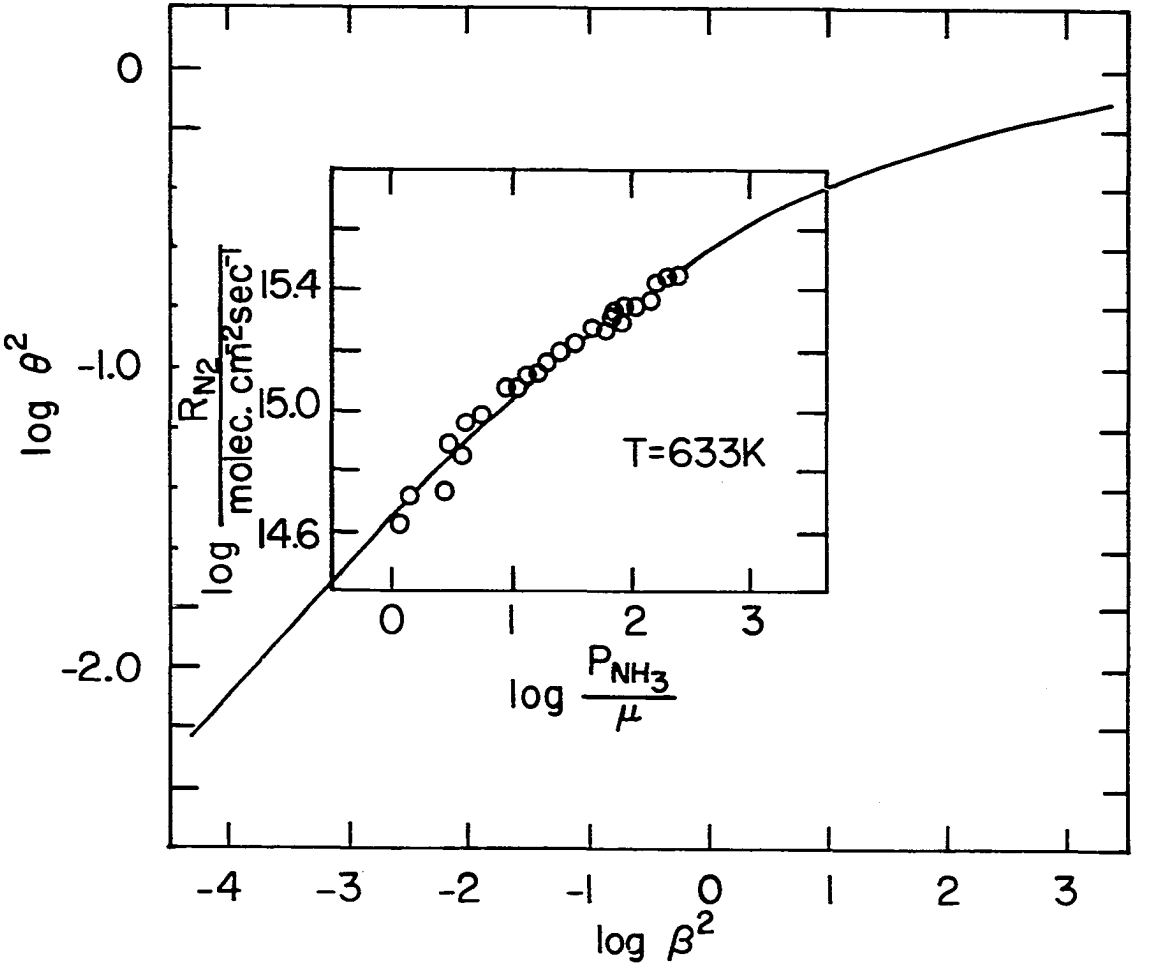

Figure I-26. Correlation of pure NH_3 data at 633K with the log θ^2 <u>versus</u> log β^2 curve obtained from equation I-30, showing the actual and theoretical decrease in NH_3 order. A value of 9×10^{15} molec cm^{-2} sec^{-1} for k_4 is extracted from this curve and other information available

concentration of Rh_2NH may also be building up. However, the 633K data fit rather well and provide a semiquantitative means of obtaining the rate constant, k_4. From this superposition, $\beta^2 \cong .224$ at $P_{NH_3} = 100\ \mu$. Now the data for $P_{NH_3} < 17\ \mu$, can be fit reasonably well to 1/2 order in NH_3 (see equation I-22). The slope from this fit is given by:

$$\text{Slope} = \left(\frac{k_1 k_2 k_3}{6k_{-1}}\right)^{1/2} = 4.06 \times 10^{14} \text{ molec cm}^{-2}\text{sec}^{-1}\mu^{-1/2} \quad \text{(experimental)} \qquad \text{(I-31)}$$

All the other parameters in equation I-30 are known so that:

$$k_4 = \left(\frac{k_1 k_2 k_3}{6k_{-1}\beta^2} P_{NH_3}\right)^{1/2} \cong 9 \times 10^{15} \text{ molec cm}^{-2}\text{sec}^{-1} \qquad \text{(I-32)}$$

This value of k_4 should be only qualitatively accurate as the theory is obviously oversimplified. However, the chemical basis for the theory is sound and indeed the curve in Figure I-26 does mimic the kinetic trends observed. At the higher temperatures, the surface should be nearly devoid of N species even under reaction conditions, giving the 1/2 order in NH_3. With H_2 in the system, the number of N containing species is again small, with Rh being the major surface species. The deviation toward 1/3 order at low temperatures may account for the increased activation energy ($\sim$23 kcal/mole) in this temperature region as the 1/3 order rates are lower than they would be if the data were

proportional to the 1/2 power in P_{NH_3} as is the case for T > 673K.

Experimental and Theoretical Implications

From the results reported, it is clear that the NH_3 decomposition reaction occurs very readily on Rh in the temperature range 620-720K and NH_3 pressures of 1-500 μ. The turnover number (molecules N_2 (reactive site)$^{-1}$ sec^{-1}) is approximated as ∿.1 to 10 in this temperature region which indicates excellent reactivity. The definition of a reactive site will be considered in subsequent discussion. There are several more experimental considerations that will now be mentioned.

First, the results in this study tend to support the findings of Amano and Taylor (55) and Sokol'skii *et al.* (47). The seemingly anomalous results of Logan and Kemball (46) can be partially explained. As mentioned previously, the activation energy for the NH_3 reaction increased with increasing H_2 pressure. Hence, one would expect the activation energy for a 6:1 H_2-to-NH_3 mixture used by Logan and Kemball (∿57 kcal/mole) (46) to be "abnormally" high relative to other findings. In fact, if the 633K H_2 order data are fit to an equation like I-27 (*i.e.*, $P_{NH_3}^{1/2}$ instead of $P_{NH_3}^{1/3}$), the values of the constants, k" and k'" can be compared at 633 and 673K. Table I-5 lists the determined

parameters. This indicates that as the H_2 pressure increases, the activation energy should also increase as is experimentally observed. The rate constants determined for the H_2 pressure limits in equation I-14 are quite different, implying different activation energies. However, relative to the other Rh studies discussed, the reaction orders of Logan and Kemball (46) are yet to be rationalized and appear in error.

Table I-5. Comparison of rate parameters and energies as a means of predicting trends in apparent activation energies (see equation I-27 for definition of parameters)

T(K)	k" (molec $cm^{-2}sec^{-1}\mu^{-1/2}$)	k''' ($\mu^{-1/2}$)	$E_{k"}$ (kcal/mole)	$E_{k'''}$ (kcal/mole)
633	3.40×10^{14}	.26	+24	-12
673	1.04×10^{15}	.147		

When comparing the results of this study with those on other metals, it is clear the Rh is one of the more active NH_3 decomposition catalysts. Using Löffler and Schmidt's parameters on Pt(110) (54), the rate calculated at 10 μ NH_3 at 673K is over an order of magnitude less than the rate determined in this study on Rh. This substantiates the

contention that Rh is more active than Pt (46,47). For the most active W single crystal (35) to produce rates comparable to those reported here on the Rh(110), a temperature ∿200K higher would be required. Hence, Rh is a very efficient decomposition catalyst at very mild conditions.

A direct comparison with results reported by Pignet and Schmidt (57) is possible. Using the data reported in their figure 1, an approximate activation energy from 923K and up is determined and used to extrapolate the rate at 673K. On a Rh wire, this calculation gives a rate of 8×10^{15} molec cm^{-2} sec^{-1} at 115 μ and 673K; here the rate at those conditions was 7.5×10^{15} molec cm^{-2} sec^{-1}. Hence, the rates reported here correlate very well with Pignet and Schmidt. If the pressure conditions of Logan and Kemball's Rh film work (46) are inserted into equation I-29, a rate of $\sim 1 \times 10^{15}$ molec cm^{-2} sec^{-1} is calculated, over 3 orders of magnitude greater than they reported (46). This fact detracts further from the credibility of the Rh film study.

The kinetics of this study in general do not correlate with the Temkin-Pyzhev theory. The 1/2 order in NH_3 is not predicted by the theory and the 1:1 ratio of NH_3 order to H_2 order is not explicitly postulated by the T-P theory. It is noted that Friedlander et al. (51) determined that for low pressures (<1 torr), the revised T-P equation (17) predicts +1 and -1 orders in NH_3 and H_2, respectively. This

derivation was made using parameters for Fe (17) which may have no relevance to the study presented here. Indeed, the -1.5 order in H_2 on Pt (54) at P < 1 torr would be difficult to explain via this theory. This is another example of the questionable flexibility of the T-P theory.

The reaction orders observed in this study are not unprecedented in the literature. Mardaleishvili et al. (49,50) observed the same trends on Ni as found here for Rh. A fractional order in NH_3 was observed on W single crystals (35) and VN (45). As seen in the kinetic analysis, the data collected displayed good internal consistency from one set of conditions to the next. Considering all these factors, it is concluded that the reported results give a reasonable representation of the decomposition reaction on Rh.

The mechanism proposed for the NH_3 decomposition reaction on Rh (equations I-7) predicts the observed kinetics and seems chemically reasonable. Admittedly, there may be other mechanisms or modifications of the proposed one which will fit the experimental results. There are, however, some unique features in the mechanism presented here which make it quite attractive from a chemical standpoint.

The proposed mechanism involves the initial adsorption of NH_3 on Rh to produce species like RhH, Rh_2NH and RhN. The actual surface structure of these proposed intermediates would be of great interest. Chemically and physically

reasonable proposals for these intermediates will be given. Arguments concerning face specificity will also be presented.

The species, RhH, is simply a single H atom adsorbed on a surface Rh atom. As discussed in Part II of this dissertation, there is much evidence for single site H adsorption onto protruding surface atoms rather than in holes or defects in the surface. However, at the reaction temperatures (588-725K), the H atom should be extremely mobile on the surface and the RhH intermediate very short-lived; yet, with a high H_2 pressure, enough RhH is present to cause the reverse of the NH_3 adsorption step #1 to become significant, reducing the concentration of the critical intermediate, Rh_2NH.

The Rh_2NH intermediate is the unique species in the mechanism. The species is postulated to be a bridged NH between two Rh surface atoms. There are several reasons for choosing the particular stoichiometry indicated. The Rh_2NH satisfies the trivalency of nitrogen. The possible surface structures are depicted in Figure I-27 (a) and (b). The Rh-Rh distances on the Rh(110), (100) and (111) surfaces are 2.69Å and 3.80Å. If an approximate Rh-N distance of 2.00Å (sum of covalent radii) is chosen, the narrow bridge (a) shows a Rh-N-Rh bond angle of $\sim$85° while the wide bridge shows $\sim$144°. If there is any multiple bonding, the 2.00Å distance will be shortened, causing the (a) configuration

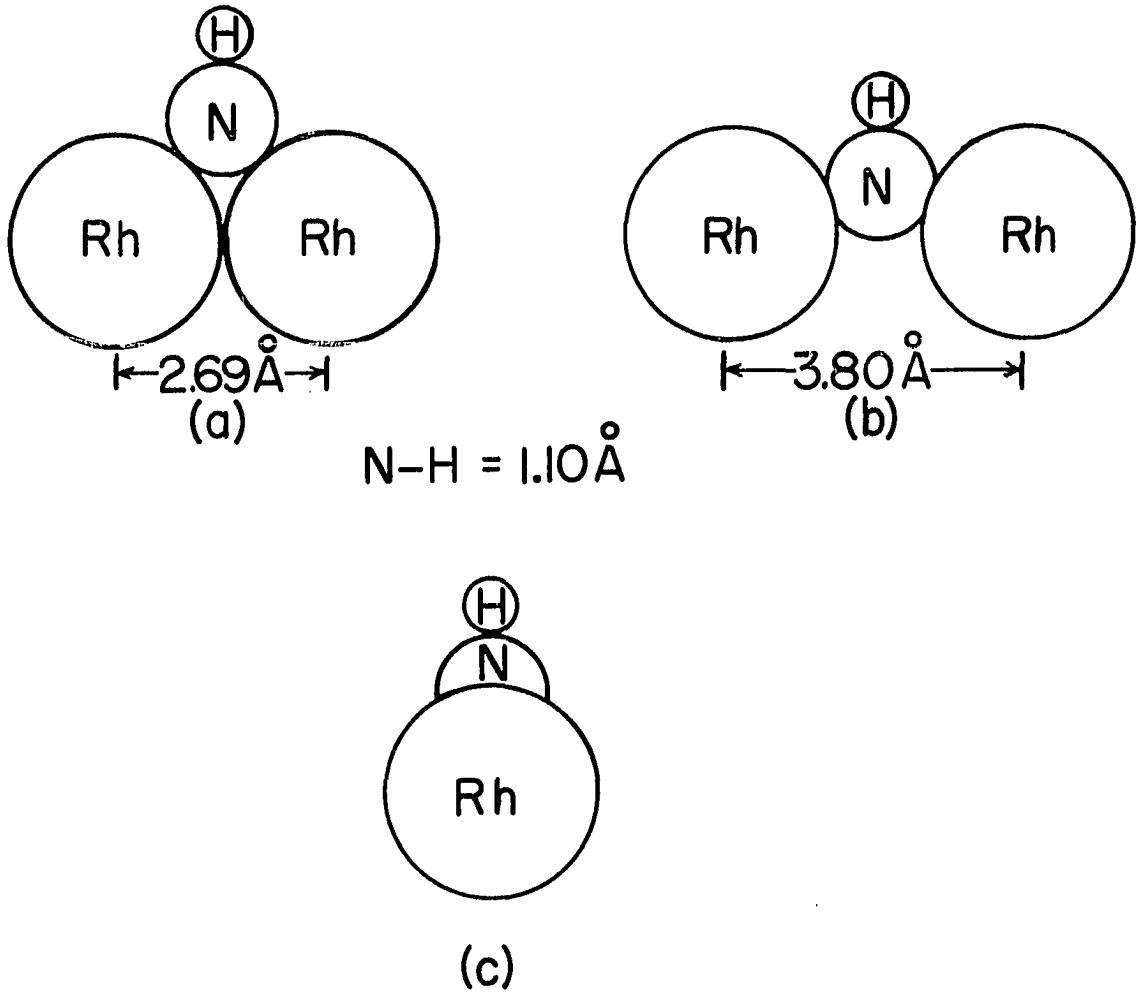

Figure I-27. Possible surface structures for the intermediate, Rh_2NH:

(a) Rh-Rh at nearest neighbor distance (Rh-N-Rh angle = 85° for Rh-N = 2.00 Å)

(b) Rh-Rh at 3.80 Å (Rh-N-Rh angle = 144°)

(c) "Side" view of planar Rh_2NH

to become more feasible from an angle standpoint. The discussion below will further clarify this point.

The N-H bond of the intermediate could be within the Rh-N-Rh plane (i.e., Rh_2NH = planar) or bent with respect to the plane (pyramidal). Chemically, the planar "structure" shown in Figure I-27(c) is deemed most reasonable. If the adsorbed intermediate were planar, the unhybridized N 2p orbital could interact with the Rh atoms via $d\pi$-$p\pi$ bonding. Indirect evidence for this exists in the form of trisilylamine, $(H_3Si)_3N$, as discussed by Cotton and Wilkinson (82). This compound is indeed planar, supposedly due to $d\pi$-$p\pi$ bonding utilizing the empty Si d orbitals. In the present case, this type of bonding would tend to stabilize the planar Rh_2NH over the pyramidal one. Furthermore, the decomposition of the planar species would be somewhat "difficult" relative to the initial dehydrogenations as the H atom is as far from the Rh surface as possible. This provides some credibility to the assumption that step #2 of the mechanism is slow. If the Rh_2NH were planar, then the large bond angle in Figure I-27(b) would not be appropriate for sp^2 hybridization on N. If, in fact, the π interaction did shorten the Rh-N bond distances, structure (a) would become more feasible due to increasing bond angle. It is not possible to distinguish fully between the wide and narrow bridge but the latter choice appears both chemically and physically feasible.

A species such as RhNH is unreasonable for two reasons. First, the decomposition of this species would require a bare Rh atom "in" the mechanism to accept the H. This introduces the possibility of a negative order in NH_3 at high nitrogen species coverage which is not evident kinetically. The Rh_2NH "mechanistically" has the Rh atom readily available to the hydrogen. Furthermore, the RhNH species would require at least a full double bond between Rh and N. The surface valency of the Rh atom is probably limited such that the possibility of a species of this form is reduced.

Finally, the RhN intermediate is considered. As mentioned in Part II of this thesis, N is believed to reside in multi-coordinate holes of four-fold symmetry on the surface. This would correspond to the troughs on the Rh(110) surface (Figure I-2). If this type of coordination site is not available, the N may prefer a top position on a protruding atom. At the reaction temperatures, the surface nitrogen atom should be relatively mobile and may choose either a hole or top position as is "convenient".

The stoichiometry of the Rh_2NH species may be misleading. It may in fact be that several Rh atoms are involved in the formation of RhN in step #2 of the mechanism. The stoichiometry stated is clearly the simplest possible and could be lacking in specific details.

The mechanism proposed is somewhat unique in that there are two reactions which are coupled in a rate limiting sense; it may in fact be inappropriate to speak of a rate limiting step in this case. In terms of the production and consumption of N surface atoms, the rate of the dehydrogenation of Rh_2NH is equal to the rate of the nitrogen desorption step. Hence, the decomposition of NH_3 on Rh under the conditions specified here is an example of a non-Temkin-Pyzhev process which has N_2 desorption as rate limiting. The isotope effect observed clearly becomes involved in step #2 of the mechanism, ND_3 producing the species RhN slower than NH_3. Therefore, internal consistency is maintained.

In the other single crystal studies of NH_3 decomposition cited (35,54), the only comments made concerning face specificity were in reference to the postulated total inactivity of the most closely packed faces. Though total inactivity seems to be too drastic a conclusion, greatly reduced activity is clearly possible. The Rh(110), (100) and (111) surface atoms have 7, 8 and 9 nearest neighbors, respectively. If a surface atom has few nearest neighbors then more orbital overlap should be possible with an adsorbing atom(s). It may be that the Rh(100) and (111) faces would be as efficient decomposition catalysts as the (110) but the initial adsorption of NH_3 may be much less on these faces. Furthermore, there are several different

near-surface atoms present on the (110) while all the atoms in the (100) or (111) are identical. Different types of sites may be required for substantial decomposition (i.e., on the Rh(110) here) though these specifically are not required in mechanism-kinetics arguments. As the kinetics are the same on each face, it is logical to assume that the mechanism (i.e., intermediates) is the same on each face. It may be that the most reactive faces form and decompose these intermediates more readily.

In summary, it has been shown that the mechanism proposed for the NH_3 decomposition reaction on Rh is both chemically and kinetically reasonable though not necessarily unique. The structures of the proposed intermediates can only be conjectured without any concrete structural evidence. The mechanism proposed differs only slightly from the McAllister-Hansen mechanism on a nitrogen covered W surface (35). This indicates that reaction pathways may not vary much from metal to metal. The basic differences concern whether a bare or covered surface is the active catalyst and the extent of the initial dehydrogenation of the impinging NH_3. The zero order in H_2 on W (35) is probably due to the very high temperatures required for reaction; the H_2 will not adsorb at these temperatures. It appears that temperature plays a vital role in determining the reaction kinetics. At very high temperatures, the impinging NH_3 may totally dehydrogenate on

Rh, doing away with the proposed Rh_2NH intermediate and changing the kinetics.

Finally, some correlation to the NH_3 synthesis reaction on Rh can be made. Rh metal, itself, appears to be relatively inactive toward the NH_3 synthesis (22); this is true for a number of pure metals (22). According to the principle of microscopic reversibility, a synthetic pathway to NH_3 would be the reverse of the postulated reactions for the NH_3 decomposition. Therefore, the low NH_3 synthesis activity of Rh may reflect either a very low rate of adsorption of nitrogen from the gas phase (reverse of step #4 of the mechanism) or a very low rate of hydrogenation of the RhN species (reverse of step #2). As discussed previously, K promoted Rh on charcoal is quite active for the synthesis. The added K must activate the chemisorption of N_2 on Rh (i.e., make $k_{-4}(Rh)^2P_{N_2}$ relatively large) and/or increase the rate of the hydrogenation step. In general, the K probably enhances the reversibility of the critical reaction steps.

CONCLUSIONS AND SUGGESTIONS FOR FUTURE RESEARCH

The interaction of NH_3 with single crystal Rh surfaces has been studied using kinetic and isotope experiments, flash desorption spectroscopy and LEED/Auger spectroscopy. The NH_3 decomposition reaction occurs at rates of 10^{14} - 10^{15} molec cm^{-2} sec^{-1} at temperatures between 590 - 700K at NH_3 pressures of 1 - 500 μ on the Rh(110) surface. The kinetic and isotope results are explained *via* a reaction mechanism involving the dehydrogenation of a surface imine group (Rh_2NH) coupled with desorption of N_2 ($2RhN \rightarrow 2Rh + N_2$). Although the mechanism is probably not unique, there is sufficient evidence to support it as a possible explanation for the varying positive order in NH_3 and the negative order in H_2 observed. The LEED/Auger experiments along with the flash desorption results support the contention that the NH_3 decomposition reaction occurs on a fairly bare Rh surface. It appears that the least closely packed surfaces are most reactive for the NH_3 decomposition reaction while the kinetics are the same on all the surfaces studied. Finally, the reaction intermediates proposed are only speculative but are chemically and physically reasonable.

Although the initial surface characterization of the Rh(110) surface has been done in this study, a thorough investigation of the other crystal faces would be useful.

The study of activated N adsorption on Rh via LEED/AES, ESCA and UPS would be helpful in determining the exact surface environment of nitrogen on Rh. Another interesting endeavor would be the determination of poisoning effects on the NH_3 reaction on Rh. In practical catalyst systems, species such as CO, NO_x, SO_2 and O_2 are present in significant quantities such that their effect on the catalyst and reaction is of importance.

A detailed kinetic analysis of the NH_3 decomposition reaction on other metals would also be of interest. A single crystal study on Ru would be particularly useful in that Ru is an hcp metal and also the most active decomposition catalyst studied to date (47). The Ru results could then be compared to the W(bcc), Pt(fcc) and Rh(fcc) findings to determine any possible correlations to bulk metal structure on the catalytic activity.

Finally, the kinetics of both of the NH_3 reactions over supported and/or promoted Rh catalysts would be of great use. From the obvious greater activity of the "open" faces, a highly dispersed Rh catalyst consisting of very small particles would be most conducive to the NH_3 decomposition reaction. It would be of great interest to see if the kinetics of the NH_3 synthesis would correlate with the reaction mechanism proposed in this study.

PART II. HYDROGEN AND NITROGEN ADSORPTION ON A W(111) SURFACE: A THEORETICAL MOLECULAR ORBITAL APPROACH

INTRODUCTION

Recently, it has become possible to study the specific adsorption of atoms and molecules on well-defined surfaces. There are numerous surface analysis techniques which provide useful information concerning the absolute adsorption positions. In recent years, intensity analyses of LEED data have absolutely determined the surface structures of adsorbates on several surfaces. A paper by Jona (83) provides a good review of the structure determination procedures and results to date. However, this type of approach used to study adsorbate-surface interactions is extremely time consuming and expensive. A theoretical approach, though less accurate, seems justified as it can provide useful information about preferred adsorption sites. As ab initio quantum mechanical calculations are again overly expensive, the use of a semi-empirical method is appealing. The method of extended Hückel molecular orbital calculations (EHMO), though generally non-rigorous, has in the past accounted quite well for structural features in a variety of systems.

This study is a continuation of a series of investigations performed in this laboratory using the EHMO technique. The previous studies involved the adsorption of H (84) and N (85) on a truncated W(100) lattice. These investigations were performed by Anders, Hansen and Bartell. Since these studies were done, semiempirical molecular orbital theory has

been used to study numerous bulk and surface properties of metals. Excellent reviews of the recent literature have been prepared by Baetzold (86) and Simonetta and Gavezzotti (87). Examples of work on metal cluster properties have been co-authored by Baetzold (88-90).

Anderson and Hoffmann (91) and other investigators (92, 93) have recently applied the EHMO technique to appropriate surface adsorption studies. The study by Hoffmann involved the dissociative adsorption of diatomics on Ni and W. The types of generalized results obtained were a) the attraction of electrophilic species to edge atoms, b) theoretical justification for dissociative adsorption and c) fairly good correlation to photoemission results for the various gas-surface interactions. Politzer and Kasten (92) calculated stretching frequencies for CO on Ni with reasonable success using EHMO. Fassaert et al. (93), Lee and Rabalais (94) and Anders et al. (84,85) have conclusively shown that the EHMO technique is very useful for predicting preferred adsorption sites and determining the actual adsorbate-surface bonding. Other examples also tend to show that the EHMO technique can be very helpful in surface interaction studies.

The extended Hückel method does, however, have some severe limitations. In the EHMO method, excessive and unrealistic charge transfers are observed. These can be alleviated by parameter adjustment as shown later. The

electron excitation energies calculated are very crude; i.e., work functions predicted are generally extremely inaccurate. The EHMO method does not specifically take into account electron-electron and/or nuclear-nuclear repulsions. By including nonvalence orbitals, this problem can be minimized. Probably the largest source of error in EHMO is the arbitrariness inherent in the choice of matrix elements and parameters. In general, relative energies or properties can be compared with confidence while the absolute values calculated are of little use.

There are inherent difficulties with all semiempirical techniques. The CNDO method includes a lot of the same problems as mentioned for EHMO. Even though it does account for individual electron spins, CNDO neglects terms that are at least approximated in the Hückel approach. Furthermore, CNDO requires more empirical parameters than does EHMO and hence introduces even more arbitrariness.

The Hückel method does have many redeeming virtues as well. As mentioned, there are numerous instances where EHMO has successfully predicted structural geometries in molecules and on surfaces. It is useful in that both sigma and pi bonding are investigated, an extremely important feature to all areas of chemistry and physics. However, probably the most attractive quality of EHMO is its conceptual simplicity and ease of application to a number of systems. The cost of

using the technique is far outweighed by the useful qualitative chemical information which it provides. Using EHMO as a tool, scientists can qualitatively predict surface phenomena with a minimum amount of effort and expenditure.

Specifically, this work investigated the adsorption of atomic hydrogen (H) and nitrogen (N) on a truncated W(111) surface. The interactions of these species with tungsten (W) have been studied quite extensively in the literature. H adsorption on W is of interest as it produces an ordered LEED pattern on the W(100) surface (95,96), indeed a rare phenomenon. There are also numerous desorption states for H on W(111) (97,98) which could possibly be explained theoretically. For comparison purposes, there are many examples of experimental data for hydrogen on W(111) available (97-103).

Theoretical studies of N adsorption on W are of interest as N_2 adsorbs dissociatively on tungsten surfaces, a process not occurring on a number of transition metals. Data concerning N on W(111) surfaces are also available for comparison with the calculated results (44, 103-105). Finally, it is of interest to see if the Hückel method can produce chemically significant results on a number of different crystal orientations. Comparing the results of this work with previous studies on the W(100) surface (84,85) will give useful evidence concerning the universal application of the extended Hückel molecular orbital method.

PROCEDURE

The extended Hückel theory was formulated by Roald Hoffmann (106) in 1963 and was successfully applied to the determination of structural conformations of hydrocarbons. Since that time, the theory has been applied to numerous geometric and surface problems, including ionic crystals. Extended Hückel theory is semiempirical in nature and includes all overlap integrals. It is a much simplified version of the exact Hartree-Fock theory.

The molecular orbitals (MO's) are developed from a linear combination of atomic orbitals (LCAO),

$$\Psi_i = \sum_j C_{ij} \chi_j \qquad \text{(II-1)}$$

where χ_j are the single parameter, nodeless, Slater type atomic orbitals. The standard variation principle states that the function above leads to a set of j simultaneous linear homogeneous equations each containing j coefficients C_{ij},

$$\sum_j (H_{kj} - e_i S_{kj})C_{ij} = 0 \qquad \text{(II-2)}$$

The determinant of the coefficients must vanish for this set of equations to have nontrivial solutions. Hence,

$$||H_{kj} - e_i S_{kj}|| = 0 \qquad \text{(II-3)}$$

The eigenvalues e_i obtained by the solution of the above determinant are the molecular orbital energies. By inserting the e_is into the set of simultaneous equations, the coefficients C_{ij} can then be obtained. These coefficients provide the individual contributions of the atomic orbitals to the molecular orbitals at each energy.

The overlap integrals, S_{kj}, are calculated using the Slater type orbitals with appropriate parameters. In the Hückel formalism, the diagonal matrix elements, H_{kk}, are set equal to the valence orbital ionization potential (VOIP) of χ_k. The off-diagonal elements, H_{kj}, are approximated by the Mulliken-Wolfsberg-Helmholtz expression (107):

$$H_{kj} = 0.5\ K\ (H_{kk} + H_{jj})\ S_{kj} \qquad \text{(II-4)}$$

where the Helmholtz constant, K, is equal to 1.80. The program used in these studies has been listed by Leon Anders (108).

Excessive charge transfers are a major problem in the extended Hückel formalism. In the truncated lattices used in this study, the outer "edge" atoms tended to build up negative charge at the expense of the inner atoms. This problem was partially alleviated by adjusting the substrate VOIP's as functions of charge and iterating to self-consistency. In general, the equation used to incorporate the charge dependence of VOIP was (109):

$$\mathrm{VOIP}(q) = Aq^2 + Bq + C \qquad \text{(II-5)}$$

The charge, q, was computed using the method developed by Mulliken (110). A charge of zero was obtained for each "surface" atom *via* this adjustment. Energy minima calculated showed similar shifts when the VOIP's were shifted such that conclusions on preferred adsorption sites were unaffected by changing the VOIP's in this manner.

The parameters used in these calculations were the same as used by Anders *et al.* (84,85) and are shown in Table II-1.

Table II-1. Atomic orbital parameters for extended Hückel molecular orbital calculations. Orbital exponents are for the Slater-type atomic orbitals. VOIP parameters show charge dependence according to $VOIP(q) = Aq^2 + Bq + C$. Parameters are those reported by Anders *et al.* (84,85)

			VOIP Parameters		
Atom	Orbital	Exponent	A	B	C(eV)
H	1s	1.20	13.60	27.20	13.60
N	2s	1.95	3.48	20.25	28.02
	2p	1.95	3.72	14.14	16.05
W	5p	4.91	0	0	46.08
	5d	2.40	0	3.50	9.00
	6s	1.40	0	3.50	8.00

Parameters for the H 1s orbital and the N orbitals were obtained from Basch, Viste and Gray (109). The orbital exponents for the N orbitals and the W 5p orbitals were calculated using the method of Burns (111). The VOIP's (C) and orbital exponents for the W 5d and 6s orbitals were obtained from Lohr and Lipscomb (112) with the orbital charge dependences being linear. The VOIP for W 5p was taken from the tables of Herman and Skillman (113).

As shown by Anders et al. (84), the inner, nonvalence 5p orbitals must be included in the calculations to give the necessary repulsion at small interatomic distances. They chose to model this repulsive region by an exponential function and discontinue use of the W 5p orbitals. In this study, all the calculations were done using these orbitals. The pairwise additivity of the repulsive energies was good for the H case but not so for N (85). Hence, the entire orbital set was used throughout to eliminate any possible complications. In the correlation diagrams presented later, the W 5p orbitals were eliminated for clarity and simplicity.

In order to obtain a usable surface model for the W(111) surface, it was necessary to truncate the W surface to a finite number of metal atoms. The surface lattices were chosen such that they represent all the symmetric bonding positions possible. The W(111) surface has three distinct symmetric adsorption positions available. These are

presented in Figure II-1. The three positions are designated the TOP position, the SHALLOW 3-FOLD, and the DEEP 3-FOLD positions. The TOP position is located at the atom which protrudes most from the W(111) surface. The nearest identical position on the surface is 4.47 Å distant. This position was simulated using Lattice #1. The SHALLOW position is a three-fold hole where the central atom is 0.91 Å below the "TOP" atom. Lattice #2 was used to depict this position. The DEEP position is also in a three-fold hole but with two layers of atoms above the central atom. Again, Lattice #1 was used for this position. The central atom here is 1.82 Å below the top level of atoms.

Both lattices used contained seven tungsten atoms. They were chosen for either convenience or symmetry. If more atoms were included (generally beneath or surrounding the central atom), the preferred adsorption positions did not change though the energy minima calculated did shift somewhat. The lattices will be designated as W_7 and the "adsorbed" surface molecule being either W_7H or W_7N. If all of the VOIP's of the two lattices were set at the same value, the outer atoms accumulated a large negative charge. Adjusting the outer VOIP's to lower values caused all the charges on the lattices to become zero.

The "adsorption" of H or N on these lattices was accomplished by moving the adsorbing atom toward the surface and

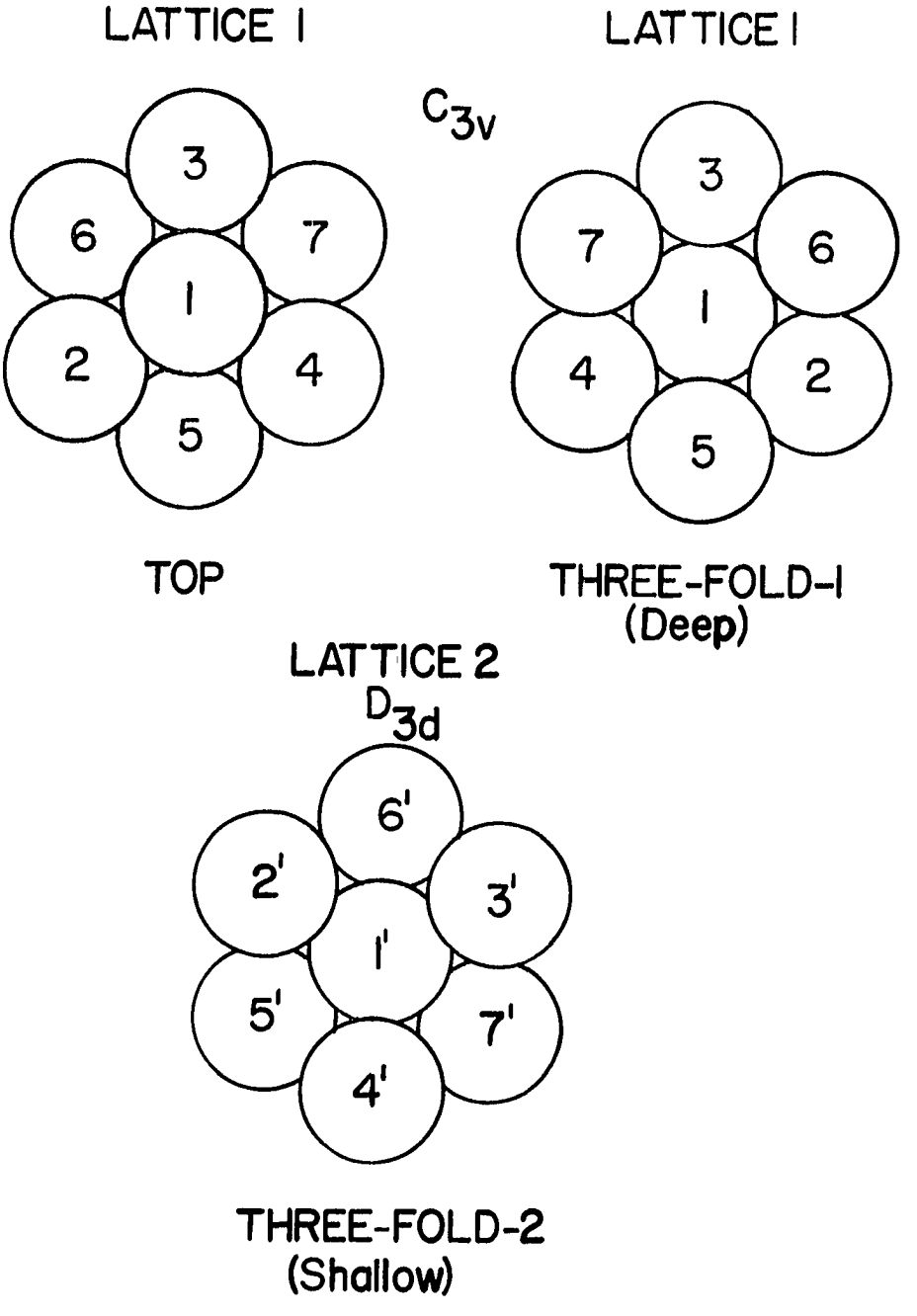

Figure II-1. Surface arrays used to model adsorption on different W(111) surface sites

computing the energy of the system at various distance intervals. The bond energy, E, was calculated using the following expression:

$$E = \sum_{W_7X} n_i e_i - \sum_{W_7} n_i e_i - e_X \qquad \text{(II-6)}$$

where the first term is the summation over the occupied molecular orbitals of the surface molecule W_7X where X is either H or N. The second term is the summation over the occupied molecular orbitals of the W_7 lattice separated from X. The last term denotes the total energy of X separated from the appropriate lattice. As mentioned previously, the repulsive energy is inherent in the calculations, hence none was included as a separate term. In all cases, the internuclear distance was the distance between the adsorbing atom (H or N) and the central atom of the lattice.

From these calculations, the bond energies and molecular orbitals of the surface molecules can be extracted. The contributions of the adatom atomic orbitals to the MO's can also be determined and presented in molecular orbital energy diagrams. The contributions of the lattice orbitals to the bonding can also be determined. Using group theoretical methods, the various orbital contributions can be estimated.

The diatomic molecules, W-W, W-H and W-N were investigated by Anders *et al.* (84,85). Hence, these calculations were not repeated. The results they obtained were basically

used to establish the empirical repulsion energy which was not used in this study.

RESULTS

The two lattices used in the calculations (Figure II-1) had to be "zeroed" as discussed previously before the adsorption of H or N could be investigated. The VOIP's of the outer atoms were reduced such that all the "surface" atoms had a charge of zero. Table II-2 shows the final adjusted VOIP's for Lattice #1 and Lattice #2. After this adjustment, the lattice VOIP's remained the same throughout the adsorption calculations.

Table II-2. Adjusted VOIP's for W_7: Lattice #1 and Lattice #2

	Lattice #1		
	VOIP (eV)		
Atom(s)	5d	6s	5p
W(1)	-9.00	-8.00	-46.08
W(2,3,4)	-8.67	-7.67	-46.08
W(5,6,7)	-8.38	-7.38	-46.08
	Lattice #2		
	VOIP (eV)		
Atom(s)	5d	6s	5p
W(1')	-9.00	-8.00	-46.08
W(2'-7')	-8.30	-7.30	-46.08

Once the lattice VOIP's were adjusted to give zero charge to the surface atoms, H and N were "adsorbed" and bond energies determined. The results for H are presented first followed by the nitrogen results.

H Adsorption

As was shown by Anders *et al.* (84), a minor variation in the H VOIP did not affect the relative energies calculated. Hence, a value of -10.40 eV for the H 1s VOIP was used for all three adsorption positions. This value is nearly identical to that reported by Anders *et al.* (84).

Figure II-2 is a plot of bonding energy *versus* internuclear distance for the W_7H molecule. The value of R is the distance from the central atom to H. Table II-3 gives the energies, distances and charges for all three positions. The preferred site for H on W(111) is predicted as the TOP position, the same type of site predicted on the W(100) (84).

Table II-3. Bond energies, equilibrium bond lengths and H charges for H adsorption on W(111)

Site	Bond Energy (eV)	R_{eq} (Å)	Charge (e)
TOP	3.23	1.75	-.32
SHALLOW 3-FOLD	2.30	1.65	-.13
DEEP 3-FOLD	1.60	1.50	+.05

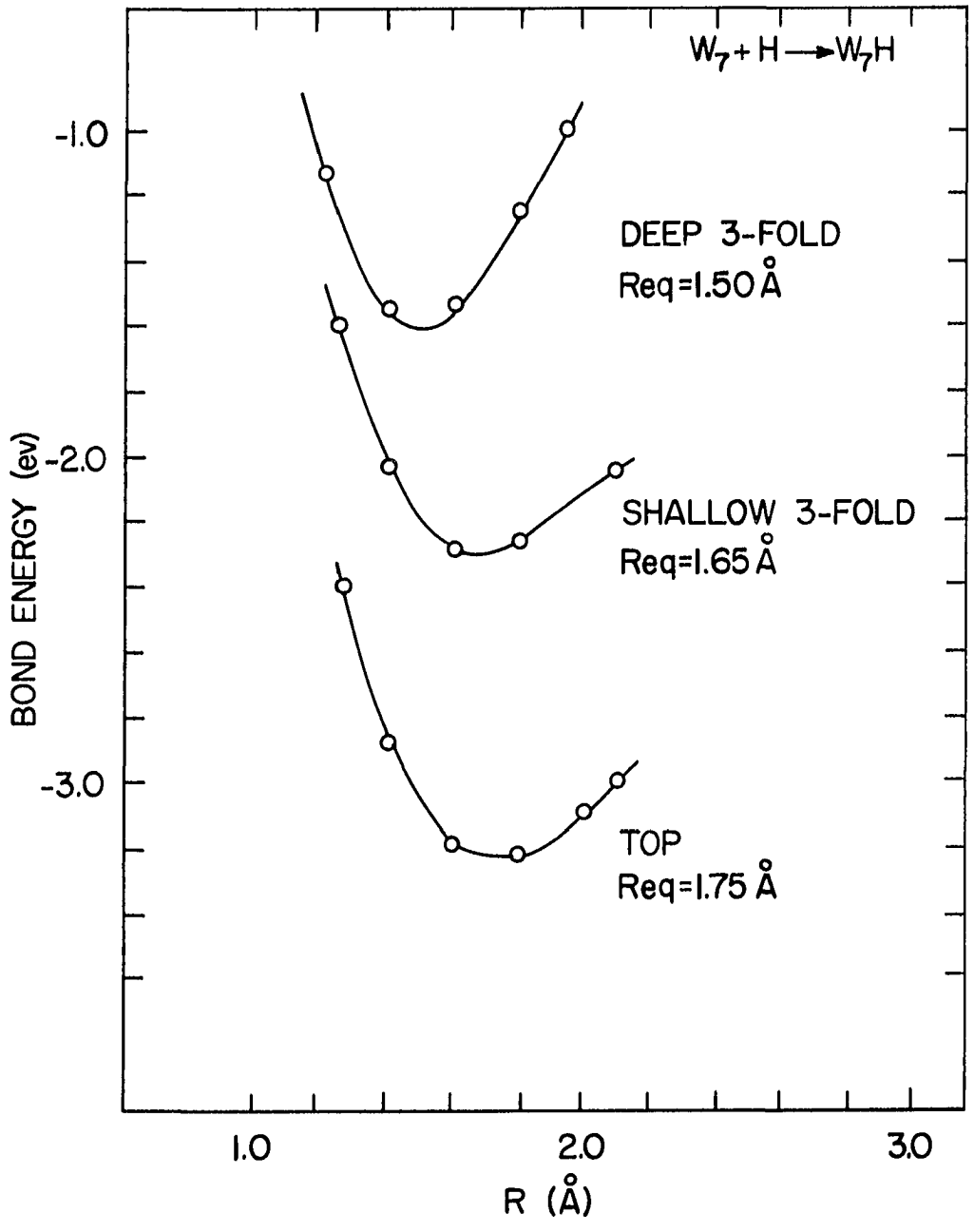

Figure II-2. Bond energies as functions of distances for hydrogen on the three W(111) adsorption sites

By using group theory, a description of the bonding in the W_7H molecules can be obtained. Lattice #1 belongs to the symmetry group C_{3v}. Lattice #2 belongs to the D_{3d} group of which C_{3v} is a subgroup. Hence, for simplicity, both lattices are considered as having C_{3v} symmetry. All the useful information concerning Lattice #2 can be extracted using this reduced symmetry. The reducible representation, Γ, for the 42 valence orbitals in either lattice is given by:

	E	$2C_3$	$3\sigma_v$
Γ_{W_7}	42	0	6

This can be broken down to the following:

$$\Gamma_{W_7} = 10A_1 + 4A_2 + 14E \qquad \text{(II-7)}$$

Hence, there are 10 totally symmetric molecular orbitals in the W_7 systems. These molecular orbitals can be determined by the projection operator procedure. As the H 1s orbital is totally symmetric, it can only interact with the totally symmetric orbitals of the W_7 lattice. Of the 10 a_1 orbitals in each of the two lattices, 5 orbitals were occupied. Tables II-4 and II-5 tabulate the atomic orbital contributions to these five occupied molecular orbitals.

Figure II-3 shows the molecular orbital energy diagram for H interacting with the lattice adsorption positions at

Table II-4. Totally symmetric occupied molecular orbitals for Lattice #1 representing the TOP and DEEP 3-FOLD adsorption sites

M.O.	ψ_1	ψ_2	ψ_3	ψ_4	ψ_5
Energy (eV)	-12.01	-10.18	-9.87	-9.18	-8.20
W(1)					
$5d_{z^2}$		-.60	.13	-.10	-.41
6s	.29				
W(2,3,4)					
$5d_{z^2}$				.44	.14
$5d_{xz}$(2,4)		±.27			
$5d_{x^2-y^2}$(2,4) (3)			-.19 .38		
$5d_{yz}$(2,4) (3)		.16 -.32			
$5d_{xy}$(2,4)			±.33		
6s	.20				
W(5,6,7)					
$5d_{z^2}$		.17			-.48
$5d_{xz}$(6,7)				±.28	±.16
$5d_{x^2-y^2}$(5) (6,7)		.12 -.06	.32 -.16		
$5d_{yz}$(5) (6,7)				-.32 .16	.18 -.09
$5d_{xy}$(6,7)		±.10	±.28		
6s	.17				

Table II-5. Totally symmetric occupied molecular orbitals for Lattice #2 representing the SHALLOW 3-FOLD adsorption site.

M.O.	ψ'_1	ψ'_2	ψ'_3	ψ'_4	ψ'_5
Energy (eV)	-11.74	-10.18	-8.87	-8.82	-8.06
W(1')					
$5d_z^2$		-.66		.09	
6s	-.33				
W(2',3',4')					
$5d_z^2$			-.38	-.08	
$5d_{xz}(2',3')$		±.20			±.27
$5d_{x^2-y^2}(2',3')$				.19	-.13
$(4')$				-.38	.26
$5d_{yz}(2',3')$		.12			.16
$(4')$		-.24			-.32
$5d_{xy}(2',3')$				±.33	±.23
6s	-.18				
W(5',6',7')					
$5d_z^2$			.38	-.08	
$5d_{xz}(5',7')$		±.20			±.27
$5d_{x^2-y^2}(5',7')$				.19	.13
$(6')$				-.38	-.26
$5d_{yz}(5',7')$		.12			-.16
$(6')$		-.24			.32
$5d_{xy}(5',7')$				±.33	±.23
6s	-.18				

the equilibrium internuclear distance. The five W lattice orbitals are indicated at the left of each diagram and the H 1s orbital to the right. The middle orbitals are the molecular orbitals formed from the interaction of H and W_7. The eigenvectors for the W_7H molecules are listed in Tables II-6 - II-8. Connecting the W_7 orbitals to the appropriate W_7H orbitals indicate how the W_7 orbitals' energies change upon interaction. The contributions of the W_7 orbitals to the W_7H orbitals were determined by quantitatively analyzing the eigenvectors of W_7H in terms of the W_7 orbitals listed in Tables II-4 and II-5.

It is noted that the H 1s orbital does not contribute significantly to all the W_7H molecular orbitals. The molecular orbitals which have no "H" character are characterized by an unchanged W_7 MO. However, there are slight perturbations in some of the orbitals, with minimal contributions from other MO's in all cases. Furthermore, in the SHALLOW 3-FOLD case, Ψ_6' of the W_7H is above the HOMO (Highest Occupied Molecular Orbital) and is unoccupied; i.e., not contributing to the bonding.

N Adsorption

For N adsorption on the two chosen lattices, identical VOIP values were used to avoid oversensitivity to parameter adjustment. For N, values of -17.77 eV for the 2s VOIP and

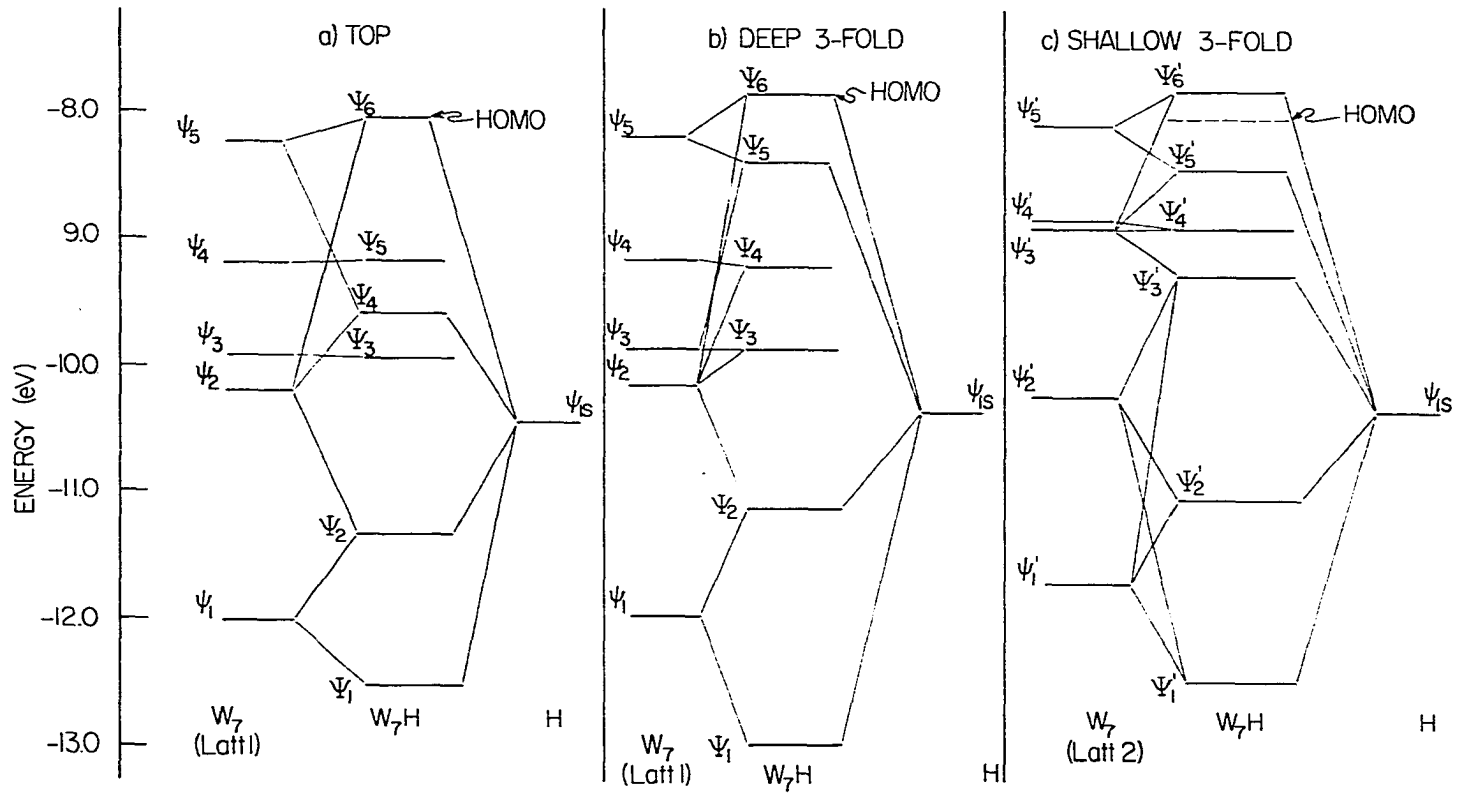

Figure II-3. Molecular orbital-energy diagrams for the totally symmetric occupied orbitals for hydrogen adsorbed on the three W(111) surface sites. (HOMO = Highest Occupied Molecular Orbital)

Table II-6. Totally symmetric molecular orbitals for the W_7H molecule; H adsorbed at the TOP site

M.O.	Ψ_1	Ψ_2	Ψ_3	Ψ_4	Ψ_5	Ψ_6
Energy (eV)	-12.48	-11.31	-9.89	-9.54	-9.16	-8.02
H						
1s	.46	.48	.07	.34	.07	.11
W(1)						
$5d_{z^2}$	.22	-.48		-.16	-.07	-.13
6s	.27	.11		.06		.05
W(2,3,4)						
$5d_{z^2}$				-.08	.43	.25
$5d_{xz}$(2,4)		±.07	±.05	±.32	±.10	±.15
$5d_{x^2-y^2}$(2,4) (3)			-.19 .38	-.07		
$5d_{yz}$(2,4) (3)		 .08		.19 -.38	.06 -.12	.08 -.16
$5d_{xy}$(2,4)			±.33	±.06		
6s	.14	.14				
W(5,6,7)						
$5d_{z^2}$				.26	.08	-.40
$5d_{xz}$(6,7)				±.11	±.27	±.26
$5d_{x^2-y^2}$(5) (6,7)			.34 -.17			
$5d_{yz}$(5) (6,7)				.12 -.06	-.30 .15	.30 -.15
$5d_{xy}$(6,7)			±.30			
6s	.10	.14		-.08		

Table II-7. Totally symmetric molecular orbitals for the W_7H molecule; H adsorbed at the DEEP 3-FOLD site

M.O.	Ψ_1	Ψ_2	Ψ_3	Ψ_4	Ψ_5	Ψ_6
Energy (eV)	-13.02	-11.17	-9.89	-9.25	-8.42	-7.88
H						
1s	.48	.30	-.03	-.09	-.20	.18
W(1)						
$5d_{z^2}$	.22	.46	.28		-.36	.13
6s	.18	-.21				
W(2,3,4)						
$5d_{z^2}$				.42		.27
$5d_{xz}(2,4)$		±.12	±.14	±.06	±.24	±.33
$5d_{x^2-y^2}(2,4)$			-.18		.05	
(3)		-.08	.36	-.07	-.10	.07
$5d_{yz}(2,4)$		-.07	-.08		-.14	.19
(3)		.14	.16	.07	.28	-.38
$5d_{xy}(2,4)$		±.07	±.30	±.06	±.09	±.06
6s	.12	-.15				
W(5,6,7)						
$5d_{z^2}$		-.07	-.11		-.40	-.26
$5d_{xz}(6,7)$			±.07	±.27	±.14	±.20
$5d_{x^2-y^2}(5)$	-.05	-.10	.28	-.10		
(6,7)		.05	-.14	.05		
$5d_{yz}(5)$				-.32	.16	.24
(6,7)				.16	-.08	-.12
$5d_{xy}(6,7)$	±.05	±.09	±.24	±.09		
6s	.10	-.12				

Table II-8. Totally symmetric molecular orbitals for the W_7H molecule; H adsorbed at the SHALLOW 3-FOLD site

M.O.	Ψ'_1	Ψ'_2	Ψ'_3	Ψ'_4	Ψ'_5	Ψ'_6
Energy (eV)	-12.66	-11.08	-9.28	-8.86	-8.43	-7.83
H						
1s	.52	.32	.26	.01	.21	-.10
W(1')						
$5d_{z^2}$	.25	.49	-.19			-.20
6s	.22	-.21	-.07			
W(2',3',4')						
$5d_{z^2}$			-.16	.33	.10	.28
$5d_{xz}$(2',3')		±.11	±.10			±.32
$5d_{x^2-y^2}$(2',3')			.15	.10		.09
(4')			-.30	-.20		-.18
$5d_{yz}$(2',3')		-.06	.06			-.19
(4')		.12	-.12			.38
$5d_{xy}$(2',3')			±.27	±.17		±.16
6s	.12	-.11				
W(5',6',7')						
$5d_{z^2}$				-.38	-.08	.28
$5d_{xz}$(5',7')		±.07	±.22		±.30	±.06
$5d_{x^2-y^2}$(5',7')			.10	.05	-.21	
(6')			-.20	-.10	.42	
$5d_{yz}$(5',7')		-.04	.13		.17	.03
(6')		.08	-.26		-.34	-.06
$5d_{xy}$(5',7')			±.17	±.08	±.36	
6s	.08	-.15	-.09		-.08	

-9.29 eV for the 2p were used; identical to the parameters reported by Anders et al. (85). As shown by these authors, the site preference remained the same using identical VOIP's for all adsorption positions. The calculation procedure was identical to that used for H adsorption.

Figure II-4 is a plot of bonding energy versus internuclear distance for the W_7N molecule. Table II-9 provides the various critical numerical results. As is seen, again, the TOP position is the predicted preferred adsorption site.

Table II-9. Bond energies, equilibrium bond lengths and N charges for N adsorption on W(111)

Site	Bond Energy (eV)	R_{eq} (Å)	Charge (e)
TOP	4.82	1.90	-1.50
SHALLOW 3-FOLD	3.27	2.10	-1.50
DEEP 3-FOLD	1.66	2.20	-.90

The equilibrium energy separations are rather large compared to those of Anders et al. (85) on W(100). If more surface atoms were included, the TOP and DEEP 3-FOLD energies destabilized somewhat while the SHALLOW 3-FOLD energy stayed about the same. The changes observed, however, were quite

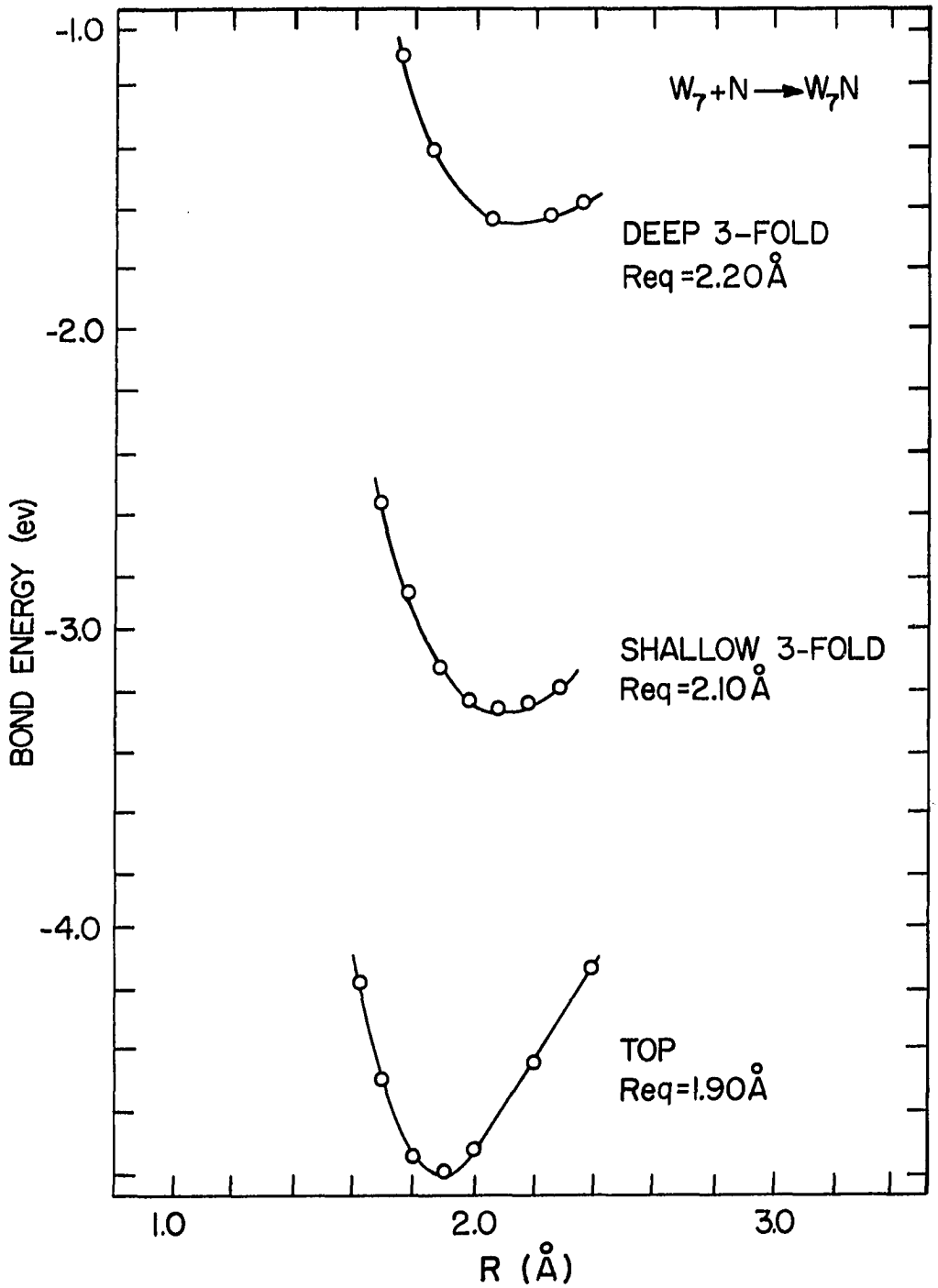

Figure II-4. Bond energies as functions of distances for nitrogen adsorbed on the three W(111) adsorption sites

minimal. It is definite that the DEEP 3-FOLD position is the least stable adsorption site. This contrasts with the results of Anders et al. (85) who determined that N preferred a multicoordinated adsorption position.

The group theoretical analysis of the W_7N molecule is very similar to that for W_7H. In the nitrogen case, the 2s and $2p_z$ orbitals belong to the A_1 representation of C_{3v} and can hence interact with the 5 totally symmetric occupied W_7 MO's. This interaction will produce 7 molecular orbitals for the W_7N molecule. Tables II-10 - II-12 present these 7 molecular orbitals for each of the three adsorption positions. By comparing these molecular orbitals to the W_7 MO's in Tables II-4 and II-5, the contributions to the W_7N MO's by the 5 lattice MO's can be determined. The results are depicted in Figure II-5 in terms of molecular orbital energy diagrams. It is noted that for the TOP position, the N 2s contributes only to the more stable W_7N MO's while for the other two positions, there are large contributions to the higher energy orbitals. In general, most all of the W_7 molecular orbitals became involved in the adsorption interaction; unlike the situation for W_7H.

In the symmetry group C_{3v}, the p_x and p_y orbitals of N belong to the E irreducible representation. Hence, they can only interact with degenerate e MO's from the W_7 lattices. As mentioned previously, there were 14 sets of e MO's in the

Table II-10. Totally symmetric molecular orbitals for the W_7N molecule; N adsorbed at the TOP site

M.O.	Ψ_1	Ψ_2	Ψ_3	Ψ_4	Ψ_5	Ψ_6	Ψ_7
Energy (eV)	-18.32	-11.78	-10.28	-9.88	-9.35	-9.14	-7.99
N							
2s	.89	-.13	.22	.03			.03
$2p_z$		.04	.66	.14	.48	.22	-.12
W(1)							
$5d_z2$	.17	-.21	-.40				-.09
6s	.13	.24	.07				
W(2,3,4)							
$5d_z2$					.19	-.39	.26
$5d_{xz}(2,4)$			±.16		±.27	±.17	±.17
$5d_{x^2-y^2}(2,4)$				.19			
(3)				-.38			
$5d_{yz}(2,4)$			.09		-.16	-.10	.10
(3)			-.18		.32	.20	-.20
$5d_{xy}(2,4)$				±.33			
6s		.20					
W(5,6,7)							
$5d_z2$			.10		-.23	-.15	-.38
$5d_{xz}(6,7)$					±.16	±.24	±.27
$5d_{x^2-y^2}(5)$			.08	-.34			
$(6,7)$			-.04	.17			
$5d_{yz}(5)$					-.18	.28	.32
$(6,7)$					.09	-.14	-.16
$5d_{xy}(6,7)$			±.07	±.29			
6s		.18	-.06				

Table II-11. Totally symmetric molecular orbitals for the W_7N molecule; N adsorbed at the DEEP 3-FOLD site

M.O.	Ψ_1	Ψ_2	Ψ_3	Ψ_4	Ψ_5	Ψ_6	Ψ_7
Energy (eV)	-18.36	-11.24	-10.10	-9.86	-8.91	-8.39	-7.91
N							
2s	.87	-.15	-.20	-.05	.16	-.19	-.17
$2p_z$		-.19	.67	.25	-.36	-.08	-.12
W(1)							
$5d_z^2$	.11	-.40	.29	-.18	-.08	-.27	
6s	.07	.23	.12		-.07	.06	
W(2,3,4)							
$5d_z^2$			-.12	-.10	-.45	.12	-.09
$5d_{xz}$(2,4)		±.11		±.13		±.26	±.38
$5d_{x^2-y^2}$(2,4)				.16		.07	
(3)		.06	.09	-.32	.07	-.14	-.09
$5d_{yz}$(2,4)		.06		.07		-.15	-.22
(3)		-.12		-.14		.30	.44
$5d_{xy}$(2,4)			±.08	±.30	±.06	±.12	±.08
6s		.17	.09				.06
W(5,6,7)							
$5d_z^2$		.07		.11	-.06	-.38	.36
$5d_{xz}$(6,7)			±.13	±.15	±.19	±.14	±.08
$5d_{x^2-y^2}$(5)		.10	.14	-.24			
(6,7)			-.07	.12			
$5d_{yz}$(5)			.16	.14	.22	.16	-.09
(6,7)			-.08	-.07	-.11	-.08	
$5d_{xy}$(6,7)		±.08	±.11	±.21			
6s		.13					

Table II-12. Totally symmetric molecular orbitals for the W_7N molecule; N adsorbed at the SHALLOW 3-FOLD site

M.O.	Ψ'_1	Ψ'_2	Ψ'_3	Ψ'_4	Ψ'_5	Ψ'_6	Ψ'_7
Energy (eV)	-18.29	-11.28	-10.12	-9.23	-8.86	-8.48	-7.80
N							
2s	-.89	.14	-.27	-.06		.08	.12
$2p_z$		-.14	-.72	.36	-.03	-.26	.05
W(1')							
$5d_z2$	-.14	.36	.35	.16			.15
6s	-.10	-.26	.08	.05			
W(2',3',4')							
$5d_z2$				.16	.33	.09	-.23
$5d_{xz}(2',3')$		±.08		±.13		±.08	±.35
$5d_{x^2-y^2}(2',3')$				-.15	.09		-.12
$(4')$				.30	-.18	.09	.24
$5d_{yz}(2',3')$		-.05		-.08		.05	.20
$(4')$		.10		.16		-.10	-.40
$5d_{xy}(2',3')$				±.25	±.16	±.08	±.21
6s		-.14					
W(5',6',7')							
$5d_z2$					-.39	-.08	-.23
$5d_{xz}(5',7')$		±.05	±.09	±.21		±.28	±.10
$5d_{x^2-y^2}(5',7')$				-.10		-.20	
$(6')$				.20	-.09	.40	-.06
$5d_{yz}(5',6')$			-.05	-.12		.16	-.06
$(6')$		.06	.10	.24		-.32	.12
$5d_{xy}(5',7')$				±.18	±.08	±.35	±.05
6s		-.18	.13	.05		-.05	

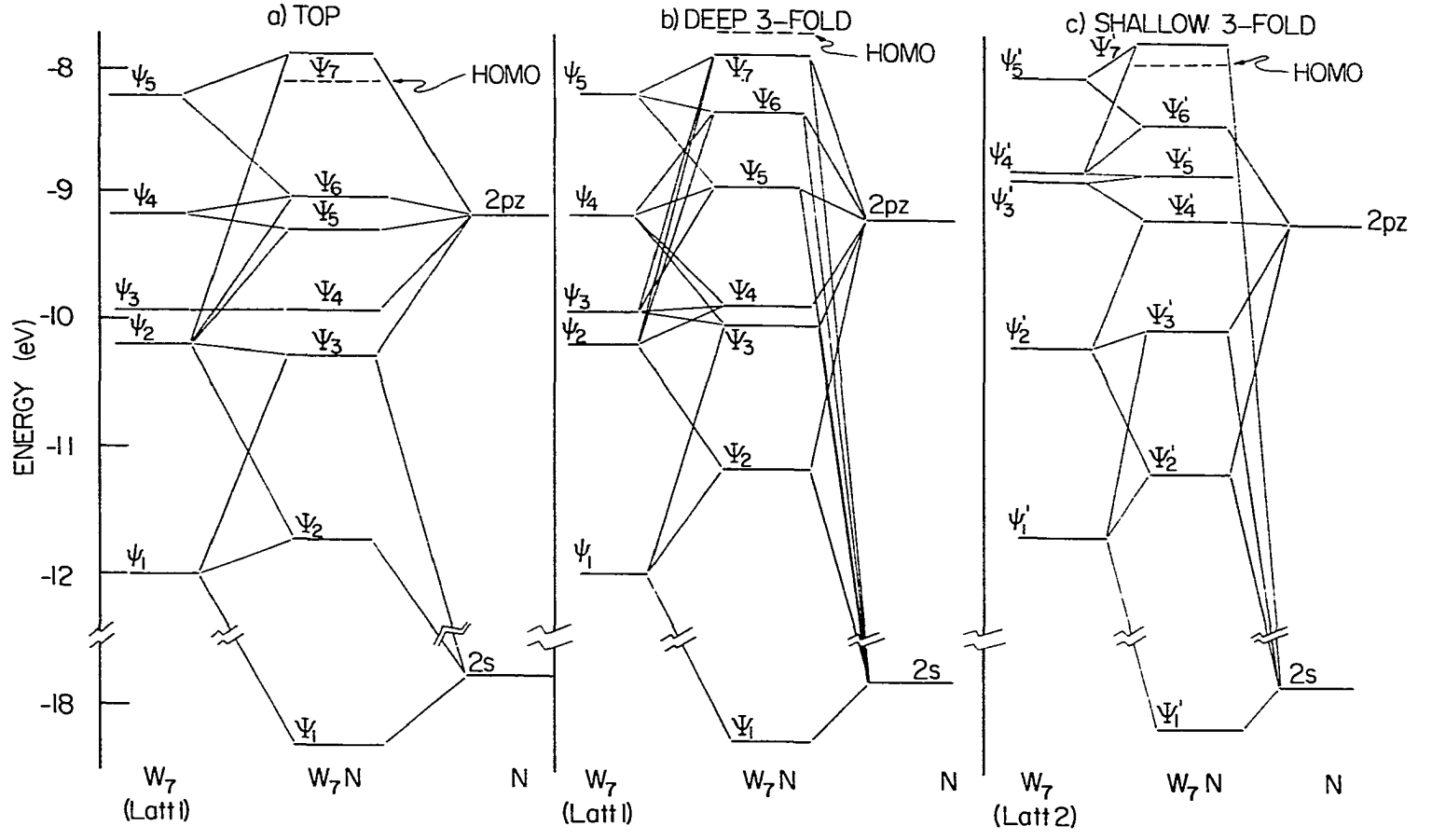

Figure II-5. Molecular orbital-energy diagrams for the totally symmetric occupied orbitals for nitrogen adsorbed on the three W(111) surface sites

W_7 system, of which 7 were occupied. Unfortunately, the resulting linear combinations were quite "nonsymmetrical" with no continuous pattern observable as for the totally symmetrical case. The LCAO's produced were by no means unique; others may show more logical symmetry. The e orbitals created were indeed degenerate and orthogonal. The inherent 3-fold symmetry of the lattices seems to have "interfered" in the production of logical linear combinations from the 4-fold symmetric d orbitals. Hence, no tabulations of the linear combinations are presented. However, qualitative information is presented in molecular orbital energy diagrams in Figure II-6. The contributions indicated for the W_7 orbitals are approximated due to the patternless MO's mentioned. It is seen that the 7 sets of W_7 MO's and the degenerate $2p_x$,p_y of N combine to form 8 sets of degenerate orbitals all of which are at least partially occupied. In all cases, the orbitals, $\Psi_{15,16}$, are the HOMOs. They are triply occupied in the TOP case and singly occupied for the other two positions. It is evident that there were several W_7 e orbitals which did not participate in the bonding.

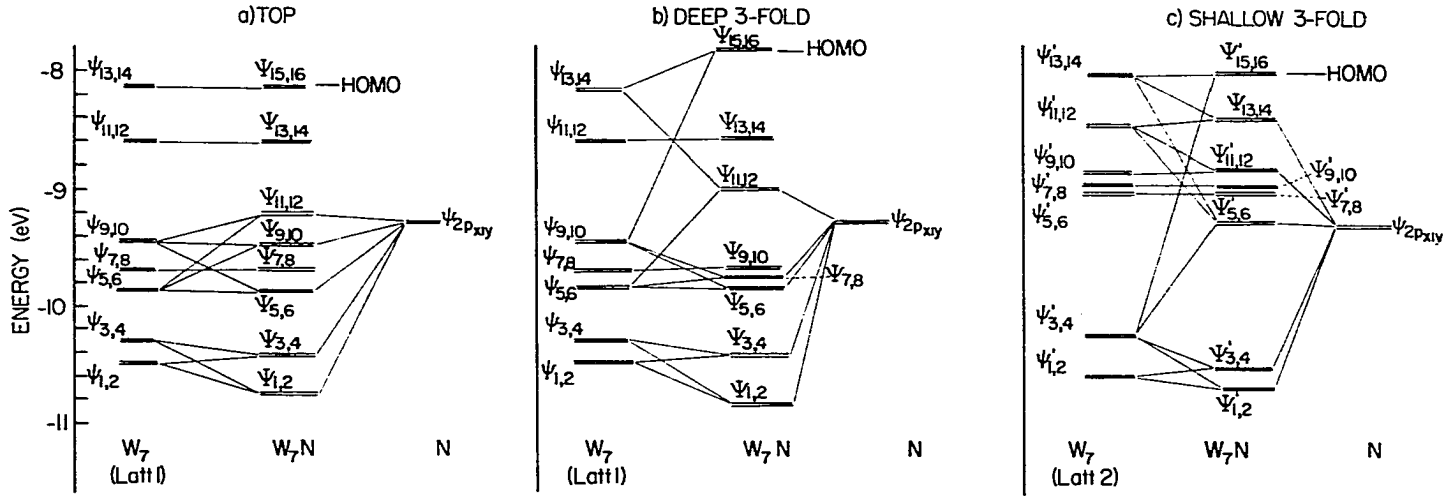

Figure II-6. Molecular orbital-energy diagrams for the occupied orbitals belonging to the E representation for nitrogen adsorbed on the three W(111) surface sites.

DISCUSSION

H Adsorption

The most fascinating item about H adsorbed on W(111) is that it produces 4 distinct beta (β) desorption peaks ranging in temperature from 200 to 600K (97,98). This seems to indicate that there should be a number of reasonable bonding sites on W(111) for H. Tamm and Schmidt (97) suggest that the three sites chosen here plus less symmetrical sites can all be used for adsorption. The other sites would be "bridging" positions between atoms 1 and 3 and also atoms 1 and 6 of Figure II-1, DEEP position. They also obtained very high coverages of H; claiming on the order of 4 Hs/top surface atom at saturation. If only the top most atoms are counted, the number of sites is 5.8×10^{14} atoms cm^{-2}. For the four desorption states (relative amounts being 1:1.5:1.5:1), they observed 2.6×10^{15} atoms cm^{-2} desorbing. Hence, if the high temperature state were due to adsorption on TOP, then the number of hydrogens should be 5.2×10^{14} atoms cm^{-2}, nearly a 1:1 correspondence with the number of TOP positions. The other states are probably populating the holes and/or bridging areas. It is also noted that the high temperature desorption peaks from W(100), (111) and (110) all came off at nearly the same temperature, indicating the bonding may be similar on all three faces. The "TOP" position is available

on all three faces (in a crude sense) and could account for the temperature equivalence.

As reported by Summers (103), only a (1X1) LEED pattern is observed upon H adsorption on a W(111) surface. Saturating all of the TOP atoms would tend to produce this pattern. Again, the choice of the TOP position as the preferred site is acceptable or at least nonrefutable in light of the observed LEED results.

If the slightly negatively charged H were residing in the TOP site, the work function of the tungsten system should increase as it would be more "difficult" for an electron to escape from the surface. Experimentally, the work function does increase by about .30 eV (99). If the H were in the DEEP hole, one would expect the work function to decrease as the negative H would be below the TOP later of atoms.

Strangely enough, even though there are four H desorption states on W(111), high resolution electron-energy-loss spectroscopy (HRELS) shows only one peak for H (102). C. Backx et al. believe that this single peak is due to H adsorption at the TOP position. This tends to support the contention of this study that H prefers the TOP position but says nothing about the other desorption states which do exist.

As seen in Figure II-3 and Table II-6, H in the TOP position tends to interact strongly with W_7 MO's that have

large contributions from W(#1). Hence, there seems to be a tendency toward a localized single bond; in contrast to the W(100) results for the 1CN site (84). It appears that the energy difference in the various symmetric sites can be explained in two ways using orbital interaction arguments.

Firstly, H in the TOP position tends to contribute less to the least stable W_7H MO's as compared to the other two positions. Hence the overall energy of the W_7-H bond may end up being greater for the TOP adsorption position. Secondly, the adsorption of H in a "hole" seems to have a disrupting effect on the lattices. The total overlap population of the W_7 Lattice #1 is less for the DEEP W_7H molecule than TOP W_7H molecule. However, the overlaps with H are about the same for both sites. Hence, H adsorbing at the TOP site tends to perturb the chosen lattice less than its adsorption in a hole. These are only qualitative arguments but are useful in interpreting the observations made.

It is also interesting to note that the H 1s orbital completely ignores W_7 molecular orbitals with large $d_{(x^2-y^2)}$ and $d_{(xy)}$ contributions from atoms 2-7 for all positions. This is puzzling in that the $d_{(x^2-y^2)}$ and $d_{(xy)}$ orbitals in the DEEP and SHALLOW positions tend to "point" toward the adsorbing H. It must be that the interaction is either nonbonding or possibly repulsive.

N Adsorption

This study predicts that N prefers to adsorb at the TOP position on the W(111) lattice. This result is in marked contrast to the usual conception that N likes to adsorb in high coordination positions. There seems to be sufficient evidence in the literature to support (at least not refute) the idea of single coordination adsorption for N on W(111).

Initially, it must be noted that N_2, in general, does not adsorb very well on W(111) relative to W(100). In a molecular beam study, King and Wells (44) determined the maximum coverage of N atoms on W(111) was 1.25×10^{14} atoms cm^{-2}, about 1/4 of a monolayer considering only the TOP atoms. They obtained a sticking coefficient of about .08 compared to .32 (114) found for N-W(100). Hence, it appears that nitrogen does not "like" the W(111) surface. Adams and Germer (114) claim that N only adsorbs on 4-coordination "W(100)-like" sites. King and Wells (44) state that placing a W atom on top of a protruding surface atom would create this type of site on the W(111) surface. The only W(111) unrearranged 4-fold position would be in the W (1-2-3-6) hole in Figure II-1, DEEP. The possibility of this position being an adsorption site is discussed later.

D. L. Summers (103) studied the adsorption of N_2 on W(111) using LEED. He found that as N_2 adsorbed, the clean (1x1) remained but the initially faint $(\bar{1},0)$, $(0,\bar{1})$ and (1,1)

spots were extinguished. He interpreted this to mean that N adsorbed in every other trigonal site. It seems that by adsorbing N on the TOP atoms (which are probably producing the most intense LEED spots), the $(0,\bar{1})$, $(\bar{1},\bar{1})$ and (1,0) spots should increase in intensity as the diffraction cross-section has been increased. This should cause the dim spots to become relatively dimmer. Hence, the TOP position seems consistent with the LEED results reported.

As mentioned by Anders et al. (85), the work function of W(100) decreases ($\Delta\phi$ = -.40 eV) upon N_2 adsorption. By placing the "negative" N in the 4-fold hole, they can rationalize a charged double layer with positive out, hence decreasing the work function. The work function for N on W(111) is found to increase relative to W(111) alone. The change is approximately +.15 eV (104) indicating a negative layer out. If N were adsorbed in the DEEP 3-FOLD hole, it would be below the TOP layer of atoms. This would produce a positive layer out. The TOP and SHALLOW positions would give a negative layer out as required. However, the calculations in this study indicate that of these two sites, the TOP is the preferred one. This type of argument can be applied to the "pseudo" 4-fold position mentioned previously. If the N did bond in the W (1-2-3-6) hole, it also would be below the top layer. Hence, this possible adsorption site is considered improbable due to the observed work function change.

The description of the bonding presented in Figures II-5 and II-6 and Tables II-10 - II-12 is also useful in explaining the site preference observed. It is seen that the N 2s orbital at both the DEEP and SHALLOW positions contributes significantly to the less stable W_7N molecular orbitals while the TOP N 2s does not (Figure II-5). These high energy orbitals generally contain large contributions from the noncentral atoms. Hence, the total s overlap for the two "hole" positions is qualitatively less than for the TOP position. A similar situation occurs when considering the degenerate e orbitals. The N $2p_x$,p_y orbitals, in general, interact more favorably at the TOP site relative to the other two (Figure II-6). However, it appears as though the e orbital interaction of the DEEP site is also quite stable. The deciding factors, it seems, are the contributions of the W_7 MO's to the W_7N molecular orbitals. In both the DEEP and SHALLOW cases, stable low energy W_7 MO's contribute significantly to less stable W_7N orbitals. This is not the case for the TOP W_7 e orbitals where the two least stable W_7 MO's are not changed at all. In fact, the overlap population for the W_7-N bond was slightly greater for the DEEP site compared to the TOP site. However, the total overlap between the lattice atoms was greatly diminished in the DEEP case. Therefore, from an orbital overlap standpoint, the choice of the TOP position appears reasonable.

Finally, a discussion of bond distances is also necessary. If the N chose to adsorb in the DEEP or SHALLOW 3-FOLD holes, the closest it could get to atoms 2-7 (or 2'-4') is 2.58 Å. This is significantly greater than the central atom-N distance calculated at approximately 2.15 Å. Hence, the covalent interaction at 2.58 Å should not be very great relative to the interaction possible at 2.28 Å on the W(100) surface (85). It appears that this long range interaction on W(111) does not compensate for decreased W-W interaction caused by adsorption.

CONCLUSIONS

This study predicts that both H and N favor the TOP position upon adsorption on the W(111) plane. Both the literature and orbital overlap considerations tend to qualitatively support these claims. It may be the case that the TOP position for N is the "lesser of three evils" as N does not adsorb very readily on W(111). It is felt that the integrity of EHMO calculations has been preserved when considering surface adsorption. More studies may be in order to further verify this contention. As for further studies, it is this author's opinion that the proposed "pseudo" 4-fold position be investigated if an appropriately symmetric lattice can be constructed. This site should be the only other possible adsorption position available.

LITERATURE CITED

1. J. C. Schlatter and K. C. Taylor, J. Catal. 49, 42 (1977).

2. G. C. Bond, Catalysis by Metals (Academic Press, Inc., London, 1962), Chap. 16.

3. A. Mittasch, Advances in Catalysis 2, 82 (1950).

4. W. G. Frankenburg, in Catalysis, edited by P. H. Emmett (Reinhold Publ. Corp., New York, 1955), Vol. 3, Chap. 6.

5. C. Bokhaven, C. van Heerden, R. Westrik and P. Zwietering, in Catalysis, edited by P. H. Emmett (Reinhold Publ. Corp., New York, 1955), Vol. 3, Chap. 7.

6. A. Nielsen, Advances in Catalysis 5, 1 (1953).

7. P. H. Emmett, New Approaches to the Study of Catalysis (Pennsylvania State University, 1962), Chap. 5.

8. A. Nielsen, Cat. Rev. 4, 1 (1971).

9. P. H. Emmett, in The Physical Basis for Heterogenous Catalysis, edited by E. Drauglis and R. I. Jaffee (Plenum Press, New York, 1975), pp. 3-34.

10. A. Ozaki, H. S. Taylor and M. Boudart, Proc. Roy. Soc. A258, 47 (1960).

11. K. Aika and A. Ozaki, J. Catal. 13, 232 (1969).

12. K. Aika and A. Ozaki, J. Catal. 19, 350 (1970).

13. K. Aika, H. Hori and A. Ozaki, J. Catal. 27, 424 (1972).

14. A. Ozaki, K. Aika and Y. Morikawa, in Proceedings of the Fifth International Congress on Catalysis, edited by J. W. Hightower (North Holland Publ. Co., Amsterdam, 1973), Vol. 2, p. 1251.

15. M. I. Temkin and V. Pyzhev, Acta Physicochim. (U.R.S.S.) 12, 327 (1940).

16. P. H. Emmett and J. T. Kummer, Ind. Eng. Chem. 35, 677 (1943).

17. M. I. Temkin, N. M. Morozov and E. N. Shapatina, Kinetika i Kataliz 4, 565 (1963).

18. R. Brill, J. Catal. 16, 16 (1970).

19. A. Nielsen, J. Kjaer and B. Hansen, J. Catal. 3, 68 (1964).

20. S. R. Logan and J. Philp, J. Catal. 11, 1 (1968).

21. S. Carrá and R. Ugo, J. Catal. 15, 435 (1969).

22. A. Ozaki, K. Aika and H. Hori, Bull. Chem. Soc. Japan 44, 3216 (1971).

23. K. Aika, J. Yamaguchi and A. Ozaki, Chem. Letters 161 (1973).

24. K. S. Love and P. H. Emmett, J. Am. Chem. Soc. 63, 3297 (1941).

25. S. R. Logan, R. L. Moss and C. Kemball, Trans. Far. Soc. 54, 922 (1958).

26. D. G. Löffler and L. D. Schmidt, J. Catal. 44, 244 (1976).

27. N. Takezawa and I. Toyoshima, J. Phys. Chem. 70, 594 (1966).

28. A. Kazusaka, J. Res. Inst. Cat., Hokkaido Univ. 19, 42 (1971).

29. J. Enomoto, J. Horiuti and H. Kobayashi, J. Res. Inst. Cat., Hokkaido Univ. 3, 185 (1955).

30. H. F. Franzen, Prog. Solid St. Chem. 12, 1 (1978).

31. P. T. Dawson and R. S. Hansen, J. Chem. Phys. 45, 3148 (1966).

32. P. T. Dawson and R. S. Hansen, J. Chem. Phys. 48, 623 (1968).

33. K. Matsushita and R. S. Hansen, J. Chem. Phys. 51, 472 (1969).

34. K. Matsushita and R. S. Hansen, J. Chem. Phys. 52, 4877 (1970).

35. J. McAllister and R. S. Hansen, J. Chem. Phys. 59, 414 (1973).

36. P. T. Dawson and Y. K. Peng, J. Chem. Phys. 52, 1014 (1970).

37. Y. K. Peng and P. T. Dawson, J. Chem. Phys. 54, 950 (1971).

38. P. T. Dawson and Y. K. Peng, J. Phys. Chem. 77, 135 (1973).

39. Y. K. Peng and P. T. Dawson, Can. J. Chem. 52, 1147 (1974).

40. P. T. Dawson, J. Catal. 33, 47 (1974).

41. R. Sheets and G. Blyholder, J. Phys. Chem. 76, 970 (1972).

42. K. Matsushita and R. S. Hansen, J. Chem. Phys. 54, 2278 (1971).

43. M. Abon, G. Bergeret and B. Tardy, Surf. Sci. 68, 305 (1977).

44. D. A. King and M. G. Wells, Surf. Sci. 29, 454 (1972).

45. W. J. McGill and F. Sebba, J. Catal. 2, 104 (1963).

46. S. R. Logan and C. Kemball, Trans. Far. Soc. 56, 144 (1960).

47. D. V. Sokol'skii, T. V. Kuzora, L. F. Kozin and A. I. Shcherbak, Dokl. Akad. Nauk SSSR 230, 620 (1976).

48. K. Tamaru, K. Tanaka, S. Fukasaku and S. Ishida, Trans. Far. Soc. 61, 773 (1965).

49. R. E. Mardaleishvili, H. Sin-Chou and Zh. Ya. Smorodinskaya, Kinetika i Kataliz 8, 786 (1967).

50. R. E. Mardaleishvili, H. Sin-Chou and Zh. Ya. Smorodinskaya, Kinetika i Kataliz 10, 1278 (1969).

51. A. G. Friedlander, Ph. R. Courty and R. E. Montarnal, J. Catal. 48, 332 (1977).

52. A. J. B. Robertson and E. M. A. Willhoft, Trans. Far. Soc. 63, 476 (1967).

53. D. G. Löffler and L. D. Schmidt, J. Catal. 41, 440 (1976).

54. D. G. Löffler and L. D. Schmidt, Surf. Sci. 59, 195 (1976).

55. A. Amano and H. Taylor, J. Am. Chem. Soc. 76, 4201 (1954).

56. A. G. Friedlander, Ph. R. Courty and R. E. Montarnal, J. Catal. 48, 312 (1977).

57. T. Pignet and L. D. Schmidt, J. Catal. 40, 212 (1975).

58. K. Aika, T. Ohhata and A. Ozaki, J. Catal. 19, 140 (1970).

59. K. M. C. Davis and C. F. Sayer, J. Chem. Soc., F1 68, 1884 (1972).

60. M. L. Unland, J. Catal. 31, 459 (1973).

61. T. P. Kobylinski and B. W. Taylor, J. Catal. 33, 376 (1974).

62. C. T. Campbell and J. M. White, Appl. of Surf. Sci. 1, 347 (1978).

63. B. A. Sexton and G. A. Somorjai, J. Catal. 46, 167 (1977).

64. C. T. Campbell and J. M. White, J. Catal. 54, 289 (1978).

65. R. S. Hansen and V. J. Mimeault, in Experimental Methods in Catalytic Research, edited by R. B. Anderson (Academic Press, Inc., New York, 1968), pp. 217-264.

66. A. R. Miller, Proc. Cambridge Phil. Soc. 43, 232 (1947).

67. K. A. R. Mitchell, F. R. Shepherd, P. R. Wilson and D. C. Frost, Surf. Sci. 64, 737 (1977).

68. D. G. Castner, B. A. Sexton and G. A. Somorjai, Surf. Sci. 71, 519 (1978).

69. J. T. Grant and T. W. Haas, Surf. Sci. 21, 76 (1970).

70. C. W. Tucker, Jr., J. Appl. Phys. 37, 3013 (1966).

71. C. W. Tucker, Jr., J. Appl. Phys. 37, 4147 (1966).

72. R. A. Marbrow and R. M. Lambert, Surf. Sci. 67, 489 (1977).

73. P. B. Masterson, Ph.D. thesis, Iowa State University, 1971 (unpublished).

74. K. Matsushita and R. S. Hansen, J. Chem. Phys. 52, 3619 (1970).

75. J. L. Gland, Surf. Sci. 71, 327 (1978).

76. L. R. Danielson, M. J. Dresser, E. E. Donaldson and D. R. Sandstrom, Surf. Sci. 71, 615 (1978).

77. B. A. Sexton, General Motors Corp., Warren, Mich., private communication.

78. L. R. Danielson, M. J. Dresser, E. E. Donaldson and D. R. Sandstrom, Surf. Sci. 71, 599 (1978).

79. L. E. Davis, N. C. MacDonald, P. W. Palmberg, G. E. Riach and R. E. Weber, in Handbook of Auger Electron Spectroscopy (Physical Electronics Industries, Inc., Eden Prairie, Minn., 1976).

80. J. T. Yates, National Bureau of Standards, Washington, D.C., private communication.

81. W. A. Van Hook, in Isotope Effects in Chemical Reactions, edited by C. J. Collins and N. S. Bowman (Van Nostrand Reinhold Co., New York, 1970), Chap. 1.

82. F. A. Cotton and G. Wilkinson, Advanced Inorganic Chemistry (Interscience Publishers, New York, 1972), 3rd ed.

83. F. Jona, Surf. Sci. 68, 204 (1977).

84. L. W. Anders, R. S. Hansen and L. S. Bartell, J. Chem. Phys. 59, 5277 (1973).

85. L. W. Anders, R. S. Hansen and L. S. Bartell, J. Chem. Phys. 62, 1641 (1975).

86. R. C. Baetzold, Advances in Catalysis 5, 1 (1975).

87. M. Simonetta and A. Gavezzotti, Struct. and Bond. 27, 1 (1976).

88. R. C. Baetzold, J. Chem. Phys. 55, 4355 (1971).

89. R. C. Baetzold, J. Chem. Phys. 55, 4363 (1971).

90. R. C. Baetzold and R. E. Mack, J. Chem. Phys. 62, 1513 (1975).

91. A. B. Anderson and R. Hoffmann, J. Chem. Phys. 61, 4545 (1974).

92. P. Politzer and S. D. Kasten, J. Phys. Chem. 80, 385 (1976).

93. D. J. M. Fassaert, H. Verbeek and A. van der Avoird, Surf. Sci. 29, 501 (1972).

94. T. H. Lee and J. W. Rabalais, Surf. Sci. 75, 29 (1978).

95. P. J. Estrup and J. Anderson, J. Chem. Phys. 45, 2254 (1966).

96. K. Yonehara and L. D. Schmidt, Surf. Sci. 25, 238 (1971).

97. P. W. Tamm and L. D. Schmidt, J. Chem. Phys. 54, 4775 (1971).

98. T. E. Madey, Surf. Sci. 29, 571 (1972).

99. B. J. Hopkins and K. R. Pender, Surf. Sci. 5, 316 (1966).

100. P. W. Tamm and L. D. Schmidt, J. Chem. Phys. 55, 4253 (1971).

101. M. Domke, G. Jähnig and M. Drechsler, Surf. Sci. 42, 389 (1974).

102. C. Backx, B. Feuerbacher, B. Fitton and R. F. Willis, Surf. Sci. 63, 193 (1977).

103. D. L. Summers, Ph.D. thesis, Iowa State University, 1974 (unpublished).

104. T. A. Delchar and G. Ehrlich, J. Chem. Phys. 42, 2686 (1965).

105. M. Wilf and M. Folman, Surf. Sci. 52, 10 (1975).

106. R. Hoffmann, J. Chem. Phys. 39, 1397 (1963).

107. M. Wolfsberg and C. Helmholtz, J. Chem. Phys. 20, 837 (1952).

108. L. Anders, Ph.D. thesis, Iowa State University, 1973.

109. H. Basch, A. Viste and H. B. Gray, Theoret. Chim. Acta 3, 458 (1965).

110. R. S. Mulliken, J. Chem. Phys. 23, 1833 (1955).

111. G. Burns, J. Chem. Phys. 41, 1521 (1964).

112. L. L. Lohr, Jr. and W. N. Lipscomb, Inorg. Chem. 3, 22 (1964).

113. F. Herman and S. Skillman, Atomic Structure Calculations (Prentice Hall, Englewood Cliffs, New Jersey, 1960).

114. D. L. Adams and L. H. Germer, Surf. Sci. 26, 109 (1971).

ACKNOWLEDGEMENTS

The author wishes to thank Dr. Robert S. Hansen for his guidance during the course of this research and his patience, understanding and encouragement throughout the author's graduate career. The numerous and enlightening discussions with Professor Hansen were the author's major source of knowledge concerning scientific research.

The author is indebted to Dr. Paul Mahaffy and Mike Slaughter for the cutting and preparation of the single crystal samples. Thanks are also extended to the various Ames Lab service groups for their help on this project, especially the glass shop under the direction of Harold Hall. Thanks are further extended to Sue Musselman for the typing of this dissertation. In addition, the author would like to express his gratitude to all of the members of P&I Research Group III and X-ray Group I for the many hours of enjoyable discussions and interactions throughout the author's graduate education.

Finally, the author is greatly indebted to his parents and family for their continued encouragement over these many years of schooling. The author wishes to thank his wife, Sharry, for her patience and support during his graduate work and also to our children, Amy and Eric, for the love and enjoyment they have provided.